FRAGILITY ASSESSMENT OF RIVER-CROSSING HIGHWAY BRIDGES UNDER FLOOD-INDUCED LOADS AND SCOUR

A Thesis

by

Züleyha Kanpara Cıvaş

Submitted to the

Graduate School of Science and Engineering

In Partial Fulfillment of the Requirements for

The Degree of

Master of Science

in the

Department of Civil Engineering

Özyeğin University

August 2020

FRAGILITY ASSESSMENT OF RIVER-CROSSING HIGHWAY BRIDGES UNDER FLOOD-INDUCED LOADS AND SCOUR

Approved by:

Asst. Prof. Taner Yılmaz, Advisor,
Department of Civil Engineering
Özyeğin University

Asst. Prof. Derya Deniz
Department of Civil Engineering
Özyeğin University

Professor Alp Caner
Department of Civil Engineering
Middle East Technical University

Date Approved: 26.08.2020

To my deepest love, my handsome and kindhearted father

ABSTRACT

Flood hazard is a major threat to the safety and serviceability of transportation infrastructure systems causing sudden loss of life and property. High levels of discharge values occurring in flood events may produce excessive scour and accumulations of debris around the piers of river-crossing highway bridges. The hydrodynamic loading induced by the increased flow velocities can cause damage and even collapse of the bridges with the increase in lateral displacement response and the reduction in the lateral resistance at the pier foundations due to scour. In the meantime, the accumulation of debris can aggravate the scour depths and enhance the drag force acting on the piers. Although flood-induced scour is one of the most common causes of past bridge failures, still there is a lack of structural risk assessment methodologies to address this issue.

This thesis study aims to evaluate the vulnerability of river-crossing highway bridges subjected to flood-induced loads and scour through the generation of fragility curves. For this purpose, firstly a sensitivity analysis is conducted to identify the key modeling parameters affecting the bridge response under flood effects. Then, a simulation-based probabilistic framework is developed to produce the flood fragility curves in the absence and presence of debris accumulation. Within the applied methodology, finite element models of a bridge bent are generated and nonlinear analyses are performed under the applied flood-induced load and scour effects to compute the bridge structural response. It is found out that bridge failure probabilities are significantly increased due to the presence of debris accumulation. The fragility curves generated in this thesis can be used in future studies on risk assessment of highway bridges under flood hazards.

ÖZETÇE

Seller ulaşım ağlarının güvenliğinin ve işletilebilirliğinin tehlike altına girmesine neden olabilen ve aynı zamanda ani can ve mal kaybına yol açabilen doğal afetlerdir. Sel olayları süresince ortaya çıkabilecek yüksek seviyedeki debiler, nehir geçen köprülerin orta ayakları etrafında aşırı oyulma ve moloz birikmesine yol açabilir. Köprü orta ayak temellerinde oyulmadan dolayı yatay zemin direncinin azalması ve artan akış hızları neticesinde oluşan hidrodinamik yükleme, köprülerin yatayda yaptığı deplasman tepkisinin artmasına ve köprülerin hasar almasına ve hatta yıkılmasına neden olabilir. Bu esnada, moloz birikmesi oyulma derinliği ve orta ayağa etki eden sürükleme kuvvetini şiddetlendirebilir. Sel kaynaklı oyulmanın geçmiş köprü yıkımlarının başlıca sebeplerinden biri olmasına rağmen, halen bu konuya yönelik risk değerlendirme metodolojilerinde bir eksiklik bulunmaktadır.

Bu tez çalışmasının amacı nehir geçen karayolu köprülerinin sel tarafından tetiklenen yükler ve oyulma altındaki hasar görebilirliğini değerlendirmek üzere kırılganlık eğrileri üretmektir. Bu amaçla ilk önce sel etkileri altında köprü tepkisine etki eden en kritik modelleme parametrelerini saptamak üzere bir duyarlılık analizi gerçekleştirilmiştir. Sonrasında simülasyon temelli probabilistik bir çerçeve çalışma geliştirilerek moloz birikiminin olduğu ve olmadığı durumlar altındaki sel kırılganlık eğrileri üretilmiştir. Bu çalışmada uygulanan yöntem kapsamında, bir köprü ayağının sonlu elemanlar modelleri oluşturulmuş ve köprü yapısal tepkisini elde etmek üzere sel tarafından tetiklenen yükleme ve oyulma altında doğrusal olmayan analizler gerçekleştirilmiştir. Çalışma sonunda moloz birikiminin mevcut olmasının köprülerin sellere karşı kırılganlığını önemli bir seviyede arttırdığı bulunmuştur. Bu çalışmada üretilen kırılganlık eğrilerinin ileride karayolu köprülerin sel tehlikesi altındaki risk değerlendirmesi çalışmalarında kullanılabileceği düşünülmektedir.

ACKNOWLEDGMENTS

I would first like to thank my father, Nurettin Kanpara, whom I have started to study after say that ‘Good morning, I will work hard for us’ to his handsome picture every single day. Without his endless support when both with me and from heaven, I could not reach writing this lovely page.

I am so happy that express my gratitude to my husband, Cihan Civan Cıvaş, who never quits supporting me in every condition and time since our undergraduate periods although he studies a separate area from engineering.

I would like to thank my supervisor, Dr. Taner Yılmaz for his valuable guidance and support. Also, I am so grateful for the financial support provided by The Scientific and Technological Research Council of Turkey (TÜBİTAK) within the project number 118M618 titled as “Lifetime Risk and Resilience of Highway Bridges under Multi-Hazards” during my thesis studies.

I would like to thank my big happy family; they have supported me a lot without even awareness. I am so lucky person because I have my mother, like Semahat Kanpara, my elder sisters Hatice Kanpara Elçi and Ayşe Kanpara Cömert, my too naughty nephew Barış Cömert, my game addicted nephew Eymen Alp Cömert and my little lovely niece Ahla Elçi.

I would like to thank my best friend at Özyeğin University, Yasmin Moaiyedfar, whom I have studied for every course and prepared every homework with her. Besides her technical advice, her continuous support after my father's loss is unforgettable for me. Coffee break with her was one of the most entertaining motivations during my thesis study.

I would also like to thank my office mates who are Mesut Adalı, Shaghayegh, Efecan Kor, Osman Oğuzcan, Cem Demirci, Buğra Ceyhan, Levent Coşar, Wasim Nawaz, Onur Cem Aygın, and Hasan Ölmez. We all have tried to manage our affairs well, but we also have not forgotten to support and consult each other within the two years.

TABLE OF CONTENTS

LIST OF TABLES

LIST OF FIGURES

CHAPTER I

INTRODUCTION

1.1 Background and Motivation

Bridges are the critical components of highway transportation networks that have essential roles in national economies. Any disruption in the highway networks due to the damage or collapse of bridges can fail the transportation of goods and people. The importance of highway networks and bridges is more evident in the time of natural hazards (e.g. earthquakes, floods, landslides) as the need for transporting aids is more vital during those conditions. Therefore, to prevent such undesired socio-economic consequences, bridges are required to sustain service under hazards (natural or man-made) by bridge owners. For this reason, the design of bridges should consider the possible effects of multiple hazards instead of focusing on a single hazard effect. For example, bridge design criteria under earthquake hazards are very well presented in widely used codes and manuals such as AASHTO LRFD 2014 [1] or Caltrans Seismic Design Criteria [2]. However, the design procedures against the flood-induced loads and scour are not addressed in the bridge design codes adequately and considered by practicing engineers, although flooding and scour are reported to be the most common reasons for bridge collapses [3], [4].

The studies examining the past bridge failures stated that the major cause for the collapsed or heavily damaged bridges is the hydraulic effect during flood events [3]–[8]. Within the 1989-2000 period in the United States, 503 bridge failures caused tremendous losses to the country according to Shirole and Holt [8], more than 1,000 of the 600,000 bridges in the U.S. were damaged since 1950. %60 of the 823 bridges collapsed in the U.S. between 1950 and 1990 is due to the hydraulic effects. This ratio for the bridge collapses between 1966 and 2005 was around 58% [9]. Figure 1.1 shows the distribution of the causes of bridge failures in the U.S. between 1989 and 2000 [3]. In 1987, Schoharie Creek Bridge collapsed as a result of scour around piers during a heavy flood event, and ten people were killed due to the collapse of the bridge. This disaster became a milestone for the start of the researches on the scour effects for bridges. The impact of scour induced by flood events can vary in different ways. For instance, the collapse of the Route 66 Bridge over Piney Creek during a 50-year flood in 1996 was caused by the combined effect of local and contraction scour around bridge abutments. On the other hand, in 1973 the Route 51 Bridge over the South Fork Forked Deer River had been damaged because of local scour around the pier, rapid channel degradation, and widening following channel straightening.

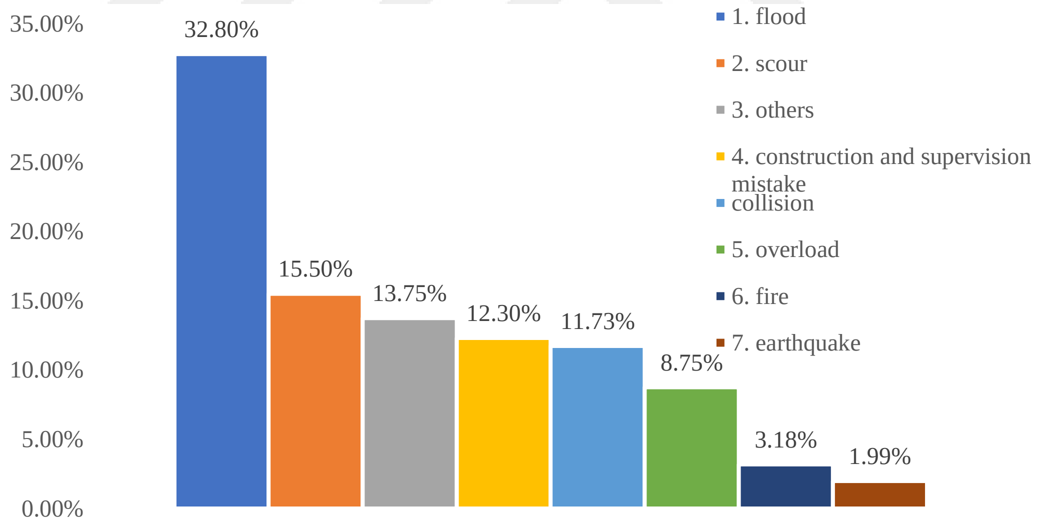

Figure 1.1: The distribution of the causes of bridge failures in the U.S. between 1989 and 2000 [3].

On the other hand, in Turkey, there are a total of 8030 bridges and 85% of them are river bridges [5]. There occurred several incidents in Turkey in the past resulting in the damage or collapse of bridges during flood events. Some examples of the bridges damaged or collapsed in those incidents occurred between 2011-2018 are Cüridere, Efirli and Cevizdere Bridges in Ordu (Figure 1.2), Yarpuz 1 Bridge in Osmaniye, Güzelceçay 2 Bridge and Abdest Bridge in Sinop, Kadıköy Bridge in Mersin, Çaycuma Bridge in Zonguldak (Figure 1.3), Karşıyaka Bridge in Samsun, Yayakent Bridge in İzmir. The most devastating bridge failure among these incidents is the collapse of the Çaycuma Bridge since 15 people lost their lives in this disaster as well as the great economic loss due to the disruption of traffic over the Çaycuma River. The cause of this collapse is associated with the loss of the resistance at the foundation level with the scouring around the piers [10]. Moreover, this failure did not occur during the flood event but triggered by the accumulated effect of local scour at the pier foundation in the previous flood events. The failures of the bridges in the past due to the effects of flood-induced loads and scour show the importance of the risk assessment of bridges subjected to these effects as it can be very critical for taking the necessary precautions such as inspection and maintenance planning [11].

Figure 1.2: Failure of Cevizdere Bridge in Ordu due to flood event

Figure 1.3: Failure of Çaycuma Bridge in Zonguldak due to scour

Yanmaz [7] listed several hydraulic effects that can instigate bridge failures including the local scouring around bridge piers and debris accumulation on the opening between piers. During a flood event, the increased velocity of the water flow exerts a hydrodynamic pressure on the bridge piers in water. Floodwaters can sometimes carry debris in front of the piers and the horizontal pushing force acting on the pier can be amplified considerably as a result of the enlarged surface area of the water pressure. In addition to the hydrodynamic loading, the increased velocities in a flood condition can induce local scour at the pier foundations and this can result in a decrease in the lateral resistance of the piers. Thus, the bridge can become more susceptible to structural or geotechnical damage or even instability with the combined effect of the hydrodynamic loading and local scour at the foundation.

Risk assessment of bridges is crucial for avoiding the damage and even collapse of bridges during possible natural hazards. It also allows for better maintenance planning that can lead to an enhanced lifetime performance of bridges. The assessment of bridge risk against earthquake hazards has been intensively investigated by many researchers in the last two decades. The effect of multiple hazards (multi-hazards) has also gained attention in the research society in recent years. The combined effect of flood-induced scour and earthquake can be given as an example for such a multi-hazard effect on bridges. In probabilistic risk assessment of structures, fragility curves are utilized as the fundamental tools which have been derived in many research studies for seismic and multi-hazard risk assessment of bridges. However, such structural risk assessment methodologies have not been adequately studied under the single-hazard of floods. Thus, in order to address the lack of knowledge on this issue, this thesis aims to develop a methodology to evaluate the vulnerability of river-crossing highway bridges subjected to flood-induced loads and scour through “flood fragility curves”.

1.2 Objectives

The objectives of this thesis can be listed as:

1. To develop a probabilistic framework to obtain fragility curves for river-crossing highway bridges subjected to flood-induced loads and scour at pier foundations,
2. To evaluate the performance of bridges subjected to floods for the presence and absence of debris accumulation at bridge piers,
3. To determine the most significant uncertain parameters to which bridge response against flood effects is the most sensitive.

1.3 Organization of the Thesis

This thesis is composed of five chapters with the following contents:

Chapter 2 presents a literature review about the studies on performance assessment of bridges under multiple hazards, uncertainties affecting the response of bridges, and estimation of scour depth and drag force on piers.

Chapter 3 constitutes the procedure and outcomes of the sensitivity study performed to identify the key uncertain parameters affecting bridge response under floods. The considered uncertainties related to soil, scour depth estimation, and bridge modeling are presented in this chapter followed by the Tornado diagrams plotted as the tool employed for the sensitivity analysis.

Chapter 4 includes all aspects of the probabilistic framework proposed for the development of the fragility curves of bridges subjected to flood-induced loads and scour. Firstly, the study bridge features, finite element modeling and analysis method, the considered flood-induced loads and scour effects on the bridge bent model are introduced. Then, the results of the applied simulations are given in terms of the proposed

Probabilistic Flood Demand Model and the produced flood fragility curves are displayed for the presence and absence of debris accumulation at bridge piers.

Chapter 5 presents a summary of the thesis and the most significant outcomes obtained in this study. The recommendations for future studies are also discussed at the end of this chapter.

CHAPTER II

LITERATURE REVIEW

2.1 Previous Studies on the Performance Assessment of Bridges Subjected to Multiple Hazards

Performance evaluation of bridges under a hazard is a significant procedure for mitigating the risks that include possible life and monetary losses. With the progression of performance-based earthquake engineering, fragility curves that represent the performance of bridges for different damage levels under various levels of earthquake ground motions have started to replace deterministic assessment procedures based on a specific region. Seismic fragility curve is the conditional probability statement that shows the possibility of a structure to sustain or surpass a predefined level of damage for a given intensity measure of the seismic excitation [12]. Over the last two decades, various researchers have suggested and implemented different fragility curve methods and approaches, such as expert-based, empirical, analytical, and hybrid methods [13].

Basöz and Kiremidjian [14], and Shinozuka et al. [15] developed empirical seismic fragility curves by utilizing the actual damage data obtained from the 1989 Loma Prieta, 1994 Northridge, and 1995 Kobe earthquakes. On the other hand, the damage data collected after earthquakes can sometimes be lacking, thus some other researchers [12], [16]–[21] developed analytical seismic fragility curves by simulating the damage data through the analysis of the computer models of the structures. Avşar et al. [13] generated seismic fragility curves for typical highway bridges in Turkey using analytical methods. In developing both types of fragility curves, different probabilistic statistical approaches such as “logistic regression analysis”, “maximum likelihood method” and “Bayesian” approaches were implemented.

The seismic fragility of bridges has the potential to increase by some internal or external effects. For example, Zhong et al. [22], Choine et al. [23], and Ghosh and Sood [24] studied the corrosion effect on seismic fragility curves. On the other hand, the seismic fragility assessment of bridges subjected to flood-induced scour was investigated in some studies. In these studies, bridges can be considered to be under the effect of the multi-hazard condition of earthquakes and floods [25]–[30]. Although seismic (and multi-hazard as indicated above) vulnerability assessment of bridges gained great attention in a large number of studies in the past, similar studies were not sufficiently conducted for the flood condition alone.

As mentioned above, the most common causes of bridge collapses are reported to have hydraulic nature, especially originating from scour and other effects of floods [31], and these effects can be exacerbated by climate change [32]. Despite the negative impacts of floods that can instigate bridge failures, vulnerability assessment of bridges against floods has not been adequately investigated. Only a few studies on the development of flood fragility curves of bridges were published in the last five years. Lee et al. [33] presented a reliability analysis (first-order reliability method) utilizing the outputs from finite element analysis for developing flood fragility curves of bridges. In their methodology, structural deterioration and debris accumulation were considered as the flood-related risk factors that can cause structural damage and flow-induced hydrodynamic loads were applied for a real bridge as the study case. However, in their study scour was not taken into account as a flood-induced risk factor, although a large percentage of bridge failures can be associated with the occurrence of scouring. On the other side, Kim et al. [34] considered scouring at bridge foundations as a flood-induced risk factor for bridges in addition to the increased water pressure due to the accumulation of debris around piers and structural deterioration caused by corrosion of steel reinforcement. They developed flood fragility curves for the performance limits of minor, major, and collapse damage states for a real bridge in Korea, which is Wangsukcheon Bridge collapsed in 2001 due to the excessive scour around its piers.

Turner [35] investigated the vulnerability of eight bridges in Colorado subjected to flood hazards by deriving the fragility curves of the composite girders of these bridges. In his study, he focused on determining the failure risk of the inundated superstructures when subjected to flood forces and considered the inundation ratio as the intensity measure for representing the flood hazard level. Kalendher [36] carried out a fragility analysis to determine the variability in the failure probability of bridges for the flood loading and structural capacity. To develop the fragility curves, a procedure, which is applicable for all types of bridges, was established for a concrete girder bridge. In this procedure, he considered the bridge to be subjected to the hydraulic loading and impact of log and debris induced by a flood event. The other factors that can influence the bridge's structural integrity such as scouring or deterioration were disregarded in the procedure. Kalendher [36] focused only on the bridge superstructures in his study because after the 2011 and 2013 floods in Locker Valley Region in Queensland, the results of the performance analyses of the bridges revealed that the bridge decks were the most damaged components. The predicted bridge failure probabilities under flood hazards were aimed to be considered by the highway authorities to strengthen the bridges in case of a flood hazard.

Qeshta [37] derived wide-ranging methods for the fragility and resilience assessment of the bridges under extreme wave hazards. He aimed to investigate the effectiveness of carbon fiber jackets to help the decision-making process for the retrofit of bridge piers against flood hazards. In developing the fragility curves of the bridges under flood hazard, he considered four different intensity measures, namely flow velocity, inundation depth, momentum flux, and moment of momentum flux. Also, the fragility curves were generated for both the initial and strengthened bridge models and the drift of the piers was taken as the engineering demand parameter to relate the bridge response with damage.

2.2 Previous Studies on Consideration of Uncertainties Affecting the Response of Highway Bridges under Multiple Hazards

Flood performance assessment of river-crossing highway bridges subject to flood-induced scour is vital for improving the design procedures and decreasing the risk of failure. Reliable performance assessment of a structure is strongly dependent on a meticulous analysis of the structural response. Bridge response under an extreme event such as floods or earthquakes obtained from the nonlinear structural analysis can noticeably vary due to the existence of various sources of uncertainties. There are mainly two classes of uncertainties, aleatoric and epistemic. Aleatoric uncertainties are originated from the inherent randomness in the components of a system such as construction material properties, soil properties, flow velocity of a flood, intensity of an earthquake ground motion, etc. Epistemic uncertainties are introduced due to the lacking knowledge within the methodology used in the system. Model error, sampling error, lack of objectivity in limit state definitions, lack of knowledge on as-built conditions can be considered as the sources of epistemic uncertainty in analytical fragility analysis [38]. Wen et al. [39] mentioned that the lack of knowledge of the directionality of strong motion, selection of ground motion suites, and assumptions made by the analyst are the additional sources of uncertainties. The present study considers the uncertain parameters associated with the modeling parameters including construction material properties and soil properties and the uncertain parameters associated with scour depth estimation.

In most of the past researches, uncertainty assessments were either investigated primarily or considered as a part of the methodologies. Some of the researchers [12], [21], [38], [40], [41] studied the seismic performance of bridges considering uncertain variables.

Padgett and DesRoches [21] evaluated the relative importance of various uncertain parameters on the seismic response of retrofitted bridges. They found that the fragility curves of retrofitted bridges are more sensitive to the uncertainty in base geometry (i.e. span length, column height, deck width) than the ground motion and modeling parameter uncertainties. Mackie and Nielson [38] attempted to show the relative contributions of aleatory and epistemic uncertainty sources on the seismic fragility curves of bridges. They considered the randomness in the ground motion suite and several modeling parameters including steel strength, concrete strength, steel mass density, concrete mass density, steel ultimate strain, concrete spalling strain, concrete ultimate strain, and damping ratio. Ma et al. [40] investigated the importance of various uncertain parameters by carrying out seismic analysis of a regular continuous highway bridge and constituted probabilistic seismic demand models of the bridge in near-fault and far-fault earthquake zones. In their study, seven different random variables were considered throughout the probabilistic seismic analysis, but three of them, which are damping ratio, pier diameter, and concrete strength, were found as the most important among others.

Some other researchers [6], [30], [42]–[45] studied the seismic performance of bridges under scour effects by incorporating uncertainties. For instance, Ghosn and Johnson [45] determined the reliability of bridge piers under the coupled effect of scour and earthquakes by using a modified Ferry-Borges algorithm. In that study, maximum yearly discharge, Manning roughness coefficient, modeling variable, and bed material condition factor (K_3) were adopted from the study of Johnson and Dock [46].

Banerjee and Prasad [42] estimated the performance of two examples of reinforced concrete bridges in California by employing time-history analyses under earthquake ground motions representing regional seismicity and scour resulting from various regional flood events. They concluded that the bridges under flood induced-scour effect tend to be more susceptible to damage under earthquakes such that the combined effect of scouring and a moderate level of earthquake intensity may lead to the same damage level that could result from the single hazard of a strong ground motion. In the same study, for the objective of evaluating the uncertainties in the flood hazard model, a sensitivity analysis was conducted to identify the major parameters in the scour depth estimation equation. However, the uncertainties in the peak discharge for a flood event and the other parameters involved in the scour depth estimation equation were not taken into consideration in the seismic performance evaluation since the variation in scour depths was found to produce insignificant variation in the bridge seismic response. A similar sensitivity analysis for scour depth estimation parameters was also performed by Yilmaz et al. [30] and deterministic (mean) values of scour depths obtained from the average peak discharge value (with 50% confidence level) for various levels of flood events were taken for generating the fragility and risk curves of highway bridges under the multi-hazard of earthquake and flood-induced scour. On the other hand, a separate sensitivity analysis was carried out to determine the key modeling parameters that are the most effective on the bridge seismic response, and then a rigorous uncertainty analysis was performed to generate the multi-hazard fragility and risk curves where the uncertainties were quantified through 90% confidence intervals.

Alipour et al. [43] developed scour load-modification factors that can be used for the seismic design of bridges subjected to scour. For this purpose, the joint probability of failure for earthquake and scour hazards were computed and compared with the target reliability index given by design codes. To address the uncertainties present in estimating the recurrence and severity of the earthquake and scour hazards, seismic hazard curves were employed, and scour risk curves were generated. However, the randomness in bridge properties was not considered in the bridge models for deriving the seismic fragility curves. Scour risk curves showing the probability of exceeding a given scour depth were generated by accounting for the uncertainties in the parameters used in the scour depth estimation equation along with a scour modeling factor. For the objective of reaching load combinations under the same multi-hazard, Wang et al. [44] suggested a risk-based design approach that combines earthquake and scours hazards. They recommended a scour load factor of 0.59 to be multiplied with scour depth estimated from the design flood event (100-year return period) and this scour depth should be considered in the analysis under the design earthquake loading. In this study, they produced the scour hazard curve by conducting a Monte Carlo simulation that incorporates the uncertain parameters within the scour depth equation such as scour modeling factor (or also called bias), the correction factor for the flow angle of attack (K_2), the correction factor for stream bed condition (K_3), and Manning roughness coefficient (n), and channel slope (S).

In the meantime, the hydraulic uncertainties affecting the estimation of scour depth around bridge piers have drawn the attention of many researchers [47]–[55]. For example, Tung [52] performed a study to evaluate the effect of uncertainty in hydraulic design and analysis. He assumed all the uncertain parameters included in his study as triangularly distributed and accepted the coefficient of variation (COV) values as 0.10, 0.12, and 0.04 for the Manning roughness coefficient, channel slope, and discharge, respectively. Johnson [48] presented a method that provides a bridge design approach considering various uncertainties in scour. She obtained bridge safety factors by conducting a Monte Carlo simulation to compute the probability of failure due to the nonlinear characteristic of the failure function. In that study, the Colorado State University (CSU) equation (HEC-18 [56] equation), which was generally preferred for estimation of pier scour depth, was modified to capture the probability of failure due to scouring. The flow depth related to the stream of interest was assumed to be normally distributed with a COV value of 0.2. The other important parameter was sediment gradation, which was shown to be influencing scour depths especially at lower Froude numbers according to the available experimental data from the University of Auckland [50], [57]. Sediment gradation was taken as lognormally distributed with a COV value of 0.2. Johnson and Ayyub [58] presented recommendations for decision-makers and designers on the management of scouring at existing piers and pier constructions to prevent pier scour failure. They established a new technique for calculating the likelihood of failure of a bridge pier under time-varying scour progression. For this purpose, they assumed that the particle size is uniformly distributed with a COV value of 0.05, the angle of flow to the pier has a normal distribution with COV value of 0.2, and sediment gradation follows a lognormal distribution with a COV value of 0.1.

Johnson and Dock [46] suggested a probabilistic scour estimation methodology by incorporating uncertain parameters to the deterministic HEC-18 equation and applying it on a real-life bridge, the Bonner Bridge in North Carolina. This probabilistic framework takes into account the model, hydraulic, and parameter uncertainties. The model in laboratory conditions may not represent the complexities in the field, so the model correction factor or bias was suggested to be included in the scour prediction equation. The other class of uncertainty is hydraulic, which is related to the flow depth and flow velocity at a specific site. The parameter uncertainty is caused by an inability to measure parameters correctly. Correction factors in the HEC-18 equation and the pier width defined the parameter uncertainty in their study. Johnson [53] quantified uncertainties in many hydraulic parameters regarding the probability distributions and their coefficients of variation. In her study, the Manning roughness coefficient (*n*) of a stream (Paint Branch stream) was determined to have uniform distribution and the average *n* value at the channel bottom was obtained as 0.037 and 0.034 with COV values of 0.284 and 0.175 for the upstream and downstream, respectively. Similarly, the U.S. Army Corps of Engineers led a parallel study to capture the Manning coefficient for ten stream sections. They determined that the Manning roughness coefficient has lognormal distribution with the average value varying from 0.02 to 0.062 and COV ranging between 0.20-0.35.

Johnson et al. [54] assessed the model uncertainty in the HEC-18 equation [56] and in the FDOT equation [59] and the parameter uncertainties, particularly about the channel flow regime. They addressed the parameter uncertainties in four different aspects, which are discharge, energy slope, channel Manning coefficient, and floodplain Manning coefficient. The model uncertainty shows how well the scour prediction equation estimates the actual scour depth, so the model uncertainty is also referred to as bias. The bias is the ratio of the observed scour depth from available laboratory data to the estimated scour depth calculated from the empirical equations. They suggested the modeling bias values and their coefficient of variation values for two different scour prediction equations at the corresponding target reliability indices. Also, a procedure for the reliability assessment of protected and unprotected bridge piers subjected to time development of scouring is recommended. They used Monte Carlo Simulation technique and Fault Tree Analysis to forecast the probability of bridge failure. They assumed that the mean flow velocity is normally distributed with a COV value of 0.329, and flow intensity, which is expressed as the ratio of upstream shear stress to sediment critical shear stress, follows normal distribution with a COV value of 0.2. Pier width and pier foundation depth were also taken as random variables in this study and were assumed to follow normal distribution with COV values of 0.05 and 0.1, respectively. The properties of flow depth were adopted from Johnson [48], and the median values were also adopted from Johnson and Ayyub [58]. Furthermore, they presented that scour depth has a normal distribution with a COV of 0.05.

Yanmaz [55] performed a study to figure out the appropriate probability distribution functions (PDF) for scouring uncertainties to be applied on cylindrical and non-cylindrical pier shapes. According to this study, the relative approach flow depth could be represented with the log-Pearson Type-3 distribution for cylindrical piers. Also, 2-parameter lognormal (LN2), 3-parameter lognormal (LN3), log-Pearson Type-3 (LPT3), Pearson Type-3 (PT3) and normal distributions could all be fitted to the live bed relative scour depth, while all these distributions excluding normal distribution could be suitable for the Froude number. For the other type of pier shape; LN2, LN3, PT3, and LPT3 could be fitted to the relative approach flow depth, all considered PDFs could be used for relative scour depth, and no PDF was recommended for the Froude number.

Johnson [60] utilized fault tree analysis to reach the probability of failure of bridges considering different combinations of scouring and channel instabilities. She studied three different real-life example bridges exposed to scouring, and site-specific distribution parameter values and COV values for considered for random variables. She concluded that the estimation of the COV for all uncertain parameters may play a more critical role than the choice of distribution type. Yanmaz and Üstün [61] studied the reliability of uniform piers with different shapes under the local scour effect. They assumed that resistance and loading are lognormally distributed as adopted in many previous studies and demonstrated that it is a reasonable assumption based on the results of the Chi-square and Kolmogorov-Smirnov tests. The mean and standard deviation values were determined from the method of maximum likelihood for cylindrical and non-cylindrical types of piers separately. Yanmaz and Çalamak [62] developed a reliability model to evaluate the risk of live-bed scour around bridge foundations by using Monte Carlo simulation technique. They incorporated the uncertainties in the hydraulic parameters and bed material properties affecting the scour around a pier. The approach flow depth and velocity, and the median size (D_{50}) of bed material were considered as random variables and their statistical distributions were adopted from various past studies [53], [55], [60], [63]–[65]. Khalid et al. [66] performed a sensitivity analysis to show the effect of several uncertain parameters on the reliability of pier foundations. The sensitivity analysis showed that scour depth is exacerbated by the increasing values of flow depth and flow velocity, which were described as load variables. On the other hand, scour depth was reduced with the increasing values of mean sediment size and foundation depth, which were called resistance parameters that contribute to the safety of the bridge. They also performed a parametric study to estimate the impact of different random variables on the reliability of piers.

2.3 Previous Studies on Scour Depth Estimation

Scour depth estimation is an essential task for the hydraulic design and assessment of bridges, since the occurrence of scour and its depth can affect the behaviour of bridges and also scour depth can be affected by many factors. For this reason, many researchers have focused on investigating better estimations of scour depth.

Scour is the removal of bed material surrounding piers and abutments as a result of the action of flowing water. A wide range of factors such as depth of water, angle of attack of the flow, flow velocity, shape of the pier, properties of river bed material influence the extent of scour around piers. The total scour depth is estimated by the sum of three primary scour types, which are long-term degradation, contraction scour and local scour as detailed below [56].

1. Local Scour: It is defined as the removal of river bed material from around the base of piers or abutments resulting from the rapid water flow and horseshoe vortices caused by obstructions to the river flow by piers or abutments. A schematic representation of local scour occurring at a pier is presented in Figure 2.1.

2. Contraction Scour: This type of scour is described as the removal of sediment from the bottom and side of the river bed induced by the narrowing of the river channel cross-section.

3. Long-term degradation: It is the lowering of the bottom of a stream caused by natural or man-induced reasons which are resulting from the modifications to the stream. It is generally a natural process and the trend for the long-term degradation may show different characteristics throughout the bridge service life. A large amount of sediment removal should be avoided because it may lead to channel instability problems [56].

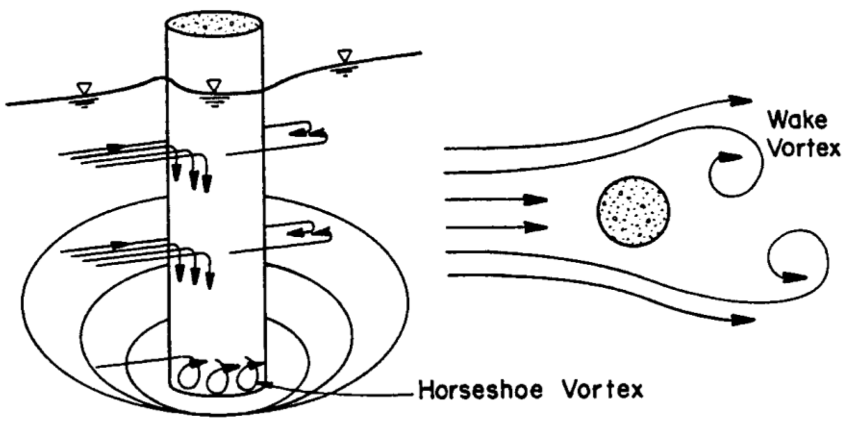

Figure 2.1: Schematic representation of local scour at a pier [56]

For contraction and local scour, the condition of whether clear-water scour and live-bed scour occurs should be evaluated. If river bed material is transported from the upstream of the bridge to the downstream, this condition is live-bed scouring, but if there is no substance carried with the flow, this is called clear-water scour. Base material properties affect the scouring. For example, loose and granular river beds are eroded rapidly by water flow than cohesive and dense river beds. However, the scour at cohesive and dense bed materials can be deeper than those with sandy soil. The evaluation of pier scour depth in time for clear-water and live-bed conditions is presented in Figure 2.2.

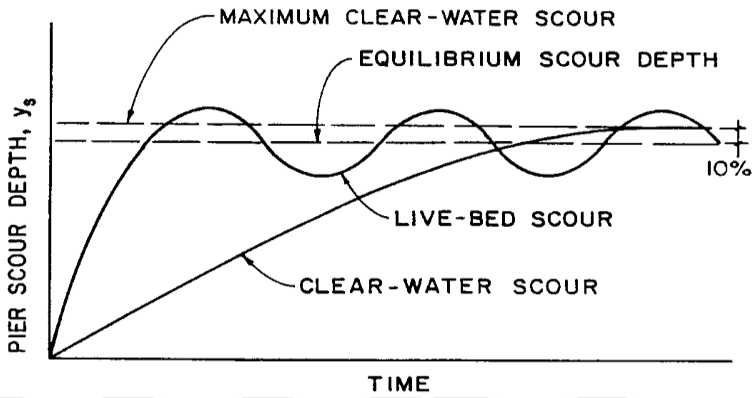

Figure 2.2: The change in pier scour depth with respect to time in sandy bed material. [56]

The practice of scour prediction is generally handled by calculating the scour depths through empirical equations, but sometimes other methods such as neutral network procedures can be used to estimate the scour depths [67]. Researchers have performed several studies on this issue and developed different scour prediction equations. The parameters considered in empirical equations may be different from each other as these models are usually constructed based on the findings from the laboratory or field data. Therefore, this can lead to inconsistencies in the scour depths estimated by using different equations. Also, more importantly, the resulting scour depths obtained from these equations and the actual scour depths measured at a site may not well-suit. The reason for this variance can be attributed to the process of developing a model for scour depth estimation based on laboratory studies. Despite the error margins included in the scour depth estimation equations, the *Colorado State University equation,* which is the most commonly used method for scour depth estimation among others, is suggested in the U.S. Department of Transportation's Hydraulic Engineering Circular No. 18 (HEC-18) [56] for both live-bed and clear-water cases. This equation is given in Equation 2.1 below. The parameters existing in this equation are schematically displayed in Figure 2.3.

$$\frac{y_s}{y_1} = 2.0 \quad K_1 \; K_2 \, K_3 \; \left(\frac{a}{y_1}\right)^{0.65} {Fr_1}^{0.43} \qquad (2.1)$$

where;

y_s: Scour depth around piers,

y_1: Flow depth at the pier,

K_1: Correction factor for the pier nose shape,

K_2: Correction factor for the angle of flow attack,

K_3: Correction factor for the river bed condition

a: pier width

Fr_1: Froude number directly upstream of the pier

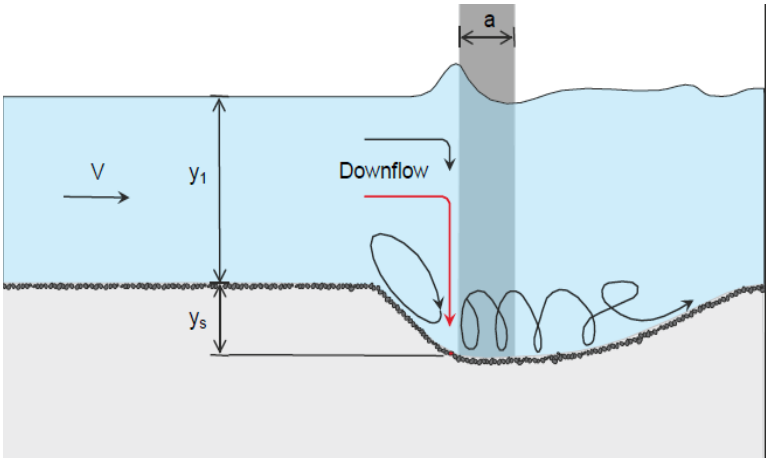

Figure 2.3: The pier scour and the associated parameters [56].

HEC-18 suggests a limitation for the scour depth calculated from Equation 2.1. The scour depth (y_s) should not exceed 2.4 times the pier width when the Froude number is lower than 0.8, and it should not exceed 3.0 times the pier width when the Froude number is greater than 0.8. Apart from the widely used HEC-18 equation for scour depth prediction, the remaining part of this subsection presents the scour depth prediction equations proposed in various other researches. The readers are referred to the original references for the detailed explanation of the below mentioned models.

The scour depth prediction developed by Laursen and Toch [68] was presented by Neil [69] as follows:

$$y_s = 1.35a^{0.7}y_1^{0.3} \tag{2.2}$$

Shen et al. [70] suggested the following scour depth prediction equation:

$$y_s = 0.00022\left(\frac{V * a}{\nu}\right)^{0.3} \tag{2.3}$$

where;

V: Average velocity of the approach flow,

$\nu = 1\text{x}10^{-6}\ \text{m}^2/\text{s}$

Breusers et al. [71] developed the below equation for the prediction of scour depth.

$$y_s = a\ f\ K_1\ K_2\ \left[2\tanh\left(\frac{y}{a}\right)\right] \tag{2.4}$$

where; $f = 0$ for $\nu/\nu_c \geq 0.5$, $f = 1$ for $\nu/\nu_c > 1$,and $f = (2\nu)/\nu_c - 1$ for $0.5 < \nu/\nu_c \leq 1$.

Jain and Fischer [72] recommended the below equations to estimate scour depth.

$$y_s = 2.0a(F - F_c)^{0.25}\left(\frac{y_1}{a}\right)^{0.5}\ (F - F_C) > 0.2 \tag{2.5}$$

$$y_s = 1.85a(F_c)^{0.25}\left(\frac{y_1}{a}\right)^{0.5}\ 0 < (F - F_C) \tag{2.6}$$

where; F_c is the critical Froude number and it can be calculated with the equation $\frac{V_c}{(gy_1)^{0.5}}$ for the condition of $0 < (F\text{-}F_c) < 0.2$. The greater value resulted from the Equations 2.5 and 2.6 should be considered as the estimated scour depth.

Hancu's [73] equation to estimate the scour depth is given below:

$$y_s\ = 2.42\ a\left[2\left(\frac{V}{V_c}\right) - 1\right]\left[\frac{V\ c^2}{ga}\right]\quad for\ 0.05\ \leq \frac{V_c^2}{ga} \leq 0.6 \tag{2.7}$$

where;

$$V_c = 1.2\sqrt{gD_{50}[(p_{s-}p)/p]}\ \left(\frac{y_1}{D_{50}}\right)^{0.2} \tag{2.8}$$

V: Flow velocity

V_c: Critical velocity

$(2\ \frac{V}{V_c} - 1)$ is equal to 1.0 for the condition of clear-water scour. Meanwhile, the above Equation 2.7 is not applicable for $\frac{V}{V_c} \leq 0.5$.

Froehlich [74] developed the following equation that can be used for scour depth estimation:

$$ys = 0.32\ a\ \phi\ F_{r_1}^{0.2} \left(\frac{b_e}{a}\right)^{0.62} \left(\frac{y_1}{a}\right)^{0.46} \left(\frac{a}{D_{50}}\right)^{0.082} \tag{2.9}$$

where; ϕ is the coefficient related to the pier nose shape, b_e is the width of the bridge pier projected normal to the approach flow; D_{50} is the median grain size of bed material.

Melville and Sutherland [75] suggested the below equation that is composed of several correction factors:

$$y_s = k_l\ k_d\ k_y\ k_a\ k_S\ a \tag{2.10}$$

where;

k_l: Flow intensity factor,

k_d: Sediment size factor,

k_y: Flow depth factor,

k_a: Pier alignment factor,

k_s: Pier shape factor.

The abovementioned scour depth estimation equations have been compared to each other by some researchers. For example, Jones [76] compared several scour depth estimation equations by using the limited field data and laboratory data. He broke down into three different classes that are namely, the University of Iowa, Colorado State University (CSU) and others based on foreign literature. He found that the CSU equation shows the best fitting performance with respect to the field data. Johnson [47] also compared the most commonly-used seven different equations, and she concluded that some of them yielded serious overestimations. Landers and Mueller [77] found that none of the equations they examined could predict the depth of scour for all conditions accurately in both live-bed and clear-water.

2.4 *Estimation of Drag Force on the Piers*

Bridge design codes or technical reports provide various methods to calculate hydrodynamic loads on bridge piers due to flowing water. Some of the researchers have used these equations to calculate the loads in their studies for the performance assessment of bridges against flood hazards. For instance, Kim et al. [34] and Lee et al. [33] followed the SI-unit version of the equations of AASHTO [78] and KHBDS [79] to apply the water pressure as an external load to the bridge piers for generating flood fragility curves of their investigated bridges. Kalendher et al. [80] employed the AS5100.2 code provision [81] to apply the force caused by a flood event and produced fragility curves for reinforced concrete girder bridges under flood hazard accompanied with debris impact force. Lokuge et al. [82] utilized the Australian Standards [83] and [81] for calculation of flood loads and analysed a real-life bridge to determine the flooding effect on the bridge. Jordan [84] analysed a case study of Tenthill Creek Bridge exposed to flood loads considering various design standards around the world. The below subsections give details on the estimation of drag force of flowing water according to different bridge design standards from around the world.

2.4.1 Australian Bridge Design Standard (AS 5100.2, 2004) [81]

The drag force acting on a pier ($\mathrm{F}^*_{\mathrm{du}}$) can be computed with Equation 2.11 below.

$$\mathrm{F}^*_{\mathrm{du}} = 0.5\, C_d\, V_u^2\, A_d \tag{2.11}$$

where;

C_d: Drag coefficient, which can be obtained from Table 2.1 for different pier shapes.

V_u: Mean velocity of flowing water,

A_d: Projected area of pier exposed to flood load (The bottom level of superstructure or debris level is considered as the ultimate point where the water pressure is exerted on the pier.)

Table 2.1: Drag coefficients per AS 5100.2, 2004 [81]

C_d	**Shape of pier**
Semi-circular pier nosing	0.7
Wedge, sharper than 90°, nosing	0.8
Square end pier nosing	1.4

The debris force acting on a pier can be obtained similar to the drag force by increasing the tributary area subjected to flood as much as the size of debris accumulation which is represented with A_{deb} (the tributary area of debris) in Equation 2.12. The drag coefficient for the condition of debris accumulation can be attained from Figure 2.4 below. The length of debris accumulation shall be considered as the smaller of the sum of the adjacent spans or 20 m. The middle point of debris height should be chosen as the point where the debris force acts on the pier per AS 5100.2, 2004.

$$\mathrm{F}^{*}_{\mathrm{du}} = 0.5\ C_d\ \mathrm{V}_{\mathrm{u}}^{2}\ \mathrm{A}_{\mathrm{deb}} \qquad (2.12)$$

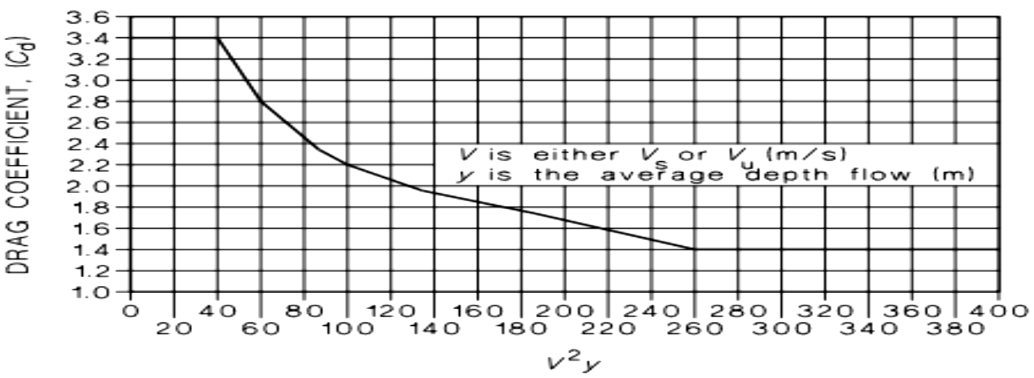

Figure 2.4: The chart of drag coefficients for debris accumulation conditions (adopted from the Australian standard 2004b [81]).

2.4.2 European Bridge Design Standard (Ba 59/94) [85]

The hydrodynamic pressure according to European Bridge Design Criteria [85] can be calculated with Equation 2.13 below for only under the condition where the flow water is acting perpendicular to the piers.

$$P = 0.51\, K\, U^2 \tag{2.13}$$

where; P is the pressure (kN/m^2). The coefficient K in Equation 2.13 depends on the shape of the pier and it has a wider range of values compared to the drag coefficients of the Australian standard presented in Section 2.4.1. The values of K is presented in Table 2.2. The parameter U stands for the velocity of river flow (m/s). It is assumed that the flow velocity varies linearly from zero value at the river bed level, which can change due to scouring, to a maximum value at the water surface.

Table 2.2: The values of *K* per European Bridge Design Standard [85]

Pier type	***K***
Square ended piers	1.5
Circular piers	0.66
Piers with triangular cutwater angle (<30°)	0.5
Piers with triangular cutwater angle (30° to 60°)	0.5 to 0.7
Piers with triangular cutwater angle (60° to 90°)	0.7 to 0.9

The drag force and lift force can be estimated by utilizing Equations 2.14 and 2.15 below per European Bridge Standards for the circumstances where the flow water acts on the pier with an angle.

$$F_D = \frac{C_D \, \rho U_0^2 \, y_0 \, L}{2000} \tag{2.14}$$

$$F_L = \frac{C_L \, \rho U_0^2 \, y_0 \, L}{2000} \tag{2.15}$$

where U_0 represents the flow velocity (m/s), y_0 is the depth of pier, L is the diameter of a single cylindrical pier or length of the pier, and ρ is the density of water. The drag coefficient C_D and the lateral drag coefficient C_L in Equations 2.14 and 2.15 are not provided in the European Bridge Design Standard, but another paper provide these coefficients in a chart form [84].

To account for the extra hydrodynamic loads acting on a pier induced by debris accumulation, the minimum debris height shall be taken as 1.2 m and the length of debris should be considered as half of the sum of two adjacent spans not exceeding the maximum debris length of 21 m. If the size of debris is not considered to reach the above-mentioned size, Equation 2.16 given below can be used to compute the increased pressure due to the accumulation of debris on piers.

$$P = 0.517 \, U_o^2 \tag{2.16}$$

2.4.3 American Bridge Design Standard (AASHTO LRFD, 2014) [1]

The stream pressure acting on bridge piers can have two components, in the longitudinal and in the lateral directions of the substructures. The longitudinal (drag) stream pressure is given in AASHTO LRFD Bridge Design Standard [1] as:

$$P = C_D \, \frac{w}{2g} \, V^2 \tag{2.17}$$

where;

P: Stream pressure (ksf),

C_D : Drag coefficient values, which can be obtained from Table 2.3,

w: Specific weight of water (kcf),

g: Gravitational acceleration (ft/s^2),

V: Water velocity (ft/s),

For calculating the drag force on the piers, the stream pressure as calculated in Equation 2.17 should be multiplied with the surface area of the pier which is exposed to flowing water.

Table 2.3: Drag coefficient per AASHTO LRFD [1]

Type of pier shape	C_D
Semi-circular-nosed pier	0.7
Square-ended pier	1.4
Debris lodged against the pier	1.4
Wedged-nosed pier with nose angle 90 degrees or less	0.8

In the case of accumulation of debris, AASHTO suggests that the draft New Zealand Highway Bridge Design Specification can be considered if site-specific data is lacking. The accumulation shape can be assumed with a triangular geometry in which the amount of accumulation decreases from the water surface (at the same level as the top of debris) to the bottom end of accumulation. The width of debris should be taken as half of the sum of adjacent span lengths or 45 ft, whichever is the smallest. The height of debris should be taken as half of the water depth, but not exceeding 10 ft. When this geometry of debris accumulation is taken into consideration, the drag coefficient in Equation 2.17 should be taken as 0.5.

2.4.4 Indian Code of Practice, 2014 [86]

The intensity of pressure (in kN /m^2) can be calculated with the following equation according to the Indian Code of Practice [86].

$$P = 52\, K\, V^2 \, \frac{9.81}{1000} \tag{2.18}$$

where;

V: Velocity of flow (m/s),

K: Pier shape coefficient, which can be obtained from Table 2.4 for different pier shapes.

The square of flow velocity is assumed to increase linearly from zero at the river bed level to the surface of water. The square root of two times the maximum velocity of the current is equal to the maximum velocity of the water.

Table 2.4: *K* values per Indian Code of Practice [86]

Pier shape	***K***
Squared ended piers (and for the superstructure)	1.5
Circular piers or piers with semi-circular ends	0.66
Piers with triangular cut and ease waters, the angle included between the faces being 30^o or less	0.5
Piers with triangular cut and ease waters, the angle included between the faces being 30^o and 60^o	0.5 to 0.7
Piers with triangular cut and ease waters, the angle included between the faces being 60^o and 90^o	0.7 to 0.9
Piers with cut and ease waters of equilateral arcs of circles	0.45
Piers with arcs of the cut and ease waters increasing at 90^o	0.5

2.4.5 Hydraulic Engineering Circular No: 9 [87]

The study of Parola [88] was taken as a model in HEC-9 [87] for developing the equation of hydrodynamic drag force in the presence of debris accumulation. The definition of debris accumulation geometry is the first step towards finding the hydrodynamic force acting on a bridge. The second step is the computation of flow hydraulics features such as water velocity. Finally, the hydrodynamic loads considering the hydraulic characteristics of the river under the presence of the debris accumulation can be computed with Equation 2.19 below.

$$F_D = C_D \gamma A_D \frac{V_r^2}{2g} \tag{2.19}$$

where;

F_D : Drag force (N, lbs),

C_D : Drag coefficient, which can be obtained from Table 2.5.

γ : Specific weight of water (N/m^3, lbs/ft^3),

A_D : Area of the wetted debris (m^2, ft^2),

V_r : Reference velocity (m/s, ft/s),

g: Gravitational acceleration (m/s^2, 32.3 ft/s^2).

Table 2.5: Drag coefficient for debris on piers per HEC-9 [87]

Value of *B*	**Value of F_r**	C_D
$B < 0.36$	$F_r < 0.4$	1.8
$B < 0.36$	$0.4 < F_r < 0.8$	$2.6 – 2.0\ F_r$
$0.36 < B < 0.77$	$F_r < 1$	$3.1 – 3.6\ B$
$B > 0.77$	$F_r < 1$	$1.4 - 1.4\ B$

To determine the drag coefficient, the blockage ratio B and Froude number F_r are required to be calculated per HEC-9 [87]. The blockage ratio can be calculated from the below equation:

$$B = \frac{A_d}{A_d + A_c} \tag{2.20}$$

where;

A_d: Blocked cross-sectional area by debris (in m^2 or ft^2),

A_c: Cross-sectional area of flow without obstructions (in m^2 or ft^2).

Froude number $F_r(= V_r/\sqrt{g\ y_1})$, which is a unitless parameter, increases with reference velocity proportionally and decreases with the square root of the multiplication of gravity acceleration and average flow depth (at the reference velocity of water).

CHAPTER III

SENSITIVITY ANALYSIS FOR PERFORMANCE ASSESSMENT OF RIVER-CROSSING HIGHWAY BRIDGES UNDER FLOOD HAZARD

3.1 Uncertainties in Performance Assessment of Highway Bridges

3.1.1 Uncertainties Associated with Bridge Modeling

Eight uncertain parameters associated with the bridge modeling are identified and elaborated in the following paragraphs. The accepted probability distributions and the related probability parameters for each of the random variables are presented in Table 3.1.

1. *Unit mass of concrete*

   To account for the variability in the bridge self-weight, Lee et al. [33] considered the unit mass of concrete as a random variable in their reliability analysis procedure. The mean value of concrete mass density was taken as 2300 kg/m^3 and COV value was 0.05, and it follows normal distribution per their study. In the present study, the mean value of concrete unit mass is taken as 2400 kg/m^3 following the Turkish Bridge Design Manual [89] with a COV value of 0.05 by following normal distribution.

2. *Unit mass of wearing surface*

   Dead load is the prominent loading source for highway bridges among live loads, environmental loads and other loads such as collision, emergency braking, etc. Each load type can be classified with some subcomponents and they can be considered through random variables by defining them with respect to available statistical data, investigations or other observations. Cumulative distribution function (CDF), mean value, bias factor (mean to nominal ratio), and coefficient of variation are some of the statistical descriptors to define a random variable. The unit mass of wearing surface, which is a subcomponent of dead load, is taken as a normally distributed random variable with a mean value of 2200 kg/m^3. The COV value for asphalt was taken as 0.25 in Nowak [90] (NCHRP Report No:368), thus this study also adopts a COV value of 0.25 for the unit mass of wearing surface.

3. *Elastic modulus of reinforcing steel*

Elastic modulus of reinforcing steel has been evaluated with different mean values in various studies. For example, the elastic modulus of reinforcing steel in piers is assumed to follow a normal distribution with a mean value of 201 GPa and a COV value of 0.033 per the study of Zhang [91]. Lee et al.[33] considered normal distribution for the elastic modulus of reinforcing steel with the mean value of 190 GPa and COV value of 0.01. This thesis adopts the recommendation of Lee et al. [33].

4. *Compressive strength of concrete*

The concrete material may have abundant sources of uncertainties because so many factors are included in its production and transfer process. For this reason, some assumptions have to be made on the concrete properties. For example, Choi [92] assumed that the compressive strength of concrete follows normal distribution. In this thesis, the expected concrete compressive strength of 32.5 MPa is used for the substructure elements (i.e. columns and pile shafts) following the work of Yilmaz [29]. The coefficient of variation for compressive strength of concrete is assumed as 0.125 as used in the studies [12], [29], [92], [93]. The bridge inventory study performed by Avşar [13] indicated that the bridges in Turkey are mostly constructed with concrete characteristic compressive strength of 25 MPa, which corresponds to an expected value of 32.5 MPa. Therefore, the mean value for the concrete compressive strength adopted for the study bridge in this thesis reflects the general practice applied for the typical bridges in Turkey.

5. *Yield strength of reinforcing steel*

Ellingwood and Hwang [94] found that yield strength of reinforcing steel follows lognormal distribution with a coefficient of variation of 0.08. Moreover, Avşar [13] found that the mean value of the yield strength of reinforcing steel applied for the bridges in Turkey is 475 MPa. By considering the findings of these two studies, the yield strength of reinforcing steel is assumed to be following lognormal distribution with a mean value of 475 MPa and COV of 0.08 in this thesis.

6. *Longitudinal reinforcement ratio*

The ratio between the longitudinal steel area to the cross-sectional area of a column is called longitudinal reinforcement ratio. Ramanathan [12] sampled longitudinal reinforcement ratio assuming a uniform distribution from a minimum value of 1% to a maximum value of 3.5% for the multi-span continuous concrete box-girder class of bridges designed in post-1990 era. Also, in Turkish bridge design practice [89], longitudinal reinforcement ratio is ranging between 1% and 4%. Considering the abovementioned studies, the longitudinal reinforcement ratio is accepted to be following uniform distribution with a minimum value of 1% and a maximum value of 4%.

7. *Internal friction angle and unit weight of soil*

In the present study, the bridge foundation (i.e. piles) is assumed to be sitting in a single layer of medium dense sand. The statistical distributions and the COV values of the modeling parameters associated with the soil properties are adopted from the probabilistic seismic performance study by Zhang [91]. According to Zhang [91], the friction angle of the medium dense silty sand has a normal distribution with a COV value of 0.12 and the saturated unit weight of the soil follows normal distribution as well with a COV value of 0.10. The mean values taken for the friction angle and unit weight of soil are in accordance with the medium dense soil.

Table 3.1: Uncertain parameters related to bridge modeling

Uncertain parameters		**Unit**	**Dist.**	**Dist. Parameters**		**References**
Unit mass of concrete	γ_{conc}	kg/m^3	Normal	μ: 2400	δ: 0.05	[33]
Unit mass of wearing surface	γ_{ws}	kg/m^3	Normal	μ: 2200	δ: 0.25	[90]
Elastic modulus of reinforcing steel	E_s	GPa	Normal	μ: 190	δ: 0.01	[33]
Compressive strength of concrete (substructure elements)	$f_{ce,sub}$	MPa	Normal	μ: 32.5	δ: 0.125	[92]
Yield strength of reinforcing steel	f_{ye}	MPa	Lognormal	λ: 6.16	ζ: 0.08	[94]
Longitudinal reinforcement ratio	ρ_{long}	%	Uniform	Lower: 1.0	Upper: 4.0	[89]
Friction angle of soil	ϕ_{soil}	degree	Normal	μ: 35	δ: 0.12	[91]
Unit weight of soil	γ_{soil}	kN/m^3	Normal	μ: 18.64	δ: 0.1	[91]

3.1.2 Uncertainties Associated with the Scour Depth Estimation

Six uncertain parameters associated with the scour depth estimation are identified and elaborated in the following paragraphs. The accepted probability distributions and the related probability parameters for each of the random variables are presented in Table 3.2.

1. *Flow discharge*

Various probability distribution models such as Extreme Type I, lognormal and log-Pearson distributions have been used for flow discharge by several experts and administrations. In NCHRP Report 489 [6], it was found that discharge follows lognormal distribution based on the lognormal probability paper results. Alipour et al. [43] took the last 50-year peak annual discharge data for two rivers from the USGS website for describing the distribution of flow discharge to be used in their study. In the current thesis study, for the objective of performing the sensitivity analysis, the flow discharge is assumed to follow asymmetrical triangular distribution with a mean value of 3500 m^3/s.

Besides the sensitivity analysis that is presented in Section 3.2, the flow discharge values are increased gradually from 100 m^3/s to 5800 m^3/s with an increment of 10 m^3/s to capture a wide range of discharge values within the simulation-based flood fragility curve generation methodology presented in Section 4.6.

2. *Channel slope*

In the literature, channel slope has been considered differently in terms of its probability distribution and the related distribution parameter values such as [52], [53], [95], [96]. In a study to determine the uncertainty of levee capacity by first-order analysis, Lee and Mays [51] found that channel slope and Manning roughness coefficient are the key parameters affecting the uncertainty. Johnson [48] assumed that channel slope is normally distributed with a COV value of 0.2. However, in a following study by Johnson [53], lognormal distribution with a

COV value of 0.25 was taken into account in a probabilistic framework used for vulnerability analysis. This thesis also adopts lognormal distribution and COV of 0.25 for the channel slope with a mean value of 0.2 %

3. *Manning's roughness coefficient*

Cesare [97] applied first-order reliability methods to integrate the uncertainty in Manning equation for determining discharge. He assumed that the Manning roughness coefficient to be having a normal distribution. Mays and Tung [96] evaluated the uncertainty of discharge resulting from a first-order analysis of the Manning equation assuming that manning roughness is significant parameter because the manning roughness coefficient is not constant, on the contrary it has a large variability because of the curved character of rivers, the bed material and the average grain size of soil, channel bedforms, channel obstructions, changing of geometry between sections, and vegetation in the channel [98]. This situation can bring a significantly high coefficient of variation for the Manning roughness coefficient. NCHRP Report 489 [6] remarks that it may vary between 0.025 to 0.035 according to the river conditions. The Hydraulic Engineering Center [99] advised that lognormal distribution with a COV value between 0.20-0.35 can be used to describe the Manning roughness coefficient. In the present study, lognormal distribution with a mean value of 0.025 and COV of 0.275 is adopted for the Manning roughness coefficient. The considered COV value is taken as the average of the possible range recommended by [6]. Since the present study does not use site-specific data, the accepted values for the probability distribution can be thought of covering a broad range of river roughness within the general framework.

4. *Correction factor for the angle of flow attack, K_2*

   K_2 is a correction factor used in the HEC-18 scour depth estimation equation for incorporating the effects of the flow angle of attack in rivers. Some researchers included K_2 as a random variable in their studies. For example, Johnson and Dock [46], Banerjee, and Prasad [25], Wang et al. [44] assumed that K_2 has a normal distribution with a mean value of 1.0 and COV value of 0.05. However, HEC-18 [56] indicates that K_2 can have a maximum value of 5.0 and a minimum value of 1.0 based on the angle of attack ranging between 0-90 degrees. The study bridge which will be introduced in Section 4.2 has no skew, but the flow may not be perfectly acting perpendicular to the bridge pier. Therefore, in order to capture the effect of the uncertainty in the flow angle of attack on the scour depth estimation, uniform distribution with the lower value of 1.0, upper value of 1.5 and mean value of 1.25 is assumed for K_2.

5. *Correction factor for the bed condition, K_3*

   K_3 is a factor used in the HEC-18 [56] scour depth estimation equation for representing the variability in river bed condition and it depends on the presence and height of the dunes at the river bed. For the case of clear water scour, horizontal bed condition, antidune flow and small height dunes, HEC-18 suggested a value of 1.1 for K_3. In the present study, it is assumed that it follows normal distribution with a mean value of 1.1 and a COV of 5% according to the studies [6], [47], [100].

6. *Scour modeling factor*

   Uncertainties associated with the estimation of scour depth may alter the final result causing a noticeable difference between the measured and the predicted scour depth values. As can be seen from Equation 3.1, the scour modeling factor can be described as the ratio of the (actual) measured scour depth to the one calculated by using the HEC-18 equation. It can be added into the HEC-18 equation presented in Equation 3.2 as a random variable affecting the final result and it can be described as the modeling uncertainty [6].

$$\lambda_{sc} = \frac{y_{s,measured}}{y_{s,estimated}} \tag{3.1}$$

$$y_s = \lambda_{sc}\, 2.0\, y_1\ K_1\ K_2\, K_3\ \left(\frac{a}{y_1}\right)^{0.65} Fr_1^{\ 0.43} \tag{3.2}$$

Johnson and Dock [46] assumed asymmetrical triangular distribution for the scour modeling variable and used a mean value of 0.93 and COV value of 0.051. Wang [100] followed the same assumption of Johnson and Dock [46] and used the same mean value of 0.93, but he took the COV value as 0.6. Ghosn et al. [6] considered normal distribution for the scour modeling variable with a mean value of 0.55 and COV of 52% as referenced by Johnson [47]. Also, Johnson [48] assumed that it has a normal distribution with a COV value of 0.18. The present study follows the recommendation of Ghosn et al. (NCHRP Report 489) [6].

Table 3.2: Uncertain parameters related to the estimation of scour depth

Uncertain parameters		Unit	Dist.	Distribution Parameters		References
Correction factor for the flow angle of attack	K_2	-	Uniform	Lower: 1.0	Upper: 1.5	[56]
Correction factor for bed condition	K_3	-	Normal	μ: 1.1	δ: 0.05	[6]
Channel slope	*S*	-	Lognormal	μ: 0.002	δ: 0.25	[53]
Manning's roughness coefficient	*n*	-	Lognormal	μ: 0.025	δ: 0.275	[99]
Scour modeling factor	λ_{sc}	-	Normal	μ: 0.55	δ: 0.52	[6]
Discharge	*Q*	m^3/s	Asymmetrical triangular distribution	μ:3500	a:300 c:6000	assumed

3.2 The Sensitivity of Bridge Response to the Uncertain Parameters under Flood Hazards

The response of bridges exposed to floods may change significantly on account of the uncertainties related to hydrologic, hydraulic, scour depth estimation, and modeling parameters when the bridge structural response is computed through finite element analysis. In the present study, a sensitivity analysis is conducted to identify the most critical parameters to which the bridge response is sensitive under the applied flood effects.

For this thesis, Tornado Diagram Analysis (TDA) method is used to perform the sensitivity analysis. Tornado diagrams are generated on the basis of nonlinear static analyses of the finite element models of a river-crossing highway bridge, which is explained in detail in Section 4.2. The aim of creating tornado diagrams is to determine the most critical uncertain parameters influencing the response of the bridges exposed to floods. These critical uncertain parameters are further considered in the probabilistic framework developed in Chapter 4 to generate the flood fragility curves. Within the analyses performed for the sensitivity analysis herein, the same bridge bent model as considered in Chapter 4 is employed and nonlinear static analyses are carried out to obtain the structural response of the bridge under the hydrodynamic loads and scour depths at the pier foundation caused by the given flood discharge. The details on the bridge modeling, the calculation of the flood-induced loads and scour acting on bridge piers and nonlinear static analysis are presented in Sections 4.3, 4.4 and 4.5, respectively.

In TDA, the first step is the calculation of the bridge response by taking the mean values of all uncertain parameters, as this result is used for drawing the vertical axis of the tornado diagram. Secondly, for each uncertain parameter, analyzes are carried out by using two standard deviation smaller and greater values than the mean value, whereas all other parameters are remained at their mean values. This procedure is repeated for each parameter. The number of analysis is equal to twice the number of uncertain parameters plus one which is for the mean value. The difference of the analysis results obtained from the use of upper and lower values are called swing, which shows the sensitivity of the bridge response to an uncertain parameter. The swings of all random variables are plotted in the descending order, which resembles the shape of a tornado. Figure 3.1 shows the tornado diagrams produced when the maximum curvature ductility demand and maximum displacement of piers are considered to represent the bridge response.

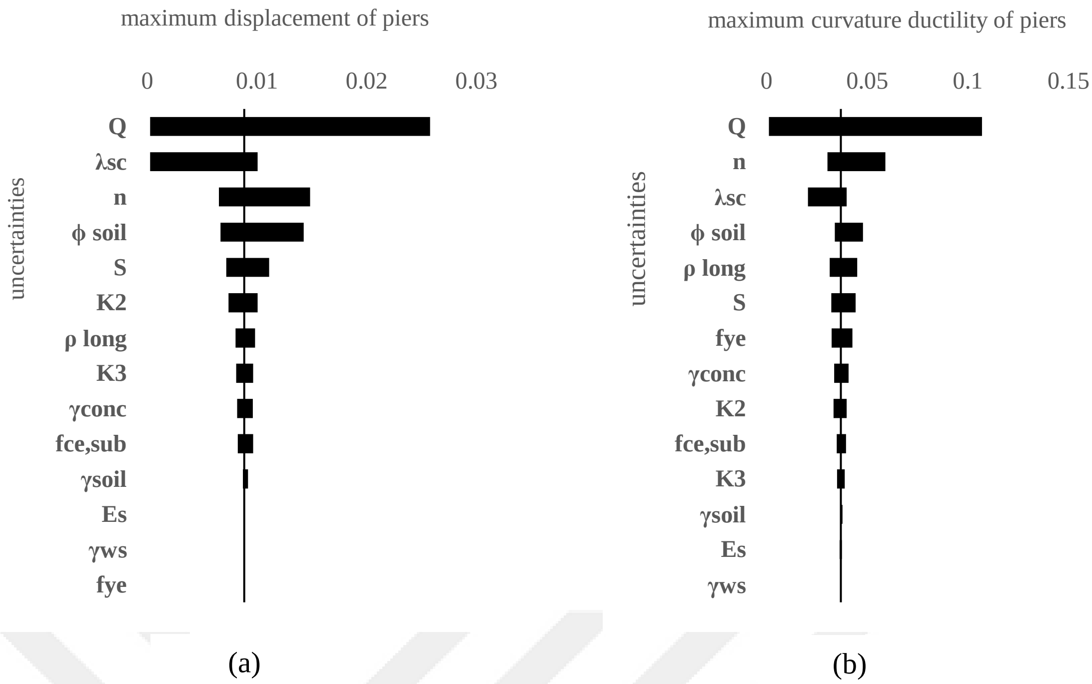

Figure 3.1: Tornado Diagrams for (a) maximum displacement of piers; (b) maximum curvature ductility of piers.

The swings of each uncertain parameter displayed in the tornado diagrams in Figure 3.1 show the extend of the impact of these parameters on the bridge response under flood effects. It can be noticed that the order of these random variables is different between the tornado diagrams produced for two different engineering demand parameters. Thus, in order to sort the criticality of these random variables, Table 3.3 is presented below that demonstrates the order of importance of the random variables in terms of the swings that they produce in the two tornado diagrams.

Table 3.3: The importance order of uncertainties for two different demand parameters

The importance order of RV's	Maximum displacement	Maximum curvature ductility
1	Q	Q
2	λ_{sc}	n
3	n	λ_{sc}
4	ϕ_{soil}	ϕ_{soil}
5	S	ρ_{long}
6	K_2	S
7	ρ_{long}	f_{ye}
8	K_3	γ_{conc}
9	γ_{conc}	K_2
10	$f_{ce,sub}$	$f_{ce,sub}$
11	γ_{soil}	K_3
12	E_s	γ_{soil}
13	γ_{ws}	E_s
14	f_{ye}	γ_{ws}

It is known that flow discharge (Q) in a river increases in proportion to the severity of a flood event. In the sensitivity analysis, the upper value of discharge is taken as 6000 m^3/s to monitor the bridge response during a possibly severe flood event through the sensitivity analysis. The results show us the most important uncertain parameter in which the bridge is most sensitive is the flow discharge. Since the increase of discharge causes to rise of flow depth and flow velocity, hydrodynamic loads on the piers and the scour depth at the foundation are simultaneously increased. Because of that, the hydrologic uncertainties affecting the bridge performance should be investigated in detail, specifically during the design stages of the bridges which are located in flood-prone regions.

As can be seen in Figure 3.1, scour modeling factor (λ_{sc}) affects the response of the bridge considerably both in terms of the maximum displacement and maximum curvature ductility demands of the pier. This is because the scour modeling factor is a multiplier in the HEC-18 [56] scour depth estimation equation (given in Equation 3.2), so it proportionally affects the final scour depth. As the scour modeling factor is increased, the scour depth also increases, thus the soil supporting the foundation reduces and the pier unsupported length is increased.

The Manning roughness coefficient (n) and channel slope (S) take part in the Manning equation as the parameters influencing the resultant flow velocity. The tornado diagram analysis results revealed how effective these parameters are for the resultant flow velocity, which is a very significant factor for the response of the bridges under flood events.

The correction factor for the flow angle of attack, K_2, and the correction factor for the river bed condition, K_3 are critical parameters with respect to the results for maximum displacement compared to the ones obtained for the maximum curvature. K_2 and K_3 both increase the final scour depth, so it may be deduced that scour depth causes an increase in the displacement demands further than the curvature ductility demands.

The curvature ductility demand of a pier section can be influenced by section diameter, yield strain of reinforcing steel, compressive strength of concrete, longitudinal reinforcement ratio, and axial load on the section [101]. Comparing the tornado diagrams in Figure 3.1, the longitudinal reinforcement ratio of piers (ρ_{long}) can be considered as a critical parameter, especially based on the results obtained for the maximum curvature demand.

The angle of friction is the central parameter having an impact on the strength of the soil. The shear strength of soil improves with the increase in friction angle of soil. Therefore, friction angle of soil is a highly significant parameter directly affecting the soil resistance against deformation. As can be seen in Table 3.3, the angle of friction of soil is the fourth most important parameter among others based on the response of the bridge in terms of maximum curvature ductility and maximum displacement. The sensitivity analysis results demonstrated that local soil conditions play a vital role in changing the response of bridges against external loads.

According to the results of the TDA as presented in Figure 3.1 and Table 3.3; flow discharge, scour modeling factor, Manning roughness coefficient, channel slope, internal friction angle of soil, longitudinal reinforcement ratio, compressive strength of concrete and unit weight of concrete are determined to be the key uncertain parameters. The flow discharge parameter is treated separately from the other key uncertain parameters, as it will be sampled incrementally while the other parameters will be subjected to a random sampling process within the probabilistic framework presented in Section 4.6.

CHAPTER IV

DEVELOPMENT OF FLOOD FRAGILITY CURVES OF BRIDGES

4.1 General Methodology

Fragility curves (or fragility functions) are the fundamental tools in probabilistic risk assessment procedures for the bridges under earthquake hazards. These curves mainly provide the likelihood that the structure of interest will sustain a specified level of damage under a given ground motion intensity. In other words, fragility curves can be used for assessing component and system vulnerability of structures. Analytical and simulation-based methods have been increasingly employed in the development of fragility curves thanks to the advances in modeling capabilities and because of insufficient earthquake damage data. While generating fragility curves, different analytical modeling and analysis methods, approaches for simulating the hazard effects, assessment strategies for structural damage, and reliability assessment methods can be applied [12].

An identical path as used in generation of seismic fragility curves is followed in the present study to develop the analytical fragility curves of bridges under flood hazard. There are two major reasons for using analytical methods for the development of the flood fragility curves. The first one is that there is a lack of bridge damage data from past flood events with the corresponding flood characteristics that can be used for the construction of empirical fragility curves. The second reason is that there are advanced finite element modeling and nonlinear analysis capabilities that can simulate the bridge response under the effect of flood-induced hydraulic loads and scour.

The analytical fragility curves of bridges that will be developed under the flood hazard alone will be referred to as *Flood Fragility Curves* in the rest of this thesis. Figure 4-1 shows the general framework proposed to derive the flood fragility curves. In this framework, firstly the significant uncertain parameters affecting the bridge response under flood hazard effects are obtained from the sensitivity analysis presented in Chapter 3. Then, these key uncertain parameters are sampled randomly using the Latin Hypercube Sampling technique [102] and each sample combination of the random variables are matched with an incrementally increasing value of flow discharge. The large number of sample combinations and associated flow discharge values are utilized to construct the finite element models of the bridge bent and structural analyses are performed under the flood-induced effects to obtain the structural demands for each realization. The structural demands are described with respect to the engineering demand parameter (EDP) associated with the bridge response that defines the failure mode under investigation.

This thesis proposes the concept called *Probabilistic Flood Demand Model* (PFDM) to determine the relationship between the intensity of a flood event (IM_{fl}) and the structural demand (*D*) that can result from the flood-induced effects. This model is based on a linear regression analysis of the EDP and the associated IM_{fl} values obtained from all realizations. The probability parameters estimated from the PFDM for demand are compared with the ones adopted for capacity within the classical reliability equation to get the fragility parameters for the failure mode under consideration.

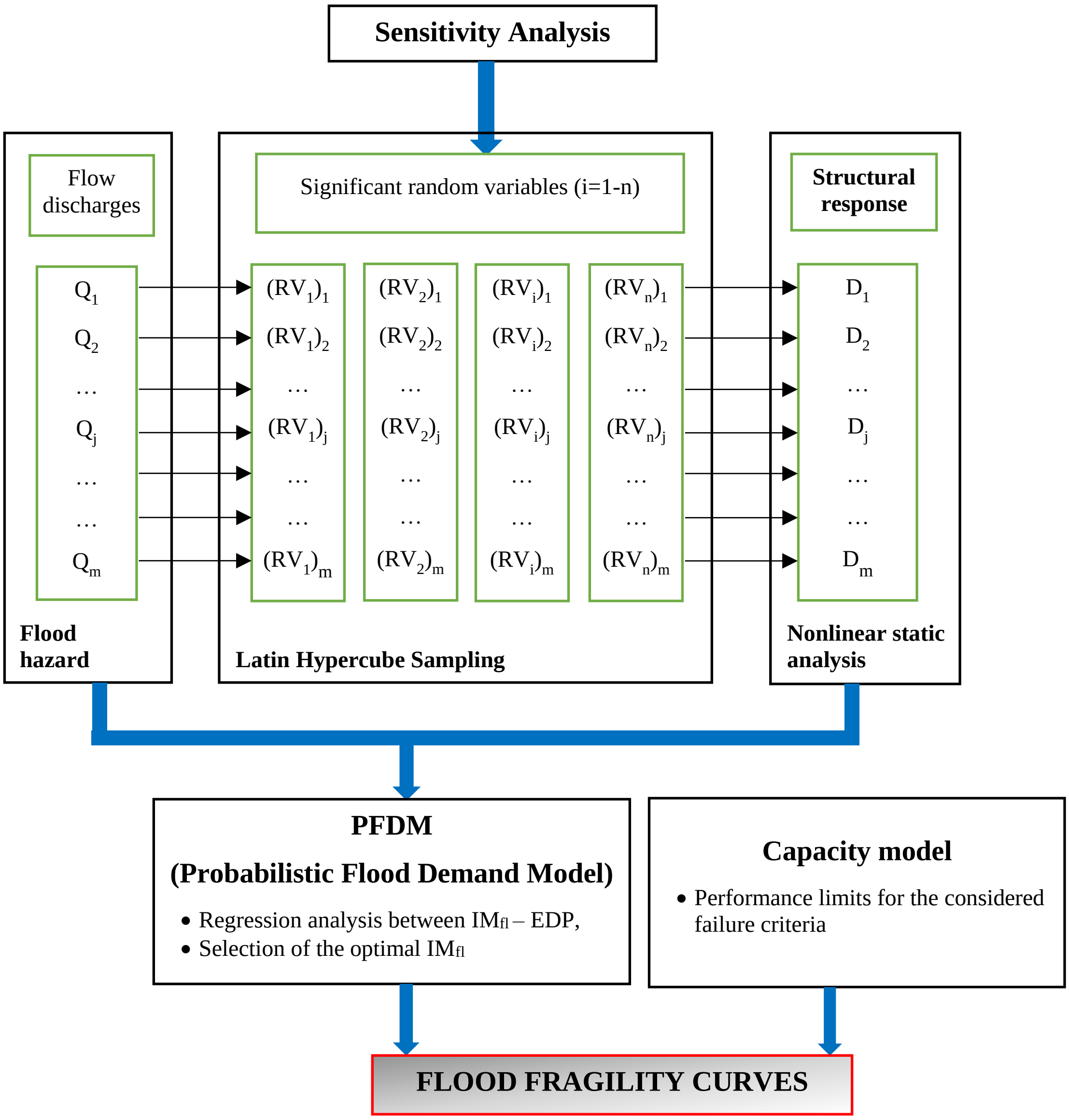

Figure 4.1: General framework for the development of flood fragility curves.

4.2 Study Bridge

4.2.1 Bridge Inventory Studies in Turkey

Akgul [103] developed a bridge management system (BMS) for Turkey. As a part of this BMS, he made an inventory study and reached the following outcomes about the general features of the highway bridges in Turkey:

1. Most of the bridges in the west of Turkey cross rivers, while valley crossings and railway crossings are more common in the east of Turkey. The Black Sea region gets heavy rain along the coastal and in mountainous hinterland areas during a year. This results in floods and bridge damage frequently occurs in this area, sometimes followed by bridge collapses causing loss of life.
2. 72% of bridges in Turkey had been constructed after 1971, so most of the bridge infrastructure in Turkey can be said to be relatively young.
3. 42% of bridges in Turkey have reinforced concrete (RC) simple beam, 32% of the bridges have prestressed simple beam for their superstructure systems. The other types of superstructures are made of RC simple slab, RC continuous beam, RC continuous slab, RC cantilever beam, RC cantilever slab, RC arch, post-tension simple beam, RC rigid frame slab, RC box section, concrete arch, masonry arch, composite, steel girder concrete slab, steel girder zores slab, steel truss beam, steel box section, ferbeton, mix. The average bridge length is 56 m.

Avşar [13] conducted a bridge inventory study to find the general properties of ordinary highway bridges in Turkey. For this purpose, he considered a selection of 52 bridges (available in Table 2.5 in [13]) that represent the highway bridges in Turkey. These selected bridges were defined as "Ordinary Highway Bridges" according to Caltrans 2006 [104] and their general properties are listed below:

1. For the ordinary highway bridges constructed after 1990, reinforced concrete is the primary material of bridge construction excluding the superstructure girders. The characteristic compressive strength is 25 MPa for the substructure components.

2. The girders of the bridge superstructures are made of prestressed concrete with characteristic compressive strength of 40 MPa. The most frequently used girder type is prestressed concrete I-girders.
3. Reinforcing steel class of S420 is used for all RC members. The minimum longitudinal reinforcement ratio is 1.0% for RC piers.
4. Bridges typically have seat-type abutment systems and multiple or single-column bents.
5. Precast prestressed concrete girders are transported from a production facility and the rest of the bridge components are generally constructed on-site. This construction method enables a shorter construction period.
6. In general, bridges have a skew angle ranging between 0-10 degrees. Bridges with a skew angle smaller than 30 degrees are considered as no-skew bridges per Avşar [13]. This implies that more than 67% of the bridges in the inventory are considered without skewness in his study.
7. More than half of the bridges have two spans and 20% of the bridges have three spans.
8. The maximum span length varies between 15-30 m and it is accepted to be statistically normally distributed. The middle span has the maximum length, which is a common design approach in Turkey. The total length of the bridges varies between 40 m to 200 m, but for more than half of the bridges, this length varies between 40 m to 60 m.
9. According to ATC-32 [105] (ATC, 1996) and Priestley et al. [106], column aspect ratio is an effective factor in the displacement ductility capacity of a bridge bents. This ratio varies between 0.5 and 1.25 for the bridges in Turkey. Most of the multiple-column bents have two columns with a section depth of 2.5m with

respect to its strong axis. According to the bridge design practice in the U.S., the beams are required to be designed stronger than the connecting columns [105]. According to Caltrans 2006 [104], nonlinearity should occur on the columns as a formation of plastic hinges at the component ends while the other parts of the bridge remain elastic. This design approach is useful and practical for maintenance and retrofit purposes, however, it may not always be satisfied for the bridges in Turkey, especially for cap beams. Avsar [13] modeled superstructure as elastic, following the recommendations of Caltrans 2006 [104].

10. There are two common types of girder spacing, which are either closely spaced or widely spaced. In Turkey, closely spaced prestressed girders application is the most common type, which enables a more practical construction than using widely spaced girders.
11. More than half of the bridges have a total bridge deck width ranging between 13-14 m.

4.2.2 Selection of the Study Bridge

Yılmaz and Banerjee [107] reviewed the National Bridge Inventory of the U.S. to obtain the general features of the river-crossing highway bridges in California and Washington states. According to results of this inventory study, they formed two major bridge classes, namely continuous concrete box-girder and continuous concrete I-girder, to represent the characteristic bridges that reflect the state-of-the-art practice of bridge design and construction in these states. In addition to these two superstructure types, two foundation alternatives, namely Type I and Type II shafts as described by Caltrans 2013 [108], were investigated to find the effect of these foundation designs on the multi-hazard performance of bridges.

The present research deals with the issue of assessing the structural vulnerability of river-crossing highway bridges subjected to the flood-induced loads and scour, which is a very common and critical problem for the bridges not only in Turkey but also in the world. Thus, the study bridge in this thesis is selected such that a generalized framework for the flood fragility assessment of bridges can be developed. For this purpose, the three-span continuous concrete box-girder bridge with Caltrans Type I shaft foundation as displayed in Figure 4.2 is adopted in the present study for performing the flood fragility assessment. Each bent of this bridge is composed of two reinforced concrete columns which are extended below ground as pile shafts.

It should be noted that the focus of this study is the bridge piers under the effect of hydraulic loads and local scour at pier foundations. Hence, a typical bent of the abovementioned bridge type will be analyzed within the scope of this thesis, so that the superstructure type is assumed to have minimal impact on the final findings. This approach will address the research problem in a global sense by covering the highway bridges in Turkey and the world.

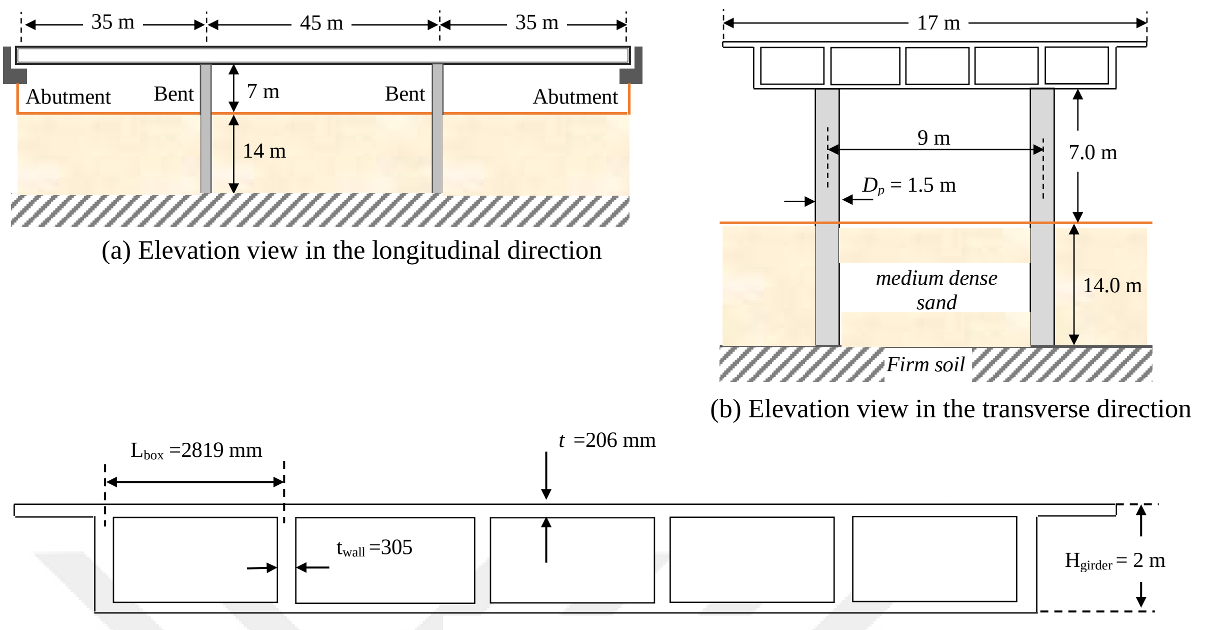

(a) Elevation view in the longitudinal direction

(b) Elevation view in the transverse direction

(c) Box-girder section

Figure 4.2: Schematic drawings of the study bridge.

4.3 Bridge Modeling

As stated in Section 4.2.2, one of the identical bents of the study bridge is investigated in this thesis. The 2-D finite element (FE) models of the bent are generated in the finite element analysis platform OpenSees [109]. The schematic elevation view and the OpenSees model of the bridge are displayed in Figure 4-3. The modeling details of the bent are explained in two parts: modeling of the structural elements and modeling of the foundation-soil interaction.

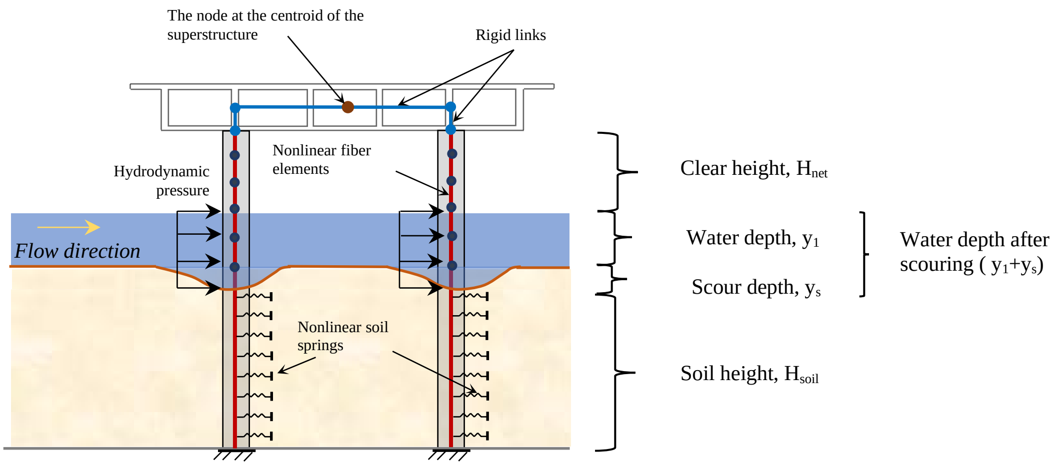

Figure 4.3: The schematic elevation view and modeling properties.

4.3.1 Modeling of the Structural Elements

The superstructure of the bridge type studied in this thesis is only composed of a post-tension box-girder which is monolithically connected with the bent columns. Because the bridge bent is modeled in 2-D, the bridge girder which extends in the longitudinal direction of the bridge is not included in the model as a structural element. However, the dead loads acting on the tributary length of the bridge in the longitudinal direction are transferred to the master node located at the centroid of the superstructure in terms of mass and weight quantities. These dead loads are comprised of the self-weight of the bridge girder and wearing surface on the deck. The master node through which the box-girder passes is connected to the top nodes of the bent columns with rigid link elements. These elements are modeled with dummy elastic beam-column elements with considerably high stiffness strength and zero mass and weight properties.

The substructure of the bridge bent is composed of two reinforced concrete columns and the pile shafts extending below ground with the same diameter. The inelastic response of the columns and extended pile shafts are modeled with displacement-based fiber elements. In the section definitions of these elements, cover and core concrete areas are divided into a decent number of fibers in the radial and circumferential direction and the concrete material definitions with the corresponding unconfined and confined concrete properties, respectively. The uniaxial material definition “Concrete07” which is based on Mander’s Concrete Model [110] are assigned onto the unconfined and confined concrete fibers. The longitudinal reinforcing steel bars are also represented with fibers distributed uniformly in the radial direction with respect to the number of bars as dictated by the utilized longitudinal reinforcement ratio. The uniaxial material definition “Steel02” which represents the uniaxial stress-strain relationship of the reinforcing steel is assigned to the longitudinal reinforcing bar fibers.

4.3.2 Modeling of the Foundation-Soil Interaction

The interaction between the piles and the surrounding soil is considered through nonlinear soil springs in the horizontal direction. These soil springs are placed at small intervals along the length (H_{soil} as shown in Figure 4.3) below the ground level which is associated with the scour depth considered in the analysis. The pile elements are assumed to be fixed at the bottom due to the firm soil below the piles.

The ultimate soil resistance (p_{ult}) that describes the *p-y* curve property of a soil spring varies according to the depth with respect to the river bed level. The relationship between the horizontal soil resistance (P) and the lateral deflection (y) can be calculated with the following equation API [111]:

$$P = A \; x \; p_u x \; tanh \left[\frac{k \; x \; H}{A \; x \; p_u} x \; y \right] \tag{4.1}$$

where; H is depth of the spring from the ground level (in m), k is the initial modulus of subgrade reaction (in kN/m^3) which is a function of the angle of internal friction (ϕ) for the sandy soil. The coefficient A in this equation is the factor to consider whether the loading is cyclic or static. This coefficient is recommended to be equal to A = 0.9 for cycling loading, while the following equation is given for static loading:

$$A = \left(3.0 - 0.8 \; \frac{H}{D} \right) \geq 0.9 \tag{4.2}$$

At a given depth, the ultimate bearing capacity p_u (in kN/m) given in Equation 4.1 is taken as the smallest of the values resulting from the below equations:

$$p_{us} = (C_1 \times H + C_2 \times D) \times \gamma \times H \tag{4.3}$$

$$p_{ud} = C_3 \times D \times \gamma \times H \tag{4.4}$$

where; γ is the effective soil weight (in kN/m^3), D is the average pile diameter (in m) and C_1, C_2, and C_3 are the coefficients determined as a function of ϕ from the figure given in [111] which is also presented in Appendix B.

When river bed level changes with the occurrence of the scour hole in a flood event, the soil springs along the scour depth are removed since soil no more provides resistance for the scoured section of the pile. In addition, the *p-y* curve properties of the remaining soil springs are updated based on the new soil depths.

In order to implement the modeling procedure properly, the total length of each extended column-shaft is classified into three segments as shown in Figure 4.3. The first segment (H_{soil}) is the length from the bottom of the piles to the river bed level and it can be calculated by subtracting the scour depth from the intact pile length. Soil springs are applied within this segment. The second segment is the length from the river bed level to the water level and this length is actually the summation of the scour depth (y_s) and the average flow depth (y_1) resulting from the discharge value of interest. Hydraulic loads are exerted on the extended column-shaft within this segment. The third segment (H_{net}) is the remaining length of the extended column-shaft and it is free of hydraulic loading and soil springs. Considering these three segments in modeling becomes very useful while performing a large number of simulations that include many FE model realizations with different combinations of flow and scour depths. For a given set of flow and scour depths; nodes and structural elements are introduced, soil springs and their properties are assigned automatically in the OpenSees input file by using a parametric scheme. This procedure provides great ease in conducting reliability analysis for different flood intensity levels that results in different sets of flow and scour depths, and thus it allows for working with a large number of sample size in a more convenient way.

4.4 Effect of Flood Hazard on Bridges

Excessive precipitation or melting of snow can cause flood events resulting in extreme discharge values in rivers and sometimes overflow of the stream channel. Floods can have various adverse impacts on bridges. According to Yanmaz [112], the main hydraulic effects reducing the capacity of bridges are associated with the following reasons: change in river bed level due to natural or humankind effects, contraction scour, local scour around piers, hydraulic jumps at bridge spans, debris accumulations between piers, debris impacts of drag materials, pressure and weir-type flow, improper locations of bridges or bridge piers. Among all these effects, scouring around piers or abutments is regarded as one of the most common causes of bridge failure. Nevertheless, the general bridge design procedures do not take hydraulic effects into account sufficiently besides structural effects [112].

Although widespread studies were carried out on scour, only a limited number of them studied how to assess the impact of scour on piles [113]. Scour damage on bridges may have a broad range of effects varying from the minor removal of bed material around piers and abutments to the complete failure of bridges. According to Mondoro and Frangopol [114] the weakening of foundations due to scouring and the hydraulic load on bridge elements can ultimately cause foundation collapse.

Lin et al. [115] reviewed 36 bridge failures attributed to scour and characterized the failure modes in four key types, which are vertical failure, lateral failure, torsional failure, and bridge deck failure. Vertical failure due to scour can be caused by inadequate bearing capacity of the shallow foundation, penetration of friction piles, undermining of pile toe, and pile buckling. Lateral failure involves the pushover failures of piers, structural hinging of piles, kick-out failures of foundations, and excessive lateral movement of piers or foundations. Pushover failure of a bridge subjected to scour may develop with the increasing lateral flow load and debris as the lateral capacity of the bridge is reduced due to a deep scour hole. For the structural hinging mode, the bending moment resistance in structural elements including piles can be lower than the substantial bending moments produced by transverse loads under the excessive lateral movement. The kick-out failure of foundations can arise once piles washout from the pile tips because of scouring.

Being parallel to the classification of Lin et al. [115], the proposed framework in this thesis study considers only the lateral failure mode where the bridge damage or failure is instigated by the excessive lateral movement and the resulting inelastic response of the column-shafts. For this objective, the fragility assessment of the study bridge is performed by incorporating the below listed three main effects acting on bridge piers. These effects are further explained in Sections 4.4.2-4.4.4.

(i) Hydrodynamic pressure occurring from the increased stream velocity,

(ii) Local scour occurring at pier foundations,

(iii) Increased hydrodynamic pressure owing to the accumulation of debris in front of the upstream side of piers.

The hydrodynamic pressure effects (stated in items i and iii) create a dragging force that acts on bent columns and shafts (if exposed due to scour), while simultaneously local scour (stated in item ii) causes a reduction in lateral soil resistance along with the scour depth at pier foundations. These combined effects can lead to structural damage, even a total failure of the bridge stability. It should be noted that other possible scenarios of bridge failures under flood hazards such as the occurrence of scour at abutments or the uplift of submerged bridge superstructure are beyond the scope of the present study.

4.4.1 Calculation of Flow Depth and Flow Velocity

The purpose of the study is not a risk analysis of a site-specific bridge, so capturing the wide range of possible flood events is the main idea. The discharge values are increased from the 100 m^3/s to 5800 m^3/s in the sort of ascending.

For a given flow discharge value Q, the flow depth (y_1) and the flow velocity (V) are calculated from the Manning's equation:

$$Q = VA = \frac{1}{n} A \left(\frac{A}{P}\right)^{2/3} (S)^{1/2} \tag{4.5}$$

where; n is the Manning roughness coefficient, A is the cross-sectional area of the flow, P is the wetted perimeter and S is the channel slope. In the present study, the flow cross-sectional area is assumed to be rectangular, so Manning's equation can be expressed in the following form:

$$Q = \frac{1}{n}(b\, y_1)\left(\frac{b\, y_1}{b + 2\, y_1}\right)^{2/3} (S)^{1/2} \tag{4.6}$$

where; b is the channel width which is taken as the total bridge length. In Equation 4.6, all the parameters except the channel width (b) are taken as random variables in the reliability analysis. For the given input parameters of Q, n, S, and b, the first objective here would be to solve for the unknown parameter of y_1. For this purpose, a trial and error procedure can be used where an assumed value of y_1 is updated until the Q value resulting from this equation is validated with respect to the given value of Q.

The reliability analysis applied in this study is based on simulations requiring the calculation of flow depth and flow velocity for a high number of realizations. In order to overcome the difficulty in repeating the trial and error process for all realizations, an iterative approach is utilized where a close prediction of y_1 can be obtained in maximum 2-3 iterations. Equation 4.6 can be expressed in the following form:

$$Q = \frac{1}{n}\,(y_1)^{2/3}(S)^{1/2}(y_1 b)\,C_x \tag{4.7}$$

where C_x is a correction factor that can be expanded as:

$$C_x = \left(\frac{b}{b+2y_1}\right)^{2/3} \tag{4.8}$$

The value of y_1 can be calculated directly from Equation 4.7 as shown in the below equation:

$$y_1 = \left(\frac{Q\,n}{(S)^{1/2}\,b\,C_x}\right)^{3/5} \tag{4.9}$$

In the first iteration of this procedure, the term C_x is taken to be equal to 1.0 under the assumption that $(2y_1)$ is small compared to the channel with b. Then, the flow depth y_1 is calculated from Equation 4.9 and it is used in Equation 4.8 to calculate the new value of C_x. This process can be continued in each iteration such that the updated value of C_x is considered to find the new value of y_1 until the consecutive values of y_1 are close enough.

Once the flow depth (y_1) is determined, the mean flow velocity (V) can be computed from the equation below:

$$V = \frac{Q}{A} = \frac{Q}{b\,y_1} \tag{4.10}$$

4.4.2 Calculation of Scour Dept at Pier Foundations

According to an analysis of 36 bridge failure cases attributed to scour, 64% of the bridge failures are caused by local scour, while the rest of them are associated with contraction or general scour [115]. Therefore, it can be said that local scour is the leading type of scour for bridge failures.

Flood events can cause extreme flow pressure on water surface. The flow pressure getting increased from the bottom to the water surface causes a vertical flow (from the bottom to the water surface). As a result, horseshoe vortexes occur on the upstream face of piers as the vertical flow runs into the horizontal flow. During this process, river bed materials are displaced with the vertical flow and dragged to the downstream because of the horseshoe vortexes. This is the process that explains how excessive scouring starts during a flood event according to Yurtseven [116].

Within the scope of this thesis, the scour depth equation as recommended in FHWA Hydraulic Engineering Circular No.18 (HEC-18) [56] and shown in Equation 4.11 is employed to calculate the scour depth (y_s) for a given set of flow depth (y_1) and mean flow velocity (V) values.

$$y_s = \lambda_{sc}\, 2.0\, y_1\, K_1\, K_2\, K_3 \left(\frac{a}{y_1}\right)^{0.65} {Fr_1}^{0.43} \tag{4.11}$$

In this equation, a is the pier width, K_1, K_2 and K_3 are the correction factors for pier nose shape, angle of flow attack, and river bed condition, respectively. An additional coefficient λ_{sc} is included in the above equation to account for the discrepancies between the actual scour depths measured at sites and the estimated one obtained through the HEC-

18 equation. Fr_1 is the Froude number directly upstream of the pier that can be calculated from the following equation.

$$Fr_1 = \frac{V}{\sqrt{g\ y_1}} \tag{4.12}$$

According to the outcome of the sensitivity analysis presented in Chapter 3, only the scour modeling factor λ_{sc} is included in the Latin Hypercube Sampling design as a random variable. All the other parameters in Equation 4.11 (K_1, K_2, K_3) are taken at their deterministic variables. The removal of soil with the occurrence scour causes a reduction in lateral and rotational stiffness of shaft foundations and pile group foundations, thus increase the vibration period of reinforced concrete bridges compared to intact bridges [117]. The same conclusion can be acquired from Table 4.1 which demonstrates the variation in the fundamental period of the bridge bent investigated in this study for increasing scour depths.

Table 4.1: The variation in the fundamental period of the bridge bent with respect to increasing scour depths

Scour depth (m)	Periods (sec)
1	0.787
2	0.866
3	0.949
4	1.035
5	1.124
6	1.210
7	1.286
8	1.342
9	1.376
10	1.392

4.4.3 Effects of Hydrodynamic Loads on Piers

Bridge bents in water are subjected to two main hydraulic load cases: hydrostatic pressure and hydrodynamic pressure. At any point on a pier under water, the hydrostatic pressure is equal to the water depth multiplied by the unit weight of water. However, since this hydrostatic pressure acts on a pier from all directions equally under the assumption that the water level change from the upstream to the downstream is negligible, the resultant force acting on the pier due to hydrostatic pressure would be equal to zero. Along with the horizontal component of the hydrostatic pressure, buoyancy force which is the vertical component of it can act on all submerged elements. However, in this study the water level is assumed to not reach the bridge superstructure level, so the buoyancy force will not develop.

The hydrodynamic pressure considered in this thesis is based on the stream pressure arising from the increased velocity of the flow during a flood event. The stream pressure acting on bridge piers can have longitudinal and lateral components, but in this study only the longitudinal component is taken into account. This is because the bridge studied here is assumed to be straight, so the flow direction is parallel to the longitudinal axis and this makes the lateral component to be equal to zero.

The longitudinal drag force is the multiplication of the longitudinal stream pressure and the projection area exposed to this pressure. The equation given in AASHTO (2012) [78] is adopted to calculate the longitudinal stream pressure:

$$p = C_D \frac{w}{2g} V^2 \tag{4.13}$$

where; p is the flow pressure (in ksf), w is the specific weight of water (in kcf), V is the flow water (in ft/s) and g is the gravitational acceleration constant (32.2 ft/s^2). C_D in Equation 4.12 is the drag coefficient and its value depends on the pier shape and the presence of debris as in Table 4.2.

Lee et al. [34] converted the above equation into SI units and expressed the hydrodynamic force as follows:

$$p = 5.14\ 10^{-4}\ C_D\ V^2 \tag{4.14}$$

$$F_{drag\ force} = p\ A \tag{4.15}$$

where; p is the water pressure (in MPa), V is the flow velocity (in m/s), A is the projection area of the pier subjected to the water flow pressure.

Table 4.2: Drag coefficients (given in AASHTO (2014) [1])

Type of pier	C_D
Semicircular-nosed pier	0.7
Square-ended pier	1.4
Debris lodged against the pier	1.4
Wedged-nosed pier with nose angle 90 degrees or less	0.8

In this study, the drag coefficient is taken as $C_D = 1.4$ for the case when debris accumulation is present in front of the piers while $C_D = 0.7$ for the case of no debris accumulation.

Water velocity increases from the bottom to the top and it reaches the maximum value at the water surface. Since the hydrodynamic load is a function of water velocity, its distribution has a parabolic shape with an increasing intensity up to the water surface. Nevertheless, this study uses the mean water velocity corresponding to the given flow discharge, thus hydrodynamic load is exerted on the piers (column and pile elements) with uniform (rectangular) distribution along the flow depth. The water depth after scouring will be equal to flow depth as calculated in Section 4.4.1 plus the scour depth as calculated in Section 4.4.2.

4.4.4 Effects of Debris Accumulation on Bridges

Flood waters acting on bridge piers are frequently accompanied by debris such as drifts, logs, and others in rivers. Accumulation of debris at the upstream face of bridges can aggravate the scour depth. Also, this accumulation in front of the piers can escalate the lateral flow loads acting on bridges. The combination of these two effects can enhance the possibility of bridge failures.

In addition to the effects of debris accumulation mentioned above, floods carrying massive and weighty debris such as large stones or rocks may strike piers or piles, so structural hinging may occur [118]. Also, debris accumulation can block the flow channel cross-section leading to a rise in water levels and bridges can become more vulnerable as their decks are submerged during flooding. This can cause a total failure of a bridge if the bridge superstructure is not adequately connected to the substructure, as in the case of simply supported bridges. Nevertheless, this study investigates only the two effects of debris, which is the aggravation of local scour around piers and the enhancement of drag force acting on piers. The below subsections in this chapter explain these effects in detail.

4.4.4.1 Effect of Debris Accumulation on Local Scour Estimation

Floating woody debris can be stuck and pile up at the upstream face of a bridge pier. Debris has the tendency to thrust the flow downwards causing a much deeper scour hole compared to the condition of having no debris. Furthermore, the projection area of a pier on which the stream flow pressure acts can get increased due to the obstruction of floating woody debris. Therefore, an empirical formula estimating the effective pier width is utilized to calculate the enhanced scour depth in the presence of debris.

The size and shape of the debris accumulated in front of bridge piers during floods can be estimated based on past experiences or experts' judgments, particularly regarding the river basin characteristics. For this purpose, the features of the basin catchment in which bridges are located should be examined. NCHRP Report 653, "Effects of Debris on Pier Scour" [119] and HEC-20 "Stream Stability at Highway Structures" [120] mentioned the possible mechanisms and reasons for debris accumulation at bridge piers and also presented procedures for forecasting potential woody debris accumulation at piers. Debris can accumulate in various geometries but it can be generally idealized in the form of triangular or rectangular shapes. The figures 7.16 and 7.17 in HEC-18 [56] displays the idealized geometries of debris, as described in [119]. The rectangular shape for debris accumulation can cause more severe scour because of the high obstruction rate than the triangular one. But for both shapes scour depth levels are increased, since the blockage against river flow is higher compared to the absence of debris at piers. When the length of the debris in the upstream direction reaches the flow depth, a more severe depth of scour was observed [119].

For prediction of the local scour around bridge piers subjected to debris accumulation, the HEC-18 pier scour equation is considered by employing the effective pier width estimated from an empirical equation, which was based on the NCHRP Report 653 [119] . The effective width of the pier a^*_d (in m) when debris is present is calculated from the following equation:

$$a^*{}_d = \frac{K_1 \, (HW) + (y - K_1 H \,)a}{y} \tag{4.16}$$

where; a is the pier width perpendicular to flow (in m), H is the height (thickness) of the debris (in m), W is the width of the debris perpendicular to the flow direction (in m) and y is the approach flow depth (in m). In Equation 4.16, the coefficient K_1 is taken as 0.79 for rectangular or 0.21 for triangular geometry of debris.

4.4.4.2 Effects of Debris Accumulation on Hydrodynamic Loads

It is obvious that the reduction in flow cross-section area (A_1) due to debris accumulation amplifies the flow pressure acting on piers. This is because the continuity equation states that the flow rate should be constant through the channel ($Q_1 = Q_2$ in consecutive sections 1 and 2), thus if the flow area reduces from A_1 to A_2, then the flow velocity must increase from V_1 to V_2 per the continuity equation. It should be noted that the discharge is equal to the multiplication of flow velocity and flow area ($Q_1 = Q_2 = V_1 A_1 = V_2 A_2$).

This study assumes that the top level of debris is the water surface and adopted the shape of debris accumulation as triangular following the recommendation of AASHTO [1]. In calculation of the hydraulic loads acting on bridge piers when debris accumulation is present, the debris raft having the geometry as demonstrated in Figure 4.4 is considered as the projection area on which hydrodynamic pressure acts. However, in this case the drag coefficient is taken as $C_D = 0.5$ per the recommendation of AASHTO [1].

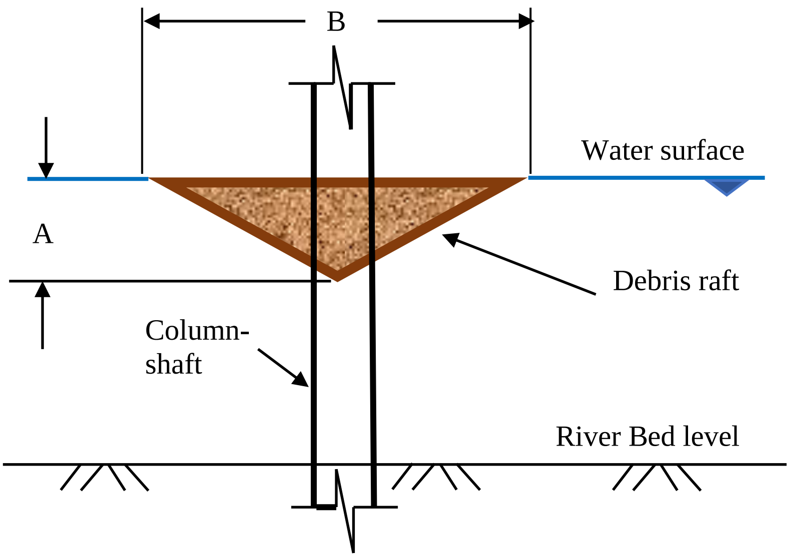

Figure 4.4: Debris raft as viewed from the upstream side (adopted from AASHTO [1])

According to AASHTO [1], the dimension A in Figure 4.4 stands for the height of the debris raft and it should be taken as half of the water depth but not greater than 10 ft (3.05 m). The dimension B is the length of the debris raft between two adjacent bridge bents and it should be taken as half of the sum the adjacent span lengths, but not greater than 45.0 ft (13.72 m). For the study bridge considered in this thesis, the sum of the adjacent span lengths is equal to 40 m, so the dimension B is taken as 13.72 m. On the other hand, the value of dimension A will vary based on the flow depth computed under the given flow discharge.

In this thesis study, the impact of debris accumulation on the fragility assessment of bridges under floods is investigated for three conditions:

Case-1 represents the condition when no debris is accumulated in front of the bridge piers. The drag coefficient used in calculation of the hydrodynamic pressure is taken as C_d =0.7 in this case.

Case-2 is the condition when debris is accumulated in front of the bridge piers but there is no information on the shape and degree of debris accumulation. Therefore, the effect of debris accumulation on scour depth calculation is not taken into consideration in this case, while the drag coefficient is taken as C_d =1.4 as recommended by AASHTO [1] .

Case-3 refers to the condition when there is debris accumulation in front of the bridge piers. However, this time the debris raft geometry is defined with a triangular shape so the effects of debris accumulation on scour depth and hydrodynamic pressure calculations are taken into account as discussed in sections 4.4.4.1 and 4.4.4.2. In this case, for the calculation of hydrodynamic pressure acting on the debris raft, the drag coefficient is taken as C_d =0.5, but for the rest of the projection areas of the structural members it is taken as C_d =1.4.

It should be remembered the debris accumulation considered in Case-3 represent the maximum degree of debris accumulation. In fact, the degree of debris accumulation contains a high level of uncertainty, so Case-2 addresses the condition when no sufficient information is available on the size and degree of debris accumulation.

4.5 Finite Element Analysis

4.5.1 Modal Analysis

Modal analysis is an analysis type for identifying the intrinsic dynamic characteristics of a system in the form of natural frequencies, mode shapes. [121]. The outputs of modal analysis are generally obtained in advance for seismic analysis of structures to calculate the inertial forces in modal spectrum analysis or to determine Rayleigh damping coefficients for time-history analysis. Nevertheless, in this thesis modal analysis is performed to examine the mode shapes for controlling the modeling in

OpenSees and how the modal periods vary with respect to different scour depths as demonstrated in Table 4.1.

In the present study, modal analysis of the bridge samples having various flood-induced scour depths are performed in OpenSees, and the first ten mode periods of bridge samples are obtained. The first mode shape of the bridge by using the mean values of input parameters is presented in Figure 4.3.

Figure 4.5: First mode of the bridge bent.

4.5.2 Nonlinear static analysis under flood effects

Natural hazards such as floods can have unfavorable impact on bridges that may result in bridge damage and even casualties. Therefore, vulnerability analysis of bridges has a vital importance for determining at what level of flood hazard a bridge cannot sustain its serviceability or necessary precautions should be taken to prevent fatalities and economic loss associated with possible bridge failures or plan the proper schedule for bridge maintenance. That is why flood fragility curves can provide a valuable guidance for decision makers and bridge owners. The hydrologic and hydraulic analyses of a bridge site can give information about the potential of flood hazard that can influence the bridge. So, if this information is used in combination with the flood fragility curves, the failure probability of the bridge can be estimated under a certain hazard level and necessary actions including maintenance and strengthening planning, bridge closure decisions and even bridge design revisions in pre-construction stages can be taken according to specified limits.

In this study, nonlinear static analyses are performed to obtain the maximum structural demands of the bridge bent models subjected to flood-induced loads and associated scour depths for a large number of discharge values within a simulation-based reliability framework. The flood-induced loads (i.e. hydrodynamic pressure) and scour depths can change throughout a flood event as a result of the variation of flow discharge. However, this study is concerned with the maximum structural demand which is assumed to develop at the instant when the peak discharge occurs in a flood event. Therefore, the discharge value considered in each realization of the simulation represents the peak discharge for that realization (flood event) under consideration and the nonlinear static analysis captures the structural responses.

Owing to the modeling approach of the bridge bent as described in section 4.3.1, the structural response is inelastic under the applied flood-induced loads. As the flood-induced hydrodynamic load acts in the horizontal direction, the bridge bent can make excessive lateral displacements causing its vertical structural members (i.e. columns and extended pile shafts) undergo high levels of flexural and shear response and this can create damage and even loss of stability. Meanwhile, the lateral displacement of the bridge bent can be amplified with the occurrence of scour as the soil support at the foundation is reduced because of the increase in unsupported length of piles. Thus, within the scope of this thesis, only the flexural failure of the columns and extended pile shafts (evaluated together) is taken into consideration for fragility assessment of bridges under floods. The maximum curvature ductility demand is used as the engineering demand parameter (EDP) to represent the flexural damage. On the other hand, shear failure of the columns and extended shafts is neglected assuming that these members contain adequate amount of transverse steel preventing them from shear failure prior to a flexural failure.

The lowering of the riverbed level due to scour can reduce the lateral resistance of the foundation system of a bridge as some part of the supportive soil strata is removed. This can bring the possibility of some geotechnical failure conditions. One of these conditions is the tilting of piers caused by total loss in foundation stability. Another condition is that, when scour depth reach a certain level, settlement of piers may occur as a result of the reduction in pile capacities. Sometimes slender piles show a tendency to buckle under the axial loads coming from the combination of axial and lateral loads or even from the own weight of bridge superstructure [122]. The bridges with different types of foundations can be affected from scour and flood-induced loads differently. For example, the bridges with pile group foundations which is commonly applied on deep alluvial stream beds may encounter stability problems due to the rise of unsupported length [123], [115]. Besides that, shallow foundations are more vulnerable to scour than deep foundations. However, the investigation on the failure modes associated with the geotechnical failure as mentioned above is beyond the scope of this thesis.

4.6 Probabilistic Framework for Generation of Analytical Fragility Curves of Bridges Subjected to Floods

Bridge fragility curves have been classically generated by using a two-parameter cumulative lognormal distribution function defined with respect to median and dispersion (lognormal standard deviation) parameters. Using the same definition as employed for seismic fragility curves by Shinozuka et al. [124], the flood fragility curves can be expressed as in the below equation.

$$F_k\,(a_i;\ \lambda_k\,,\zeta_k) = \Phi\left[\frac{\ln\left(\frac{a_i}{\lambda_k}\right)}{\zeta_k}\right] \tag{4.17}$$

where; F() represents the fragility function, which can be defined as the probability of failure of the bridge for the damage state k (or probability of exceeding the damage state k). The parameter "a_i" stands for the intensity measure (IM) of the flood event "i". In this study, IM is accepted to be flow velocity as explained in section 4.6.2. λ_k and ζ_k are the median and dispersion (lognormal standard deviation) values of the fragility curves, respectively at the damage state "k" and they are also referred to as fragility parameters. Within the applied fragility analysis framework, the dispersion value ζ_k is the same for the fragility curves at all damage states. In the present study, four damage states, namely minor damage (k=1), moderate damage (k=2), extensive damage (k=3), and collapse (k=4) are taken into consideration.

The generation of flood fragility curves of bridges is summarized in the steps mentioned below:

1. The analytical model of the bridge bent is generated in the finite element analysis platform OpenSees [109] as described in section 4.3.1. The model input file allows for a flexibility in assigning different sets of modeling parameter values, updating the soil springs with respect to the given scour depth and exerting the hydrodynamic loads based on the given flow depth and mean flow velocity values. So, all the bridge models within the simulation process are built and the corresponding nonlinear analyses are completed within a very short amount of time.

2. The most critical (key) modeling parameters affecting the bridge response under flood effects are determined by using the outcomes of the sensitivity analysis performed in section 3.2. According to the results of Tornado Diagram Analysis in section 3.2, scour modeling factor, Manning roughness coefficient, channel slope, internal friction angle of soil, longitudinal reinforcement ratio, compressive strength of concrete and unit weight of concrete are determined to be the key uncertain parameters and considered as random variables in the rest of the fragility assessment framework.
3. A large set of incrementally increasing values of flood discharges are determined. This set is planned to cover considerably a large number of scenario flood events so that the variation of structural demands under different flood intensities can be captured. For example, the maximum value in this set can represent the peak flow discharge corresponding to a flood with a very high return period, while the minimum discharge value can be thought to represent the daily peak flow discharge in the river. Hence, this set is independent of the flood hazard of a certain region, as it only aims to serve for obtaining the variety of flow intensities that can hit the bridge. In the present study, m = 571 number of realizations are created with the discharge values varying from 100 m^3/s to 5800 m^3/s, to account for the hydrologic uncertainty.
4. The key parameters determined in Step 2 are incorporated in the Latin Hypercube Sampling [102] process to produce the random sample combinations of these parameters. The number of sample combinations is taken to be exactly equal to the number of flow discharge values created in Step 3.

5. The flow discharge set (mentioned in Step 3) and the random sample combinations of key modeling parameters (mentioned in Step 4) are matched to generate the complete set of realizations in the simulation process.
6. For the flow discharge value of each realization, flow depth and mean flow velocity are calculated as described in section 4.4.1. Then, the corresponding scour depth that would develop at the pier foundation is computed by using the procedure given in section 4.4.2. In the meantime, the hydrodynamic loads are calculated following the process as described in section 4.4.3. Using the scour depth, hydrodynamic loads and the modeling parameters for each realization, bridge model is built, and nonlinear static analysis is completed to get the structural demands. This process is repeated for all realization within the simulation process.
7. The pairs of flood intensity measure (IM) versus EDP's resulted from all realizations are plotted and linear regression analysis is performed to find the relation between flood intensity and structural demand (D). This step constitutes the base of the proposed probabilistic flood demand model (PFDM) of bridges. The details of PFDM are presented in section 4.6.1.
8. Within the linear regression analysis performed in Step 7, the optimum IM is investigated and the one that yields the best model to estimate the structural demand for a given flood intensity is selected for the PFDM. The details of this step are presented in section 4.6.2.
9. The statistical parameters for demand (i.e. a, b and β_D) are obtained from the linear regression analysis as a part of the PFDM.

10. The probability distribution parameters of the capacity for the considered failure mode is adopted from literature to specify the limiting values at all damage states. The details of this step are presented in section 4.6.3.
11. The demand and capacity are compared using the classical reliability approach to generate the flood fragility curves for the study bridge. This step is further explained in section 4.6.4

4.6.1 Probabilistic Flood Demand Model

Many studies [12], [19], [125]–[127] carried out in the past have used the concept of probabilistic seismic demand model for generation of fragility curves of bridges exposed to earthquake hazard or multi-hazard conditions. This concept was first proposed by Cornell et al. [125] and they assumed that seismic capacity and demand models follow lognormal probability distribution. Adopting an identical approach, but this time for the single hazard of floods, this thesis study proposes the **Probabilistic Flood Demand Model (PFDM)**. PFDM basically shows the relationship between the intensity measure of a flood event (IM) and the resulting structural demand identified in the form of an engineering demand parameter (EDP) for the failure mode under consideration.

In this approach, the conditional relationship between structural demand (*D*) and flood intensity measure (*IM*) can be expressed as follows:

$$PFDM = P\left[D \geq d|IM\right] = 1 - \Phi\left(\frac{\ln(d) - \ln(S_D)}{\beta_{D|IM}}\right) \tag{4.18}$$

where Φ is the standard normal cumulative distribution function, S_D is the median demand and β_D is the lognormal standard deviation (dispersion) of the demand. The demand (*D*) parameter in this equation is characterized with the EDP used to assess damage for the investigated bridge failure mode. In this thesis, maximum curvature ductility is employed for the EDP to evaluate the flexural failure of columns and piles. The relationship between the median demand (S_D) and the intensity measure of flood (IM) can be established with the following equation:

$$S_D = a\,(IM)^b \tag{4.19}$$

where; a and b are the parameters which can be obtained from a linear regression analysis that is applied on the outputs of the simulations. For mathematical simplicity, the relation between IM and S_D can be transformed into the lognormal space as follows:

$$\ln(S_D) = \ln(a) + b\ln(IM) \tag{4.20}$$

The linear regression analysis provides the best straight line fitting the data of IM versus EDP pairs obtained from all realizations. The terms ln(a) and b in Equation 4.19 represent the vertical intercept and the slope of the best line, respectively. The lognormal standard deviation (dispersion) of demand can be calculated from the linear regression analysis using the following equation.

$$\beta_{D|\,IM} = \sqrt{\frac{\sum(\ln(d_i) - \ln(a\,IM_i^b))^2}{N-2}} \tag{4.21}$$

where;

d_i: The maximum demand result obtained from the i^{th} realization,

IM_i: The intensity measure value of i^{th} realization,

N: The size of the simulation (number of realizations).

The PFDM’s developed for the three investigated cases as described in section 4.4.4.2, namely Case-1, Case-2 and Case-3, are presented in Figure 4.6, 4.7 and 4.8, respectively. The linear regression analyses displayed in these figures are performed by considering flow velocity as the intensity measure. Note that the flow velocity data used these figures are computed from the discharge values of each realization.

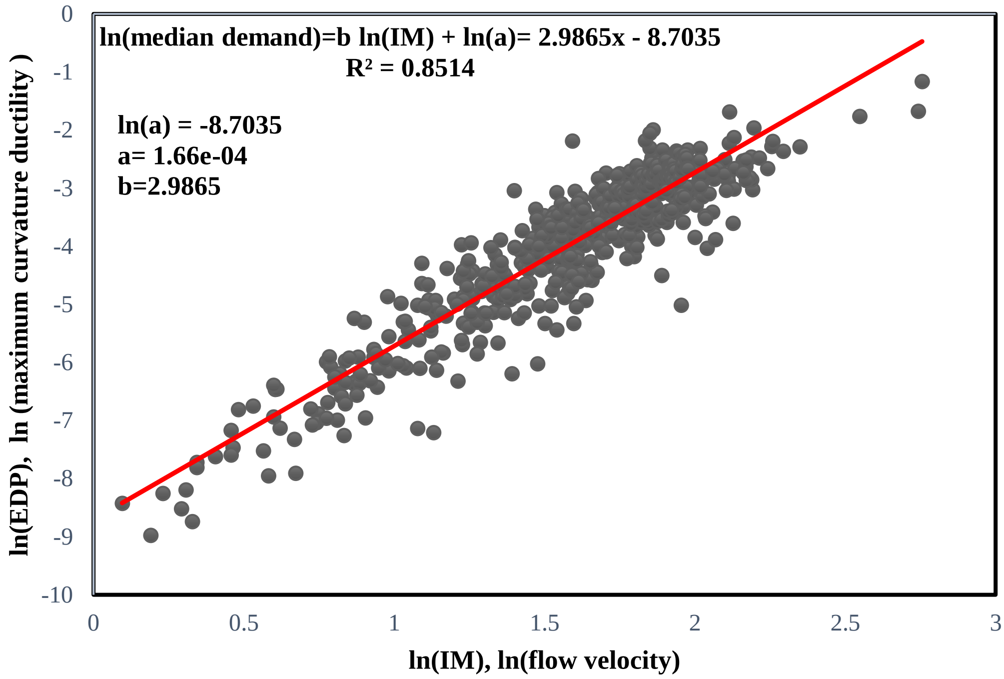

Figure 4.6: PFDM in the absence of debris accumulation (Case-1)

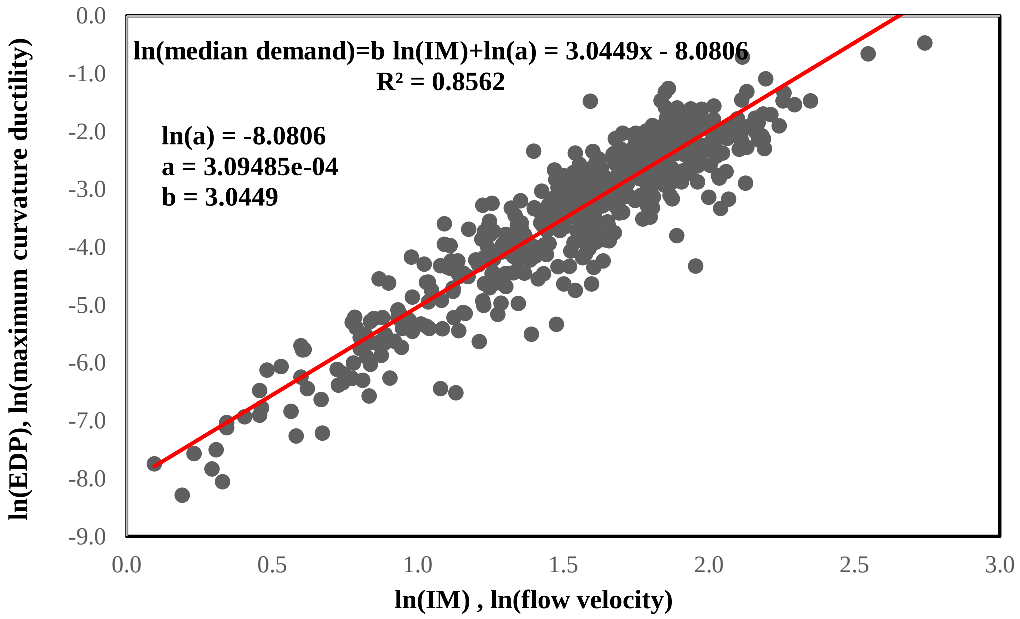

Figure 4.7: PFDM in the presence of debris accumulation with no defined geometry (Case-2)

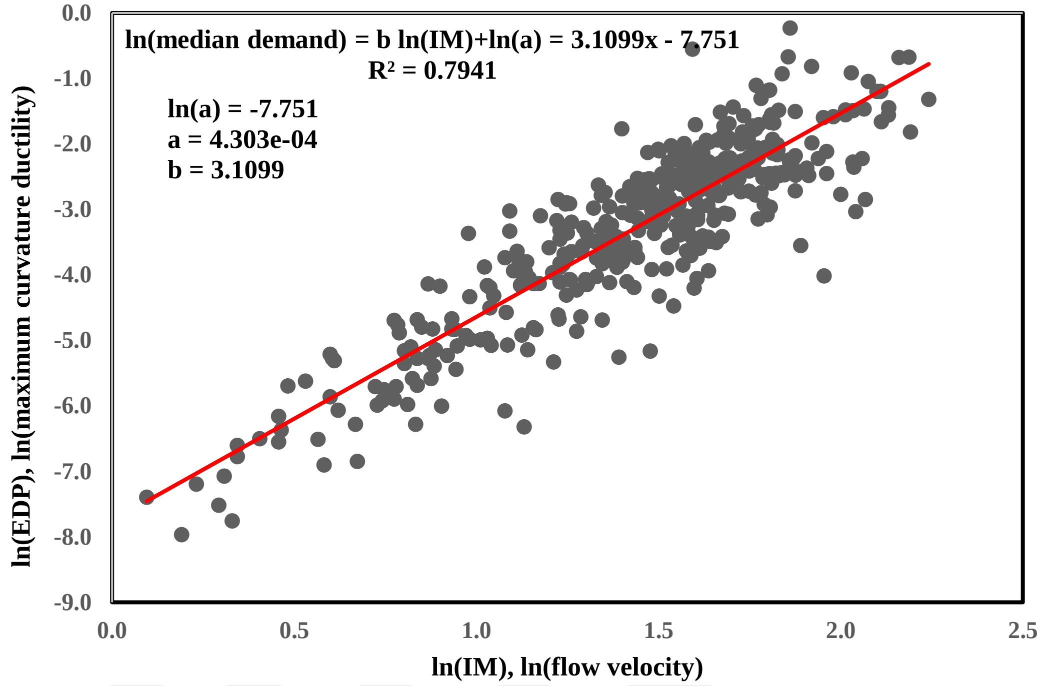

Figure 4.8: PFDM in the presence of debris accumulation defined with triangular debris raft (Case-3)

4.6.2 Selection of the Optimum Intensity Measure for PFDM

In the seismic fragility curve generation studies which employed probabilistic seismic demand model (PSDM), it is stated that PSDM should ideally be efficient, practical, and proficient [12], [100], [127]. The similar criteria are sought for the PFDM proposed in this study and accordingly the optimum flood intensity measure (IM) is investigated to reach a more accurate flood fragility curve.

The demand dispersion (lognormal standard deviation, β_D) which is predicted from the results of nonlinear static analyses of all realizations represents the efficiency of IM. A smaller value of demand dispersion indicates a more efficient IM. Practicality can be defined with respect to the regression parameter *b* (the slope of the best line fit in regression analysis) which shows the correlation between IM and EDP values. A higher value of b value shows that the selected IM is more practical. The proficiency of IM can be identified as the combination of the efficiency and practicality terms. A parameter called modified dispersion, which can be calculated by dividing the demand dispersion to the slope of the best fit line (β_D / b), is used to define the proficiency. The smaller value of modified dispersion indicates a higher proficiency of IM. Therefore, a smaller value of dispersion of demand and a higher value of b would yield a lower modified dispersion, and accordingly a higher proficiency. The R^2 value also demonstrates the capability of fitting a best line on the data of IM-EDP pairs in a linear regression analysis. As a result, the higher R^2 and b, and the lower demand dispersion (β_D) and modified dispersion (β_D / b) are considered as the proofs for selecting the optimal IM for the PFDM.

In this study, different possible intensity measures are tried out for reflecting the effect of flood hazard on bridges. For this purpose, the linear regression analyses are repeated for the intensity measures of discharge (Q), flow velocity (V), flow depth (y_1), normalized flow depth with respect to pier height (y_1/H), and Froude number ($V/(gy_1)^{1/2}$) by using the demands resulting from all bridge model realizations. It should be noted that the flow velocity and flow depth data used in these regression analyses are derived from the available set of corresponding discharge values. Also, all alternative intensity measures are assumed to be representing the flood hazard as well as the flow discharge. The regression parameters when each IM is utilized are presented in Table 4.3.

As can be observed from Table 4.3, the maximum R^2 values are obtained for discharge and flow velocity, while the use of discharge gives a slightly higher R^2 value. When the IM's are compared with respect to efficiency, it is seen that the smallest values of demand dispersion are again obtained from the use of discharge and flow velocity. Nevertheless, when the comparison is made with respect to practicality, the slope of the best line (b) for flow velocity yields is the greatest value, indicating that it is the most practical one among other IM's. When the modified dispersion values are compared, it is seen that the minimum value is obtained from the use of flow velocity, which means that it is the most proficient IM as well. As a conclusion, flow velocity is more successful in satisfying the efficiency, practicality and proficiency criteria, so it is selected as the optimum intensity measure for flood hazard.

Table 4.3: Comparison of different intensity measures for flood hazard

EDP	**IM**	**R^2**	**ln(a)**	**b**	**β_D**	**β_D / b**
Maximum Curvature Ductility Demand	**Flow velocity**	0.856	-8.0806	3.045	0.5136	0.1687
	Flow depth	0.6232	-6.2438	2.0643	0.8314	0.2117
	Normalized flow depth	0.6232	-2.2298	2.0643	0.8314	0.2117
	Froude number	0.3203	-2.6057	2.4596	1.1166	0.1934
	Discharge	0.8707	-14.8567	1.4931	0.4871	0.2690

Apart from the discussion stated above, the same selection for the optimum intensity measure could be made from another point of view. This study investigates the vulnerability of bridges under flood effects including hydrodynamic loads, local scour around piers and debris accumulation. Taking into account of all these effects, the mean flow velocity of a river is as an appropriate intensity measure since it increases with increasing flood discharge and hydrodynamic load and scour depth calculations are functions of the mean flow velocity. Moreover, it should be noted that the selection made is also dependent on the EDP considered in the regression analysis. So, this implies that the maximum curvature ductility of the columns and extended pile shafts is a successful EDP for characterizing the structural response under flood effects. In summary, flow velocity is selected as the optimum intensity measure for flood hazard, which demonstrates the most successful correlation between the flood intensity and bridge response.

4.6.3 Generation of the Flood Fragility Curves

Analytical fragility curves can be produced with describing demand and capacity with their probability distribution and distribution parameters. As mentioned above, the demand and the capacity are assumed to follow lognormal distribution. The median (S_D) and lognormal standard deviation ($\beta_{D|IM}$) of the demand are obtained by establishing the relationship between IM and demand (D) through the PFDM as explained in section 4.6.1. For this purpose, firstly the maximum structural demands of each realization are obtained from the nonlinear static analyses within the simulation framework and then regression analyses are conducted using the MATLAB computer program to calculate the regression parameters *a* and *b* and also $\beta_{D|IM}$ is computed from Equation 4.21.

Defining the capacity model is the second task after determining the demand model. The capacities of bridge components at different damage states should be determined to compare with the demands of the bridge for the procedure of generating the flood fragility curves. For this purpose, the threshold limits and their probability distributions defining the capacity of bridge components can be acquired from the literature. In the present study, the threshold limits described in terms of curvature ductility are adopted from Ramanathan [12] for the capacity definition of the columns and the extended pile shafts.

Ramanathan [12] classified the bridge components in two categories; primary and secondary components. The main idea behind these categories is to assess whether the failure of a component give a major effect on the bridge functionality. So, columns are considered as primary components since the damage to columns can alter the vertical stability and load-carrying capacity of a bridge. In the present study, fragility assessment of the bridge is conducted by evaluating the possible failure of the columns and the extended pile shafts of the studied bridge bent. Since columns and extended pile shafts have the same cross-sectional dimensions and reinforcement details, the same limit states will be applied on both types of elements.

In this thesis, flood fragility curves are generated at four discrete damage states; namely, minor damage state, moderate damage state, extensive damage state, and collapse state. Ramanathan [12] stated the definitions of these damage states for the columns of the bridges constructed after 1990 as shown in Table 4.4. This definition is also applicable for the columns and extended shafts investigated in this study. The values of median (S_C) and lognormal standard deviation (β_C) of the capacity adopted for the generation of the fragility curves are presented in Table 4.5 for different limit states. The lognormal standard deviation of capacity is taken as 0.35 for all damage states.

Table 4.4: Definition of the damage states for post-1990 ductile columns (adopted from Ramanathan [12])

Damage state	**Definition of damage state of columns**	**Repair**
Slight (minor)	Cracking	Seal and paint
Moderate	Minor cover spalling concentrated at the top and bottom of the column	Epoxy injection; minor concrete removal and patch; seal and paint
Extensive (major)	Major spalling; exposed core; confinement yield (no rupture)	Major concrete removal and patch; add Class-F jacket
Complete (collapse state)	Loss of confinement; longitudinal bar buckling or rupture; core crushing; large residual drift	Replace column or bridge

Table 4.5: The limit states of columns and extended pile shafts at different damage states (adopted from Ramanathan [12])

Component	EDP	Median values, S_C				β_C
		Minor	Moderate	Extensive	Collapse	
Columns and extended pile shaft	Curvature ductility	1.0	4.0	8.0	12.0	0.35

The definition of fragility curves as described per Shinozuka et al. [15] is presented in Equation 4.17. In order to find the fragility parameters, λ_k and ζ_k (median and dispersion) of the flood fragility curves, the classical reliability theory is used by considering the assumption that both demand and capacity have lognormal probability distribution. In this approach, the probability of failure at a desired damage state *k* can be written as in the following equation.

$$P_f = P[D > C \mid IM] = \Phi\left(\frac{ln\left(\frac{S_D}{S_C}\right)}{\sqrt{\beta_{D|IM}^2+\beta_C^2}}\right) =$$

$$\Phi\left(\frac{\ln\left(aIM^b\right)-\ln\left(S_C\right)}{\sqrt{\beta_{D|IM}^2+\beta_C^2}}\right) = \Phi\left(\frac{\ln(IM)-\left(\frac{\ln(S_C)-\ln(a)}{b}\right)}{\frac{\sqrt{\beta_{D|IM}^2+\beta_C^2}}{b}}\right) \tag{4.22}$$

The last term in Equation 4.22 can be resembled to the fragility curve definition as demonstrated in Equation 4.23. The fragility parameters λ_k and ζ_k at the damage state k can be calculated from Equations 4.24 and 4.25, respectively.

$$P[LS|\, IM] = \Phi\left(\frac{\ln(IM) - \ln(\lambda_k)}{\zeta_k}\right) \tag{4.23}$$

$$\lambda_k = e^{\frac{\ln(S_{C,k})-\ln(a)}{b}} \tag{4.24}$$

$$\zeta_k = \frac{\sqrt{\beta_D^2 + \beta_{C,k}^2}}{b} \tag{4.25}$$

4.6.4 Flood Fragility Curves of Bridges

The final step within the applied framework is to utilize the PFDM (probabilistic flood demand model) and the capacity model as presented in sections 4.6.1-4.6.3 for generating the flood fragility curves. For this purpose, the fragility parameters of median and dispersion of flood fragility curves are computed through Equations 4.24 and 4.25.

Figures 4.9, 4.10 and 4.11 demonstrate respectively the flood fragility curves developed for the three investigated cases, Case-1 (in the absence of debris accumulation), Case-2 (in the presence of debris accumulation with no definite geometry), and Case-3 (in the presence of debris accumulation with triangular debris raft). The corresponding median and dispersion values of the flood fragility curves for different damage states are also presented in Table 4.6. The median value of a fragility curve corresponds to the flow velocity value at which the probability of exceeding a considered damage state is 50%. Therefore, the smaller the median value, the higher the probability of exceedance (or failure).

Figures 4.9-4.11 show that the bridge becomes more vulnerable to floods as the mean flow velocity increases. For instance, when the fragility curves of the bridge in the presence of debris accumulation with no definite geometry (Figure 4.10) is examined, it is seen that probability of exceeding the minor damage state is 60% for the flow velocity of 15 m/s. This probability rises up to 95% for the flow velocity 20 m/s. This is an obvious outcome indeed, since the applied hydrodynamic loads considerably increase with the increasing flow velocities as the hydrodynamic pressure is proportional to the square of flow velocity as given in Equation 4.13. Bridge piers can fail due to hydraulic loads combined with axial, shear and bending transferred from the superstructure [114]. In addition to the effect of hydrodynamic loading, the increase in bridge fragilities with the increase in flow velocities incorporates the presence of scour as the soil support at foundations is diminished with the increase in scour depths. This is because the possibility of scouring around piers increases as the flow velocity reaches or exceeds the critical flow velocity to starting scouring. Also, the dragging of soil materials to the downstream is exacerbated by increasing water velocity. This phenomenon is naturally taken into account through the use of scour depth estimation equation given in Equation 4.11 where the scour depth is a function of flow velocity.

Within the framework applied in this thesis, the bridge is assumed to be in its intact condition with no scour at the pier foundations prior to the occurrence of a flood event. Therefore, the flood-induced effects of hydrodynamic loading and local scour at pier foundations are considered to act on the bridge simultaneously. However, in real life cases, scour holes from previous floods may not be refilled and a certain level of scour depth may exist before a flood event occurs at the bridge site. But this kind of investigation when the effects of hydrodynamic loading and scour are decoupled is beyond the scope of this thesis.

The flood fragility curves developed in this thesis are pertinent to the considered study bridge and the outcomes may change for a different type of bridge superstructure or pier foundation. For example, if a pile group was used for the foundation instead of extended pile shafts, then the fragility assessment would be conducted separately for the piles and columns, and component-based flood fragility curves would be have to be developed. Yilmaz and Banerjee [107] found that the impact of flood-induced scour on seismic fragility of highway bridges can change depending on the pier foundation type. Therefore, the proposed framework developed in this thesis can be extended to be applied on a study bridge with a different foundation type (e.g. pile group foundation).

Within the scope of this study, it is assumed that the water level in a flood event can rise up to the superstructure level, which means that the maximum water depth is assumed to be equal to the column height ($y_{1,max}$ = 7 m). Therefore, any probable hydrodynamic loading acting on the bridge girder is ignored in the analyses, although a greater hydrodynamic force would appear if the water depth reaches such a high level provided that the whole superstructure is not completely submerged.

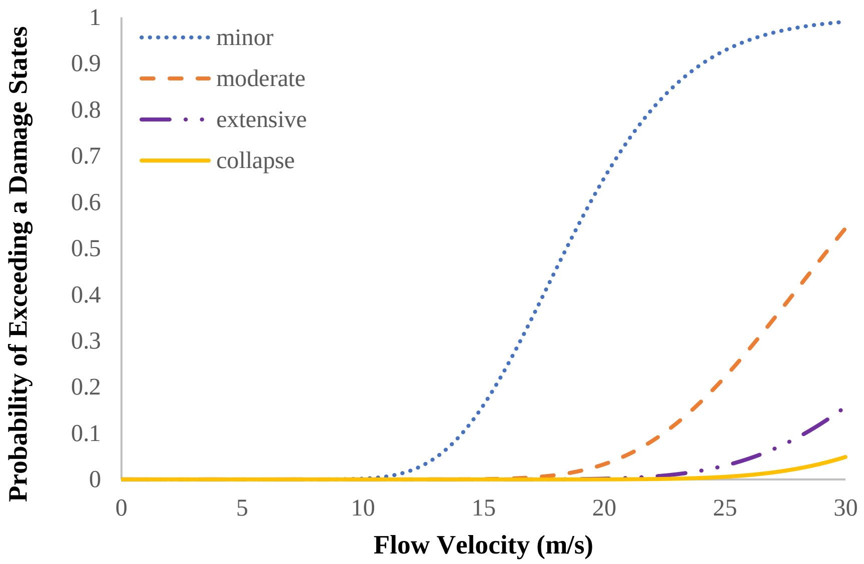

Figure 4.9: Flood fragility curves for Case-1 (in the absence of debris accumulation)

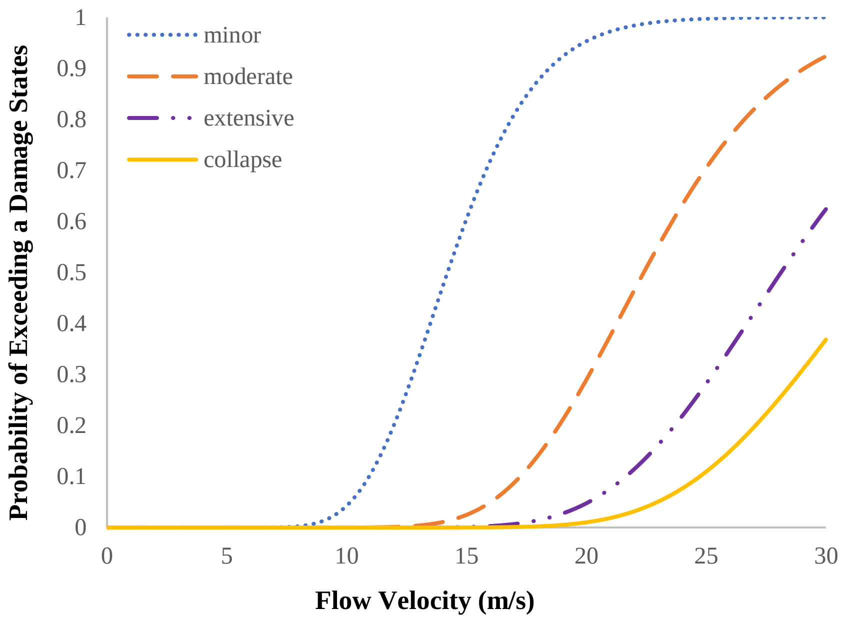

Figure 4.10: Flood fragility curves for Case-2 (in the presence of debris accumulation with no definite geometry)

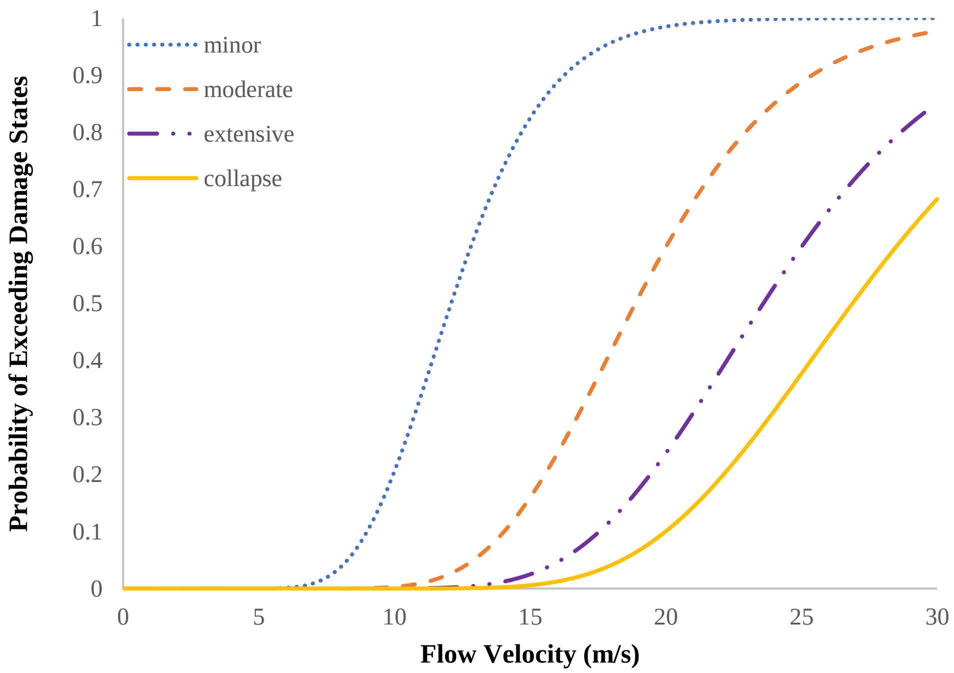

Figure 4.11: Flood fragility curves for Case-3 (in the presence of debris accumulation with triangular debris raft)

Table 4.6: Fragility parameters of flood fragility curves

	λ_k (Median V_1) [m/s]				Dispersion (ζ)
Debris accumulation effects	**Minor damage**	**Moderate damage**	**Extensive damage**	**Collapse**	
Case-1 (no debris accumulation)	18.4	29.3	37.0	42.4	0.208
Case-2 (debris accumulation with no definite geometry)	14.2	22.4	28.1	32.1	0.20
Case-3 (debris accumulation with triangular debris raft)	12.1	18.9	23.6	26.9	0.23

The debris accumulation can make an extra impact on the vulnerability characteristics of bridges subjected to floods since it can increase the effects of hydrodynamic loads and scour depth. The influence of debris accumulation on the flood fragility curves for the three conditions investigated (Case-1, Case-2, Case-3) can be observed from Figure 4.12 and from Table 4.6. It can be concluded that the presence of debris accumulation during floods increases the bridge fragilities enormously. For example, at the flow velocity of 20 m/s, the probability of exceeding moderate damage state is around 3%, 29%, and 60% for Case-1 (in the absence of debris accumulation), Case-2 (in the presence of debris accumulation with no definite geometry) and Case-3 (in the presence of debris accumulation with triangular debris raft), respectively. Also, the comparison between Case-1 and Case-2 shows that the debris accumulation can be very critical for the vulnerability of bridges as it can increase the bridge fragilities about 10 times compared to having no debris accumulation. On the other hand, Case-3 can be regarded as the maximum condition of having the debris accumulation, nevertheless, still it is recommended to consider the obtained results here for the bridge locations subjected to high level of debris accumulation during flood events.

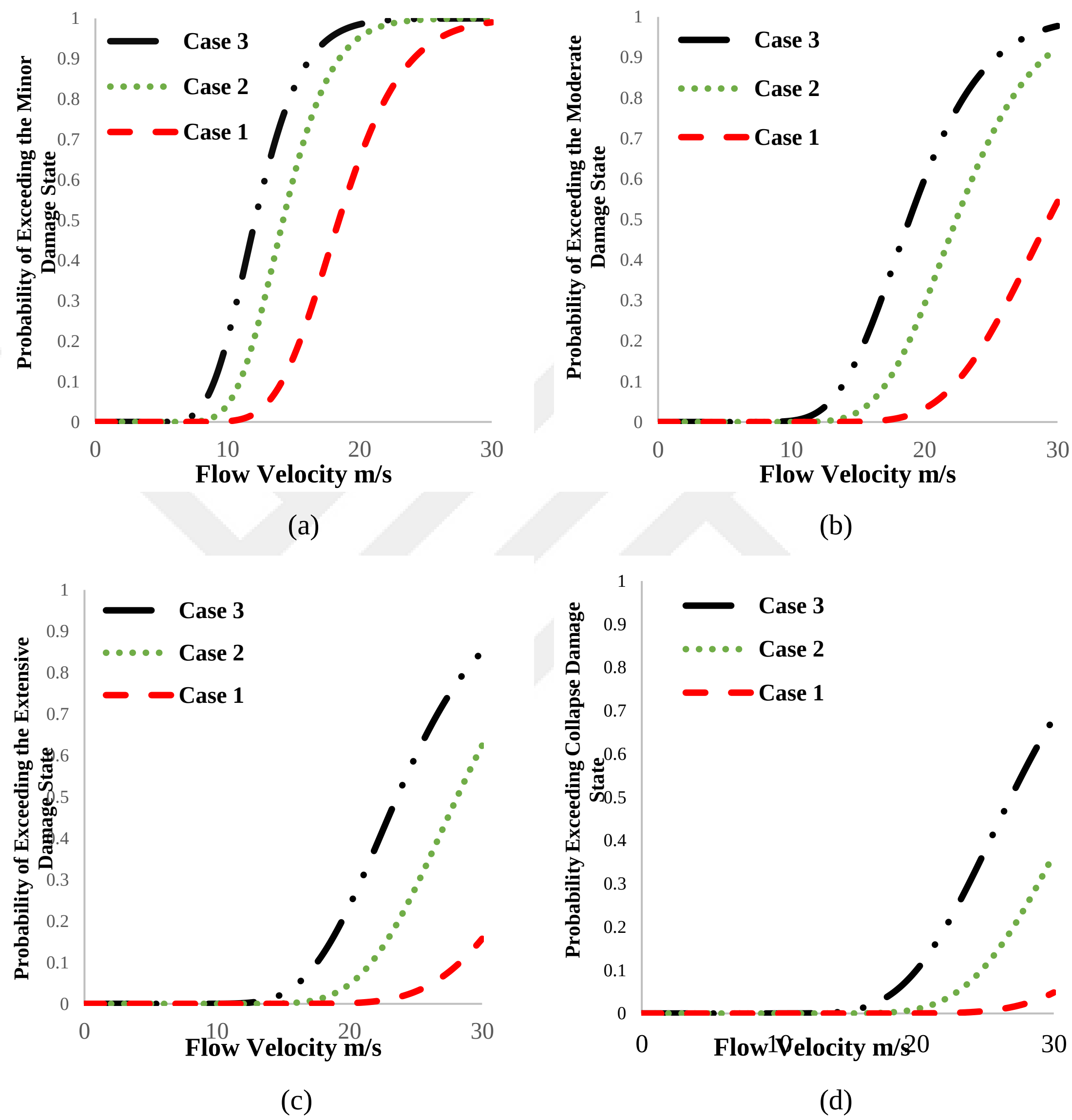

Figure 4.12: Flood fragility curves concerning Case-1, Case-2, Case-3 at different damage states; a) minor, b) moderate, c) extensive, d) collapse

CHAPTER V

CONCLUSION

5.1 Summary of the Thesis

Scouring around bridge piers induced by floods may weaken the stability of a bridge as the lateral support at pier foundations can diminish due to the decrease in the length of piles surrounded by soil. In addition, the debris brought by flood waters from upstream can accumulate in front of the bridge piers and the debris accumulation can exacerbate the scour depths and the hydrodynamic flow pressure exerting on bridge piers. Under the combined effect of flood-induced hydrodynamic loads and scouring of the foundations, bridge piers may undergo large lateral displacements, and this can cause damage on structural members. The socio-economic losses that can result from the failure of bridges exposed to flood hazards necessitates a rigorous assessment of the structural vulnerability of bridges under the single-hazard of floods.

In this thesis, a simulation-based probabilistic framework is developed to assess the reliability of bridges subjected to flood-induced loads and scour. This methodology is implemented on a generic bridge that can represent characteristic river-crossing highway bridges. As the first step of the framework, a sensitivity analysis is performed by considering 14 uncertain parameters that can influence the bridge response under flood effects and using the results of Tornado Diagram analyses, the uncertain parameters which are the most effective on bridge response are determined. Flood discharge, scour modeling factor, Manning roughness coefficient, channel slope, internal friction angle of soil, longitudinal reinforcement ratio, unit weight of concrete, and concrete compressive strength are identified as the key uncertain parameters. Then, Latin Hypercube Sampling technique is employed to create a sample set containing 571 realizations of the bridge model and these realizations are matched with the same number of discharge values incrementally varying from 100 m^3/s to 5800 m^3/s. The scour depths and hydrodynamic load effects are applied on the corresponding bridge models of the sample set and nonlinear static analyses are conducted to obtain the maximum structural demands. The maximum curvature ductility demands of the columns and extended pile shafts and the corresponding flood intensity values are used in a linear regression analysis to model the relation between intensity measure of flood and demand, which is the basis of the proposed 'Probabilistic Flood Demand Model (PFDM)'. The final step in the framework is to compare the PFDM with the accepted capacity model by using the classical reliability theory, so that flood fragility curves are generated. In this study, flood fragility curves are produced for three cases: in the absence of debris accumulation, in the presence of debris accumulation with no definite geometry and in the presence of debris accumulation with triangular debris raft.

5.2 Major Outcomes

1. A simulation-based probabilistic framework is developed to generate "flood fragility curves" to assess the vulnerability of highway bridges subjected to flood-induced loads and scour. These fragility curves can be used to estimate the probability of exceeding different damage states of bridges under a given flood effect. The presented framework is believed to be a novel contribution to the knowledge-base in risk assessment of bridges. Also, the flood fragility curves generated here can be used in future efforts for mitigating the risk imposed on river-crossing highway bridges so that more resilient bridge infrastructure systems can be obtained.
2. Within the developed framework, the approach called "Probabilistic Flood Demand Model (PFDM)" is proposed to model the relation between structural

demands with flood intensity measure values. For the proposed PFDM, flow velocity is found as the ideal flood intensity measure. So, the horizontal axis of flood fragility curves is defined with respect to flow velocity.

3. A flood fragility curve shows that the probability of failure is getting higher with increasing flow velocity as a result of the simultaneous application of increasing scour depth at pier foundations and hydrodynamic load acting on piers. For example, a bridge sustaining minor damage for a flow velocity of 20 m/s may get moderate damage when the flow velocity is increased to 30 m/s.
4. The accumulation of debris in front of bridge piers during floods is found to be increasing bridge fragilities substantially. This is because debris accumulation can aggravate scour depths and hydrodynamic loads with the enlarged projection area of piers exposed to flow. This effect is more pronounced when a definite debris raft geometry exists.

5.3 Recommendations for Future Studies

1. The drag coefficient used in calculation of hydrodynamic pressure contains a high level of uncertainty that can have a major effect on bridge response. This coefficient can be incorporated into the sensitivity analysis and Latin hypercube sampling design in future studies. Hence, the uncertainty in debris accumulation effects can be quantified and a separate flood fragility curve propagating the uncertainty in this coefficient can be generated.
2. This thesis presents only the reliability analysis of a bridge with extended pile shaft foundation. The suggested probabilistic framework can be applied for other types of pier foundations including pile group and shallow foundations.
3. In this study, only the flexural damage of columns and extended pile shafts are considered to represent the main bridge failure mode to generate the fragility

curves. Other failure modes including the shear failure of bridge pier, deck loss, geotechnical failure including tilting of piles may be investigated in future and fragility curves associated with these failure modes can be created.

4. This study is carried out with a 2-D bridge bent model by only considering the bridge response in the transverse direction of the bridge. The whole analysis framework can be repeated by using a 3-D model to capture a more accurate bridge response. Also, this can enable the incorporation of different flow angle of attack into this model.
5. Geometric uncertainties are not taken into account in the current study. Column and pile diameter, lengths of columns and extended pile shafts, distance between the two columns can be considered as uncertain parameters within the reliability framework.
6. The flood fragility curves generated in this thesis can be employed to evaluate the risk of a real-life bridge in a flood-prone region (e.g. Black Sea region in Turkey). For this purpose, flood hazard curve at the bridge location can be obtained by using a site-specific study. Then, for the flood discharges that may arise from the flood events with different return periods, the corresponding damage probability of the bridge can be computed through the flood fragility curves.

APPENDIX A

VALIDATION OF MODEL

The large-scale experimental response of a cantilever column under the full cyclic loads in both directions is compared with its analytical response for the validation of the modeling concept. The data in experiments is obtained from PEER Structural Performance Database. The column with the same material and geometric properties under the same boundary conditions which is referred to as Moyer and Kowalsky 2003 [128] modelled in OpenSees by utilizing the displacement-based fiber elements. And also, the same loading process with the experiments is applied to this analytical model. Figure A-2 shows that the analytical model used in the present study is compatible with the results of experiments.

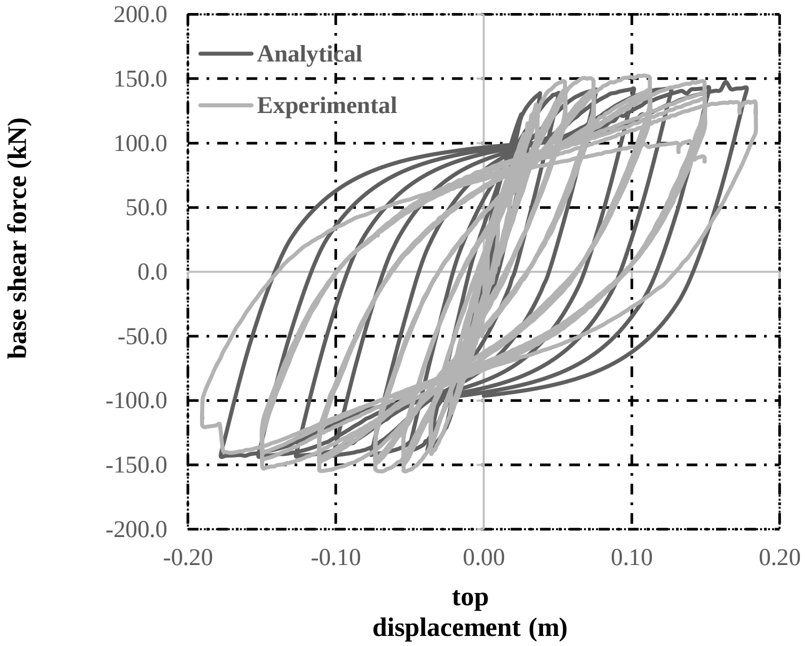

Figure A.1: The validation of the OpenSees Model with the experimental study of Moyer and Kowalsky 2003 [128]

APPENDIX B

THE EQUATIONS OF COEFFICIENTS C1, C2, C3, AND K

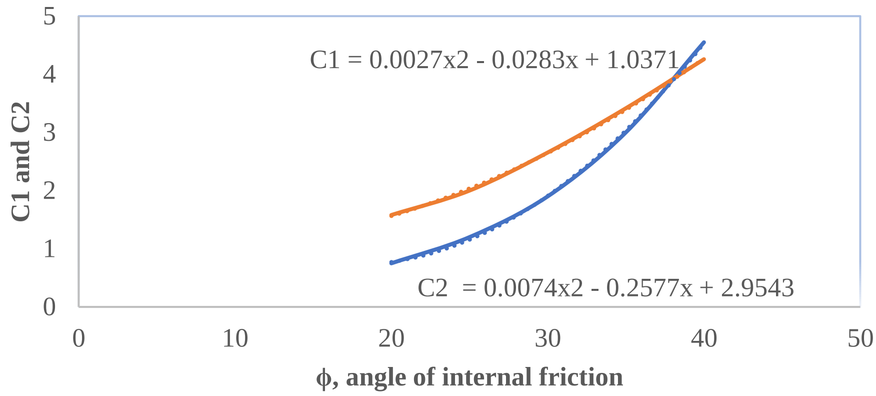

Figure B.1: The coefficients of C1 and C2

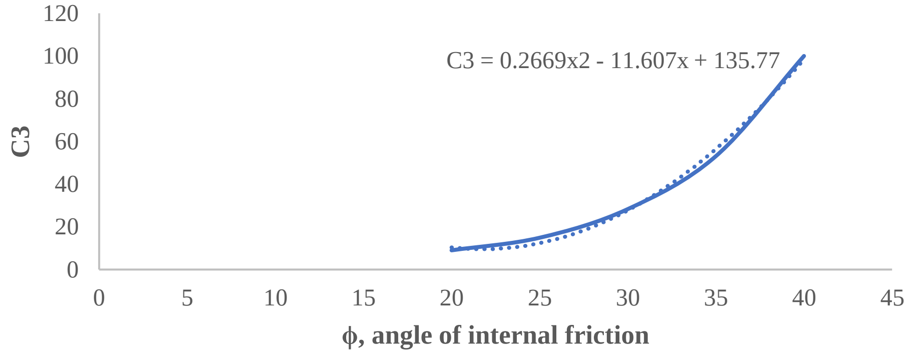

Figure B.2: The coefficient of C3

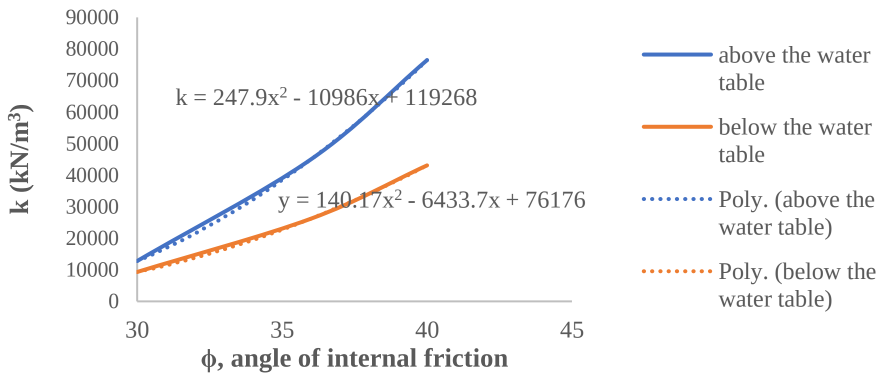

Figure B.3: The initial modulus of subgrade reaction

APPENDIX C

SENSITIVITY ANALYSIS

Table C.1: Lower and upper boundaries of the uncertain parameters for sensitivity analysis

		γ_{conc}	γ_{ws}	E_s	**Fc,sub**	**Fye**	**ρlong**	**ϕsoil**	**γsoil**	K_2	K_3	**S**	**n**	λ_{sc}	**Q**
Realization	unit	t/m^3	t/m^3	GPa	MPa	MPa	-	degree	kN/m^3	-	-	-	-	-	m^3/s
1	Mean Values	2.4	2.2	190	32.5	473	0.025	35	18.64	1.25	1.1	0.00194	0.0241	0.55	3500
2	Lower γ_{conc}	2.16	2.2	190	32.5	473	0.025	35	18.64	1.25	1.1	0.00194	0.0241	0.55	3500
3	Upper γ_{conc}	2.64	2.2	190	32.5	473	0.025	35	18.64	1.25	1.1	0.00194	0.0241	0.55	3500
4	Lower γ_{ws}	2.4	1.1	190	32.5	473	0.025	35	18.64	1.25	1.1	0.00194	0.0241	0.55	3500
5	Upper γ_{ws}	2.4	3.3	190	32.5	473	0.025	35	18.64	1.25	1.1	0.00194	0.0241	0.55	3500
6	Lower E_s	2.4	2.2	186	32.5	473	0.025	35	18.64	1.25	1.1	0.00194	0.0241	0.55	3500
7	Upper E_s	2.4	2.2	194	32.5	473	0.025	35	18.64	1.25	1.1	0.00194	0.0241	0.55	3500
8	Lower Fc,sub	2.4	2.2	190	24.375	473	0.025	35	18.64	1.25	1.1	0.00194	0.0241	0.55	3500
9	Upper Fc,sub	2.4	2.2	190	40.625	473	0.025	35	18.64	1.25	1.1	0.00194	0.0241	0.55	3500
10	lower F_{ye}	2.4	2.2	190	32.5	403	0.025	35	18.64	1.25	1.1	0.00194	0.0241	0.55	3500
11	Upper F_{ye}	2.4	2.2	190	32.5	555	0.025	35	18.64	1.25	1.1	0.00194	0.0241	0.55	3500
12	Lower ρlong	2.4	2.2	190	32.5	473	0.01	35	18.64	1.25	1.1	0.00194	0.0241	0.55	3500
13	Upper ρlong	2.4	2.2	190	32.5	473	0.04	35	18.64	1.25	1.1	0.00194	0.0241	0.55	3500
14	Lower ϕsoil	2.4	2.2	190	32.5	473	0.025	26.6	18.64	1.25	1.1	0.00194	0.0241	0.55	3500

15	Upper ϕsoil	2.4	2.2	190	32.5	473	0.025	43.4	18.64	1.25	1.1	0.00194	0.0241	0.55	3500
16	Lower γsoil	2.4	2.2	190	32.5	473	0.025	35	14.912	1.25	1.1	0.00194	0.0241	0.55	3500
17	Upper γsoil	2.4	2.2	190	32.5	473	0.025	35	22.368	1.25	1.1	0.00194	0.0241	0.55	3500
18	Lower K_2	2.4	2.2	190	32.5	473	0.025	35	18.64	1	1.1	0.00194	0.0241	0.55	3500
19	Upper K_2	2.4	2.2	190	32.5	473	0.025	35	18.64	1.5	1.1	0.00194	0.0241	0.55	3500
20	Lower K_3	2.4	2.2	190	32.5	473	0.025	35	18.64	1.25	0.99	0.00194	0.0241	0.55	3500
21	Upper K_3	2.4	2.2	190	32.5	473	0.025	35	18.64	1.25	1.21	0.00194	0.0241	0.55	3500
22	Lower S	2.4	2.2	190	32.5	473	0.025	35	18.64	1.25	1.1	0.00119	0.0241	0.55	3500
23	Upper S	2.4	2.2	190	32.5	473	0.025	35	18.64	1.25	1.1	0.003175	0.0241	0.55	3500
24	Lower n	2.4	2.2	190	32.5	473	0.025	35	18.64	1.25	1.1	0.00194	0.01405	0.55	3500
25	Upper n	2.4	2.2	190	32.5	473	0.025	35	18.64	1.25	1.1	0.00194	0.04136	0.55	3500
26	Lower λ_{sc}	2.4	2.2	190	32.5	473	0.025	35	18.64	1.25	1.1	0.00194	0.0241	0.01	3500
27	Upper λ_{sc}	2.4	2.2	190	32.5	473	0.025	35	18.64	1.25	1.1	0.00194	0.0241	1.112	3500
28	Lower Q	2.4	2.2	190	32.5	473	0.025	35	18.64	1.25	1.1	0.00194	0.0241	0.55	300
29	Upper Q	2.4	2.2	190	32.5	473	0.025	35	18.64	1.25	1.1	0.00194	0.0241	0.55	6000

Table C.2: The results of tornado diagram analysis concerning maximum curvature ductility of piers

Uncertainties	Mean: 0.03698149		
	Lower	Upper	Differences
Q	0.001210552	0.10705	0.10583928
n	0.059062174	0.030412	0.02865021
λsc	0.02066711	0.039924	0.01925695
ϕ soil	0.047924063	0.033967	0.01395726
ρ long	0.045116421	0.031483	0.01363306
S	0.032302118	0.044353	0.01205116
fye	0.04279956	0.03246	0.01033925
γconc	0.040850878	0.03373	0.00712084
K2	0.033310299	0.039924	0.00661376
fce,sub	0.03956044	0.035016	0.00454435
K3	0.035146464	0.038925	0.00377902
γsoil	0.037828192	0.036695	0.00113299
Es	0.036411354	0.037448	0.00103652
γws	0.036934409	0.037026	9.1125E-05

Table C.3: The results of tornado diagram analysis concerning maximum displacement of piers

Uncertainties	Mean: 0.00884129		
	Lower	Upper	Difference
Q	0.000257	0.0257859	0.02552938
λsc	0.01006	0.00025652	0.00980328
n	0.014856	6.53E-03	0.00832826
ϕ soil	0.014272	0.00668517	0.00758643
S	0.007198	0.0111251	0.00392754
K2	0.007413	0.0100598	0.00264685
ρ long	0.00984	0.00806326	0.0017767
K3	0.008114	0.00964069	0.00152633
γconc	0.009613	0.00818535	0.00142811
fce,sub	0.009648	0.0082549	0.00139348
γsoil	0.009193	0.00872431	0.00046844
Es	0.008872	0.0088107	6.133E-05
γws	0.008832	0.00885032	1.825E-05
fye	0.008839	0.0088431	4.27E-06

APPENDIX D

LATIN HYPERCUBE SAMPLING DESIGN

The sample-set is designed with the seven significant parameters impacting the response of the bridge, and then the flow discharge value is increased incrementally through the sample set.

Table D.1: Latin hypercube sampling design

Analysis Name	$f_{ce\ sub}$	λ_{sc}	n	S	ρ_{long}	ϕ_{soil}	γ_{conc}	Discharge
1	34.9	0.74	0.026	0.0023	0.0407	33.5	2.34	100
2	40.1	0.34	0.032	0.0021	0.0363	32.9	2.48	110
3	23.1	0.42	0.031	0.0013	0.0093	39.1	2.58	120
4	36.3	0.34	0.021	0.0027	0.0229	35.2	2.21	130
5	33.9	0.71	0.023	0.0016	0.0149	32.6	2.61	140
6	27.3	0.32	0.029	0.0016	0.0276	38.8	2.56	150
7	30.8	0.23	0.025	0.0012	0.0506	33.2	2.41	160
8	34.0	0.70	0.032	0.0019	0.0133	41.5	2.59	170
9	46.4	0.41	0.019	0.0019	0.0490	32.6	2.42	180
10	42.7	0.65	0.027	0.0018	0.0189	32.8	2.28	190
11	27.0	0.44	0.026	0.0015	0.0163	32.7	2.54	200
12	43.9	0.62	0.033	0.0011	0.0323	36.9	2.68	210
13	35.7	0.30	0.015	0.0034	0.0334	40.7	2.31	220
14	32.4	0.68	0.024	0.0027	0.0281	37.0	2.28	230
15	35.6	1.05	0.024	0.0017	0.0065	38.5	2.54	240
16	31.8	0.85	0.008	0.0018	0.0159	40.3	2.39	250
17	32.2	0.81	0.032	0.0021	0.0135	34.8	2.24	260
18	38.7	0.48	0.043	0.0019	0.0183	39.1	2.56	270
19	38.4	0.59	0.022	0.0017	0.0144	34.8	2.38	280
20	38.5	0.61	0.026	0.0024	0.0300	43.7	2.31	290
21	35.5	0.57	0.021	0.0014	0.0366	36.4	2.33	300
22	27.6	0.30	0.027	0.0029	0.0221	33.0	2.34	310
23	35.6	0.44	0.021	0.0011	0.0316	35.7	2.52	320
24	39.3	0.49	0.023	0.0018	0.0341	32.1	2.26	330
25	34.7	0.40	0.034	0.0023	0.0265	28.9	2.45	340
26	37.2	0.80	0.018	0.0020	0.0220	36.9	2.52	350
27	35.7	1.20	0.020	0.0012	0.0179	36.2	2.30	360
28	31.3	0.17	0.023	0.0024	0.0104	38.1	2.44	370

29	33.7	0.57	0.023	0.0020	0.0219	31.6	2.19	380
30	29.4	0.14	0.033	0.0015	0.0269	31.7	2.48	390
31	36.4	0.92	0.037	0.0021	0.0228	33.2	2.26	400
32	28.0	0.95	0.017	0.0023	0.0273	30.8	2.50	410
33	28.3	0.05	0.019	0.0030	0.0256	46.5	2.45	420
34	29.4	1.08	0.028	0.0019	0.0329	37.0	2.35	430
35	21.5	0.22	0.021	0.0018	0.0166	32.5	2.22	440
36	38.6	0.61	0.037	0.0017	0.0234	37.3	2.56	450
37	34.0	0.87	0.035	0.0010	0.0277	40.2	2.42	460
38	29.6	0.58	0.028	0.0022	0.0202	38.1	2.60	470
39	38.2	1.14	0.028	0.0009	0.0282	39.0	2.40	480
40	25.6	1.27	0.021	0.0018	0.0028	37.4	2.18	490
41	32.2	0.58	0.029	0.0018	0.0305	28.9	2.60	500
42	31.6	0.00	0.032	0.0023	0.0306	32.0	2.36	510
43	33.9	0.43	0.025	0.0004	0.0249	39.5	2.51	520
44	33.9	0.30	0.036	0.0024	0.0206	34.4	2.31	530
45	29.2	0.33	0.029	0.0017	0.0193	36.4	2.47	540
46	32.5	0.21	0.023	0.0013	0.0038	37.8	2.50	550
47	32.0	0.56	0.027	0.0019	0.0379	30.7	2.52	560
48	35.3	1.11	0.031	0.0020	0.0326	36.0	2.46	570
49	37.4	0.33	0.021	0.0017	0.0113	33.5	2.39	580
50	37.5	0.46	0.023	0.0012	0.0064	29.1	2.41	590
51	29.2	0.89	0.040	0.0025	0.0200	37.1	2.43	600
52	32.9	0.90	0.021	0.0020	0.0331	31.6	2.31	610
53	27.6	0.68	0.030	0.0016	0.0346	33.1	2.46	620
54	28.2	0.84	0.030	0.0025	0.0313	29.7	2.27	630
55	32.6	0.80	0.034	0.0021	0.0341	32.7	2.16	640
56	39.0	0.43	0.028	0.0013	0.0454	37.3	2.42	650
57	29.5	0.67	0.007	0.0022	0.0039	41.8	2.42	660
58	34.1	0.45	0.018	0.0010	0.0306	30.4	2.42	670
59	31.7	0.28	0.028	0.0014	0.0241	36.9	2.61	680
60	37.5	0.73	0.026	0.0020	0.0148	37.6	2.56	690
61	28.3	0.56	0.037	0.0021	0.0336	39.5	2.63	700
62	32.7	0.49	0.033	0.0020	0.0248	40.4	2.42	710
63	35.0	0.63	0.027	0.0010	0.0391	30.5	2.51	720
64	37.4	0.83	0.024	0.0023	0.0118	35.5	2.33	730
65	39.0	0.65	0.014	0.0026	0.0138	40.2	2.37	740
66	32.9	0.60	0.036	0.0025	0.0301	37.7	2.18	750
67	26.4	0.62	0.025	0.0017	0.0133	41.1	2.40	760
68	29.6	0.55	0.014	0.0017	0.0263	40.2	2.51	770
69	28.4	0.32	0.027	0.0014	0.0198	45.1	2.27	780
70	41.4	0.78	0.025	0.0020	0.0379	24.5	2.37	790
71	30.1	0.95	0.020	0.0021	0.0302	33.9	2.31	800
72	35.8	0.38	0.027	0.0015	0.0197	33.9	2.31	810
73	31.9	1.08	0.019	0.0024	0.0165	29.3	2.51	820

74	36.5	0.49	0.015	0.0023	0.0197	33.1	2.40	830
75	29.5	0.47	0.012	0.0022	0.0557	41.2	2.49	840
76	26.8	0.28	0.021	0.0016	0.0241	35.4	2.45	850
77	26.7	0.32	0.020	0.0013	0.0225	39.2	2.52	860
78	34.7	0.26	0.027	0.0022	0.0226	42.1	2.12	870
79	32.0	0.64	0.014	0.0026	0.0425	34.1	2.28	880
80	31.9	0.99	0.022	0.0013	0.0036	33.6	2.38	890
81	38.5	0.70	0.014	0.0008	0.0382	29.8	2.44	900
82	33.7	0.80	0.035	0.0026	0.0155	34.1	2.54	910
83	33.4	0.94	0.023	0.0019	0.0219	32.3	2.32	920
84	39.1	0.25	0.032	0.0025	0.0330	34.4	2.33	930
85	29.4	0.50	0.027	0.0024	0.0129	34.4	2.36	940
86	35.6	0.64	0.030	0.0013	0.0300	32.2	2.48	950
87	36.1	0.75	0.016	0.0017	0.0238	30.4	2.41	960
88	31.6	0.17	0.032	0.0015	0.0072	33.7	2.54	970
89	33.5	0.24	0.034	0.0020	0.0271	35.2	2.31	980
90	27.9	0.78	0.009	0.0025	0.0320	31.4	2.45	990
91	28.0	0.51	0.023	0.0019	0.0326	36.9	2.44	1000
92	33.0	0.71	0.019	0.0009	0.0176	34.8	2.19	1010
93	35.7	0.25	0.025	0.0026	0.0246	34.2	2.43	1020
94	42.1	0.07	0.018	0.0019	0.0324	39.0	2.61	1030
95	29.9	0.77	0.026	0.0017	0.0313	44.5	2.26	1040
96	33.4	0.90	0.028	0.0009	0.0199	38.8	2.32	1050
97	32.3	1.01	0.026	0.0021	0.0090	38.1	2.28	1060
98	24.8	0.10	0.023	0.0020	0.0280	35.2	2.54	1070
99	30.7	0.16	0.015	0.0021	0.0286	35.8	2.33	1080
100	25.3	0.12	0.024	0.0014	0.0423	37.9	2.49	1090
101	36.2	0.53	0.020	0.0016	0.0058	32.9	2.19	1100
102	29.1	0.36	0.015	0.0015	0.0206	29.0	2.17	1110
103	33.0	0.93	0.023	0.0028	0.0302	37.3	2.52	1120
104	30.4	0.13	0.022	0.0015	0.0235	32.3	2.47	1130
105	33.8	0.03	0.025	0.0018	0.0496	37.2	2.43	1140
106	30.1	0.60	0.031	0.0015	0.0203	31.7	2.52	1150
107	34.7	0.90	0.028	0.0024	0.0044	30.1	2.40	1160
108	35.7	0.31	0.032	0.0019	0.0337	29.5	2.41	1170
109	39.5	0.18	0.019	0.0020	0.0071	36.6	2.30	1180
110	31.9	0.50	0.018	0.0024	0.0409	43.0	2.40	1190
111	23.9	0.06	0.023	0.0022	0.0296	36.1	2.27	1200
112	29.3	0.55	0.033	0.0023	0.0209	37.5	2.30	1210
113	38.2	0.79	0.032	0.0009	0.0125	35.9	2.34	1220
114	28.3	0.60	0.023	0.0020	0.0467	36.2	2.41	1230
115	36.8	0.00	0.020	0.0024	0.0284	45.2	2.60	1240
116	33.1	0.38	0.014	0.0021	0.0185	31.9	2.44	1250
117	38.5	0.45	0.029	0.0024	0.0159	34.7	2.45	1260
118	24.6	1.04	0.024	0.0030	0.0229	32.4	2.46	1270

119	31.8	0.82	0.016	0.0026	0.0401	38.3	2.55	1280
120	27.6	0.52	0.022	0.0014	0.0477	36.4	2.47	1290
121	43.5	0.93	0.011	0.0015	0.0253	33.9	2.40	1300
122	36.1	0.23	0.027	0.0018	0.0300	38.4	2.35	1310
123	38.3	0.44	0.023	0.0016	0.0286	30.9	2.47	1320
124	28.4	0.95	0.035	0.0019	0.0046	35.8	2.18	1330
125	30.6	0.97	0.015	0.0026	0.0265	36.1	2.40	1340
126	31.5	0.76	0.031	0.0017	0.0184	41.8	2.52	1350
127	37.4	0.68	0.025	0.0018	0.0194	37.7	2.37	1360
128	31.4	0.37	0.024	0.0018	0.0231	35.3	2.47	1370
129	35.6	0.76	0.029	0.0022	0.0097	29.7	2.42	1380
130	24.3	0.30	0.032	0.0024	0.0152	29.1	2.47	1390
131	31.1	0.71	0.016	0.0018	0.0340	37.9	2.34	1400
132	29.3	0.62	0.033	0.0018	0.0263	32.3	2.60	1410
133	26.1	0.88	0.016	0.0024	0.0183	34.3	2.45	1420
134	34.8	0.41	0.016	0.0023	0.0210	31.5	2.41	1430
135	33.7	0.73	0.019	0.0022	0.0114	36.0	2.26	1440
136	32.7	0.78	0.029	0.0035	0.0158	36.2	2.37	1450
137	27.1	0.28	0.017	0.0019	0.0172	42.3	2.23	1460
138	37.5	0.58	0.026	0.0021	0.0228	42.5	2.36	1470
139	34.1	1.00	0.027	0.0019	0.0321	39.5	2.25	1480
140	31.3	0.57	0.025	0.0022	0.0245	39.7	2.39	1490
141	32.7	0.45	0.028	0.0017	0.0237	30.3	2.42	1500
142	31.5	0.67	0.016	0.0024	0.0140	40.5	2.34	1510
143	25.4	0.46	0.031	0.0029	0.0361	31.1	2.60	1520
144	31.4	0.67	0.025	0.0020	0.0276	28.6	2.57	1530
145	29.3	0.51	0.029	0.0019	0.0317	47.8	2.57	1540
146	28.8	0.53	0.017	0.0017	0.0274	36.7	2.47	1550
147	27.9	0.68	0.024	0.0017	0.0343	32.5	2.50	1560
148	30.4	0.94	0.030	0.0011	0.0423	35.2	2.32	1570
149	24.4	0.67	0.031	0.0019	0.0194	35.5	2.41	1580
150	36.8	1.02	0.023	0.0015	0.0315	26.4	2.26	1590
151	34.8	0.03	0.011	0.0026	0.0330	32.3	2.42	1600
152	32.5	0.41	0.016	0.0020	0.0247	37.6	2.54	1610
153	32.5	0.61	0.025	0.0019	0.0480	35.3	2.27	1620
154	29.4	0.30	0.029	0.0026	0.0126	28.5	2.37	1630
155	37.0	0.18	0.027	0.0011	0.0185	33.2	2.23	1640
156	32.1	0.73	0.020	0.0021	0.0257	34.7	2.47	1650
157	29.8	0.72	0.038	0.0014	0.0252	35.6	2.56	1660
158	38.2	0.63	0.024	0.0016	0.0224	28.3	2.54	1670
159	31.7	0.65	0.030	0.0021	0.0187	36.4	2.28	1680
160	30.2	0.29	0.021	0.0024	0.0344	41.6	2.32	1690
161	31.3	0.39	0.016	0.0015	0.0240	28.7	2.38	1700
162	29.3	0.51	0.029	0.0022	0.0142	37.3	2.35	1710
163	28.1	0.34	0.031	0.0027	0.0452	40.9	2.34	1720

164	41.9	0.64	0.036	0.0015	0.0355	37.1	2.10	1730
165	39.3	1.16	0.020	0.0015	0.0422	37.9	2.48	1740
166	33.8	0.40	0.013	0.0019	0.0244	33.3	2.37	1750
167	27.4	0.73	0.034	0.0022	0.0484	34.5	2.48	1760
168	29.2	0.23	0.026	0.0019	0.0356	30.4	2.43	1770
169	32.0	0.93	0.016	0.0015	0.0026	34.9	2.05	1780
170	35.9	0.25	0.020	0.0020	0.0091	33.0	2.36	1790
171	27.1	0.60	0.019	0.0020	0.0320	32.5	2.50	1800
172	22.6	0.36	0.032	0.0017	0.0234	41.3	2.53	1810
173	26.6	0.69	0.028	0.0014	0.0231	34.9	2.36	1820
174	34.0	0.54	0.026	0.0021	0.0374	38.0	2.46	1830
175	34.2	0.53	0.025	0.0019	0.0449	37.1	2.42	1840
176	34.6	1.30	0.018	0.0017	0.0295	30.8	2.51	1850
177	32.2	0.35	0.031	0.0016	0.0264	27.1	2.63	1860
178	33.4	0.53	0.026	0.0017	0.0510	29.3	2.29	1870
179	30.6	1.21	0.022	0.0015	0.0247	36.5	2.65	1880
180	36.3	0.21	0.022	0.0014	0.0191	34.1	2.42	1890
181	27.0	0.71	0.023	0.0026	0.0171	38.4	2.31	1900
182	34.6	0.22	0.018	0.0018	0.0151	33.7	2.30	1910
183	29.3	0.85	0.029	0.0011	0.0258	29.8	2.41	1920
184	31.1	0.64	0.033	0.0017	0.0136	35.7	2.41	1930
185	35.0	0.74	0.040	0.0025	0.0016	39.8	2.45	1940
186	37.2	0.46	0.028	0.0017	0.0086	36.5	2.50	1950
187	28.2	0.61	0.018	0.0028	0.0302	34.5	2.44	1960
188	38.0	0.97	0.025	0.0015	0.0376	33.6	2.28	1970
189	35.5	0.18	0.017	0.0016	0.0393	40.5	2.32	1980
190	32.4	0.07	0.020	0.0014	0.0528	39.0	2.31	1990
191	31.9	0.66	0.019	0.0025	0.0114	33.5	2.33	2000
192	31.7	0.35	0.018	0.0016	0.0412	29.7	2.44	2010
193	31.3	0.45	0.027	0.0021	0.0258	31.3	2.44	2020
194	32.7	0.12	0.016	0.0012	0.0189	36.8	2.37	2030
195	32.8	0.28	0.029	0.0016	0.0194	30.5	2.28	2040
196	36.1	0.42	0.030	0.0022	0.0354	33.7	2.36	2050
197	38.9	0.33	0.031	0.0013	0.0328	34.9	2.47	2060
198	34.6	0.29	0.024	0.0019	0.0027	32.5	2.38	2070
199	31.8	0.42	0.028	0.0022	0.0368	32.7	2.58	2080
200	35.3	0.26	0.035	0.0028	0.0344	34.3	2.30	2090
201	33.4	0.94	0.024	0.0022	0.0223	33.0	2.43	2100
202	28.6	0.25	0.023	0.0024	0.0124	29.7	2.54	2110
203	36.7	1.05	0.035	0.0018	0.0145	38.4	2.30	2120
204	33.8	0.43	0.007	0.0016	0.0093	31.2	2.39	2130
205	33.2	0.13	0.021	0.0019	0.0241	39.4	2.25	2140
206	34.8	0.36	0.040	0.0015	0.0199	33.8	2.29	2150
207	33.6	0.82	0.021	0.0025	0.0214	34.0	2.23	2160
208	28.9	0.85	0.020	0.0023	0.0274	40.6	2.29	2170

209	32.1	0.59	0.016	0.0024	0.0217	36.4	2.44	2180
210	32.1	0.63	0.029	0.0026	0.0044	33.7	2.37	2190
211	30.4	0.73	0.009	0.0019	0.0170	31.7	2.47	2200
212	39.4	0.13	0.019	0.0016	0.0182	33.1	2.53	2210
213	29.1	0.37	0.028	0.0022	0.0036	37.2	2.44	2220
214	30.6	0.02	0.024	0.0025	0.0353	38.8	2.50	2230
215	29.8	0.41	0.028	0.0023	0.0028	35.4	2.49	2240
216	27.7	0.82	0.025	0.0024	0.0299	33.2	2.70	2250
217	31.9	0.76	0.029	0.0027	0.0218	36.8	2.49	2260
218	31.5	1.14	0.015	0.0021	0.0204	38.1	2.22	2270
219	38.9	0.59	0.025	0.0025	0.0327	33.6	2.43	2280
220	31.6	0.08	0.013	0.0019	0.0215	41.3	2.48	2290
221	28.4	1.03	0.029	0.0023	0.0224	33.7	2.52	2300
222	39.2	0.91	0.022	0.0012	0.0134	39.0	2.50	2310
223	37.9	0.37	0.028	0.0027	0.0385	39.2	2.34	2320
224	31.7	0.61	0.020	0.0011	0.0363	35.4	2.40	2330
225	26.3	0.77	0.026	0.0020	0.0331	35.0	2.44	2340
226	30.7	0.65	0.031	0.0018	0.0312	38.9	2.42	2350
227	32.1	0.75	0.010	0.0014	0.0337	27.5	2.64	2360
228	33.6	0.51	0.011	0.0021	0.0332	35.3	2.20	2370
229	31.5	0.53	0.011	0.0021	0.0295	35.5	2.51	2380
230	34.6	0.56	0.030	0.0026	0.0325	37.0	2.55	2390
231	34.2	0.32	0.027	0.0020	0.0157	31.4	2.33	2400
232	27.4	0.96	0.019	0.0022	0.0253	29.4	2.46	2410
233	28.9	0.54	0.034	0.0020	0.0316	24.1	2.39	2420
234	29.6	0.75	0.025	0.0027	0.0154	37.7	2.28	2430
235	30.5	0.29	0.013	0.0025	0.0250	39.6	2.41	2440
236	31.2	0.23	0.017	0.0019	0.0227	33.4	2.60	2450
237	32.6	0.52	0.015	0.0020	0.0398	45.5	2.35	2460
238	20.9	0.47	0.030	0.0028	0.0307	32.6	2.48	2470
239	30.7	0.90	0.020	0.0018	0.0378	29.9	2.26	2480
240	38.0	0.72	0.016	0.0023	0.0324	34.8	2.29	2490
241	28.3	0.70	0.020	0.0015	0.0365	35.7	2.25	2500
242	36.7	0.14	0.018	0.0016	0.0236	38.2	2.23	2510
243	34.1	0.25	0.030	0.0023	0.0262	35.8	2.29	2520
244	32.5	0.60	0.027	0.0022	0.0167	32.0	2.29	2530
245	33.4	0.44	0.026	0.0025	0.0294	28.9	2.35	2540
246	26.1	0.92	0.027	0.0016	0.0647	32.8	2.19	2550
247	32.3	0.93	0.024	0.0024	0.0260	29.6	2.34	2560
248	39.2	0.37	0.017	0.0020	0.0242	38.3	2.31	2570
249	33.0	0.80	0.028	0.0019	0.0348	34.9	2.31	2580
250	32.7	0.95	0.018	0.0028	0.0057	27.1	2.36	2590
251	29.7	0.63	0.016	0.0026	0.0385	37.0	2.55	2600
252	32.5	1.01	0.016	0.0007	0.0137	31.2	2.39	2610
253	33.5	0.86	0.030	0.0021	0.0318	40.9	2.45	2620

254	34.5	0.60	0.031	0.0015	0.0281	35.4	2.59	2630
255	31.0	0.81	0.012	0.0018	0.0239	36.2	2.48	2640
256	31.6	0.60	0.023	0.0016	0.0156	31.9	2.41	2650
257	40.6	0.42	0.026	0.0027	0.0298	37.6	2.53	2660
258	23.2	0.64	0.020	0.0026	0.0384	35.5	2.67	2670
259	41.2	0.55	0.029	0.0022	0.0331	36.2	2.34	2680
260	34.0	0.43	0.026	0.0023	0.0416	34.0	2.51	2690
261	37.0	1.03	0.023	0.0022	0.0074	38.1	2.30	2700
262	25.7	0.61	0.020	0.0023	0.0252	25.2	2.25	2710
263	30.2	1.24	0.029	0.0020	0.0077	35.9	2.32	2720
264	31.4	0.45	0.030	0.0018	0.0262	39.5	2.39	2730
265	34.4	0.71	0.027	0.0022	0.0315	34.5	2.16	2740
266	25.7	0.99	0.022	0.0018	0.0146	37.8	2.20	2750
267	34.6	1.22	0.030	0.0017	0.0404	32.8	2.39	2760
268	27.6	0.63	0.018	0.0018	0.0188	36.0	2.47	2770
269	32.8	0.32	0.025	0.0019	0.0324	32.9	2.50	2780
270	35.4	0.79	0.033	0.0019	0.0208	40.0	2.45	2790
271	34.0	0.17	0.022	0.0032	0.0147	37.4	2.38	2800
272	37.4	0.46	0.018	0.0013	0.0150	41.0	2.46	2810
273	37.0	0.62	0.036	0.0014	0.0066	35.1	2.72	2820
274	30.0	0.97	0.022	0.0020	0.0426	35.1	2.64	2830
275	33.6	0.96	0.027	0.0019	0.0056	36.7	2.39	2840
276	28.9	0.53	0.019	0.0016	0.0085	41.4	2.57	2850
277	27.2	0.82	0.026	0.0021	0.0001	25.5	2.33	2860
278	36.6	0.44	0.027	0.0023	0.0079	28.3	2.44	2870
279	32.6	0.74	0.024	0.0014	0.0079	40.4	2.41	2880
280	32.4	1.07	0.026	0.0017	0.0322	42.8	2.49	2890
281	36.6	0.58	0.032	0.0013	0.0256	34.4	2.25	2900
282	35.1	0.45	0.015	0.0020	0.0119	41.0	2.48	2910
283	34.1	0.39	0.025	0.0020	0.0084	44.0	2.42	2920
284	38.0	0.75	0.010	0.0023	0.0081	36.0	2.43	2930
285	36.7	0.93	0.024	0.0014	0.0218	33.4	2.28	2940
286	33.5	1.11	0.036	0.0021	0.0008	33.3	2.35	2950
287	29.9	0.55	0.030	0.0018	0.0297	34.2	2.21	2960
288	30.0	0.59	0.024	0.0026	0.0237	38.6	2.31	2970
289	37.8	0.35	0.022	0.0021	0.0209	34.6	2.29	2980
290	25.9	1.00	0.028	0.0017	0.0328	43.4	2.36	2990
291	32.5	0.52	0.031	0.0018	0.0289	33.8	2.42	3000
292	24.8	0.40	0.024	0.0017	0.0208	32.3	2.50	3010
293	37.1	1.12	0.034	0.0026	0.0253	37.7	2.27	3020
294	36.3	0.79	0.019	0.0017	0.0232	36.3	2.43	3030
295	32.6	0.75	0.010	0.0012	0.0167	37.4	2.53	3040
296	32.3	0.24	0.019	0.0018	0.0381	26.3	2.52	3050
297	22.3	0.67	0.022	0.0025	0.0392	34.7	2.20	3060
298	35.1	0.69	0.021	0.0022	0.0257	27.2	2.49	3070

299	23.8	0.22	0.018	0.0020	0.0120	36.0	2.38	3080
300	22.9	0.48	0.033	0.0028	0.0104	38.4	2.57	3090
301	32.9	0.42	0.013	0.0016	0.0279	40.1	2.51	3100
302	28.9	0.70	0.020	0.0021	0.0220	38.4	2.36	3110
303	34.4	0.24	0.017	0.0015	0.0142	37.4	2.43	3120
304	35.5	0.86	0.021	0.0015	0.0264	38.5	2.46	3130
305	36.3	1.04	0.019	0.0018	0.0099	35.1	2.11	3140
306	29.9	0.45	0.027	0.0022	0.0288	35.1	2.33	3150
307	34.6	0.54	0.017	0.0030	0.0051	39.4	2.35	3160
308	33.0	0.69	0.018	0.0023	0.0062	39.7	2.26	3170
309	36.1	0.90	0.024	0.0014	0.0225	33.3	2.13	3180
310	34.9	0.69	0.031	0.0018	0.0124	27.6	2.50	3190
311	36.5	0.65	0.011	0.0017	0.0427	25.7	2.33	3200
312	32.1	0.40	0.035	0.0018	0.0413	28.5	2.55	3210
313	32.1	0.48	0.018	0.0025	0.0169	30.9	2.29	3220
314	37.0	0.72	0.028	0.0021	0.0127	37.3	2.52	3230
315	24.2	1.02	0.031	0.0024	0.0225	31.9	2.49	3240
316	30.5	0.71	0.033	0.0022	0.0214	35.0	2.47	3250
317	27.3	0.19	0.020	0.0015	0.0415	37.0	2.28	3260
318	31.0	0.67	0.024	0.0024	0.0207	29.6	2.38	3270
319	35.4	0.52	0.023	0.0013	0.0393	31.6	2.34	3280
320	36.1	0.47	0.020	0.0023	0.0397	32.1	2.29	3290
321	28.6	0.48	0.026	0.0022	0.0569	31.8	2.35	3300
322	30.6	0.29	0.026	0.0025	0.0202	33.5	2.20	3310
323	33.2	0.45	0.021	0.0012	0.0187	38.5	2.38	3320
324	31.3	0.32	0.025	0.0018	0.0446	33.1	2.37	3330
325	33.8	0.43	0.042	0.0019	0.0150	38.2	2.30	3340
326	34.3	0.57	0.024	0.0020	0.0024	36.8	2.48	3350
327	29.0	0.59	0.029	0.0023	0.0259	36.1	2.27	3360
328	32.0	0.49	0.021	0.0023	0.0310	39.2	2.37	3370
329	24.0	0.50	0.020	0.0022	0.0204	43.9	2.46	3380
330	37.6	0.55	0.021	0.0020	0.0207	41.4	2.42	3390
331	30.0	0.68	0.028	0.0028	0.0076	28.7	2.11	3400
332	27.6	0.91	0.019	0.0018	0.0452	37.6	2.31	3410
333	31.6	0.73	0.011	0.0020	0.0273	30.1	2.35	3420
334	26.6	0.46	0.024	0.0016	0.0178	26.6	2.33	3430
335	32.5	0.72	0.021	0.0019	0.0296	30.2	2.24	3440
336	30.3	0.47	0.026	0.0023	0.0346	26.1	2.39	3450
337	41.1	0.02	0.024	0.0013	0.0117	30.5	2.38	3460
338	37.6	0.21	0.029	0.0020	0.0276	41.0	2.56	3470
339	21.9	0.04	0.030	0.0016	0.0186	33.3	2.41	3480
340	34.5	0.48	0.015	0.0023	0.0444	46.0	2.49	3490
341	26.8	0.36	0.014	0.0010	0.0268	37.1	2.38	3500
342	31.6	0.33	0.027	0.0010	0.0107	39.3	2.17	3510
343	33.3	0.55	0.026	0.0027	0.0234	34.7	2.22	3520

344	35.7	0.34	0.017	0.0018	0.0305	34.1	2.31	3530
345	31.5	0.35	0.032	0.0010	0.0503	31.9	2.35	3540
346	39.1	0.72	0.024	0.0011	0.0255	35.9	2.47	3550
347	30.6	0.77	0.025	0.0019	0.0318	29.0	2.30	3560
348	34.0	1.18	0.026	0.0021	0.0392	31.6	2.32	3570
349	35.5	0.63	0.029	0.0021	0.0311	30.6	2.43	3580
350	32.9	0.55	0.034	0.0025	0.0134	35.9	2.33	3590
351	36.4	0.37	0.022	0.0021	0.0230	41.6	2.25	3600
352	34.0	0.49	0.012	0.0019	0.0163	44.0	2.33	3610
353	29.4	0.53	0.031	0.0025	0.0334	27.8	2.32	3620
354	25.3	0.03	0.017	0.0030	0.0429	36.9	2.48	3630
355	40.1	0.47	0.032	0.0019	0.0245	32.5	2.42	3640
356	30.1	0.76	0.020	0.0018	0.0370	30.6	2.46	3650
357	33.0	0.37	0.034	0.0024	0.0158	35.7	2.35	3660
358	35.0	0.68	0.019	0.0017	0.0268	33.3	2.65	3670
359	33.1	0.84	0.016	0.0012	0.0229	35.4	2.41	3680
360	29.0	0.86	0.030	0.0019	0.0440	38.5	2.29	3690
361	30.6	0.77	0.015	0.0020	0.0283	31.1	2.24	3700
362	32.2	0.17	0.029	0.0020	0.0341	34.7	2.41	3710
363	38.7	0.37	0.027	0.0014	0.0210	28.1	2.35	3720
364	29.2	0.81	0.023	0.0016	0.0166	33.7	2.24	3730
365	35.9	0.65	0.021	0.0016	0.0295	39.3	2.34	3740
366	33.8	0.54	0.038	0.0024	0.0141	27.9	2.19	3750
367	31.7	0.67	0.021	0.0018	0.0076	37.1	2.48	3760
368	28.4	0.88	0.022	0.0022	0.0216	29.7	2.63	3770
369	31.4	0.58	0.017	0.0022	0.0436	36.2	2.49	3780
370	32.3	0.33	0.019	0.0018	0.0199	33.4	2.36	3790
371	26.5	0.49	0.020	0.0010	0.0274	34.1	2.57	3800
372	33.4	0.49	0.035	0.0021	0.0171	28.6	2.43	3810
373	29.3	0.81	0.021	0.0023	0.0010	31.3	2.13	3820
374	32.2	0.66	0.019	0.0016	0.0250	34.5	2.38	3830
375	34.0	0.70	0.021	0.0019	0.0448	35.5	2.40	3840
376	29.0	0.58	0.029	0.0017	0.0211	34.5	2.47	3850
377	31.4	0.44	0.015	0.0028	0.0106	32.6	2.38	3860
378	34.1	0.55	0.028	0.0019	0.0123	40.8	2.55	3870
379	25.1	0.60	0.015	0.0020	0.0292	34.5	2.24	3880
380	37.2	0.15	0.023	0.0014	0.0195	31.9	2.72	3890
381	41.6	0.59	0.011	0.0016	0.0362	32.0	2.57	3900
382	36.8	0.82	0.028	0.0013	0.0219	35.0	2.37	3910
383	31.2	0.51	0.029	0.0023	0.0019	39.1	2.43	3920
384	34.5	0.99	0.019	0.0022	0.0192	33.6	2.30	3930
385	28.5	0.71	0.026	0.0015	0.0335	38.8	2.29	3940
386	40.1	0.42	0.025	0.0034	0.0368	36.2	2.40	3950
387	36.7	0.50	0.032	0.0024	0.0405	32.9	2.52	3960
388	35.9	0.46	0.025	0.0021	0.0364	31.7	2.51	3970

389	29.1	0.61	0.031	0.0029	0.0373	36.0	2.66	3980
390	33.9	0.77	0.023	0.0006	0.0476	34.9	2.36	3990
391	30.3	0.45	0.019	0.0019	0.0428	31.3	2.37	4000
392	31.2	0.68	0.024	0.0019	0.0270	31.8	2.08	4010
393	30.3	1.03	0.022	0.0020	0.0187	37.7	2.36	4020
394	28.6	0.82	0.030	0.0014	0.0218	37.6	2.41	4030
395	29.0	0.79	0.023	0.0022	0.0333	34.0	2.40	4040
396	31.8	0.31	0.018	0.0008	0.0395	38.7	2.32	4050
397	25.6	0.38	0.023	0.0020	0.0222	33.8	2.25	4060
398	35.2	0.61	0.032	0.0021	0.0424	34.9	2.35	4070
399	32.2	0.51	0.021	0.0019	0.0154	40.3	2.66	4080
400	35.6	0.07	0.019	0.0021	0.0189	33.0	2.29	4090
401	33.6	0.11	0.031	0.0015	0.0200	26.6	2.40	4100
402	34.7	0.85	0.024	0.0022	0.0162	30.0	2.26	4110
403	26.4	0.33	0.021	0.0017	0.0350	36.6	2.54	4120
404	28.6	1.11	0.019	0.0011	0.0228	34.4	2.50	4130
405	30.7	0.12	0.014	0.0018	0.0464	46.6	2.42	4140
406	33.1	0.67	0.025	0.0016	0.0247	29.4	2.39	4150
407	37.5	0.54	0.022	0.0014	0.0471	34.3	2.58	4160
408	31.4	0.33	0.026	0.0022	0.0046	35.3	2.47	4170
409	38.0	0.66	0.014	0.0019	0.0292	29.6	2.40	4180
410	34.6	0.31	0.033	0.0018	0.0282	39.7	2.41	4190
411	37.7	0.80	0.027	0.0017	0.0488	38.4	2.59	4200
412	33.2	0.56	0.013	0.0028	0.0280	41.7	2.46	4210
413	29.9	0.05	0.031	0.0025	0.0460	38.2	2.43	4220
414	26.5	0.22	0.020	0.0018	0.0474	22.3	2.47	4230
415	33.2	0.46	0.026	0.0020	0.0168	31.0	2.38	4240
416	36.1	0.89	0.025	0.0027	0.0098	36.7	2.28	4250
417	31.3	0.60	0.018	0.0028	0.0347	31.7	2.44	4260
418	30.4	0.55	0.005	0.0025	0.0141	36.6	2.20	4270
419	31.2	0.75	0.028	0.0018	0.0230	35.0	2.32	4280
420	28.2	0.15	0.021	0.0016	0.0175	33.0	2.53	4290
421	30.6	0.96	0.020	0.0023	0.0261	35.5	2.32	4300
422	32.0	0.28	0.027	0.0015	0.0321	37.6	2.43	4310
423	32.8	0.55	0.019	0.0014	0.0335	40.0	2.37	4320
424	32.4	0.44	0.029	0.0018	0.0265	31.4	2.43	4330
425	35.2	0.58	0.025	0.0024	0.0128	32.9	2.45	4340
426	33.0	0.02	0.017	0.0020	0.0139	32.2	2.34	4350
427	40.0	0.98	0.030	0.0020	0.0283	38.8	2.14	4360
428	33.8	0.70	0.027	0.0025	0.0033	41.8	2.53	4370
429	39.9	1.09	0.032	0.0020	0.0103	39.5	2.33	4380
430	29.7	0.96	0.018	0.0014	0.0056	40.8	2.43	4390
431	34.8	0.54	0.018	0.0023	0.0212	36.3	2.52	4400
432	31.5	0.26	0.026	0.0022	0.0309	31.8	2.27	4410
433	35.2	0.03	0.028	0.0019	0.0539	38.2	2.56	4420

434	35.1	0.54	0.030	0.0017	0.0249	42.3	2.49	4430
435	23.8	0.61	0.024	0.0017	0.0116	37.5	2.41	4440
436	27.2	0.85	0.022	0.0019	0.0190	39.1	2.36	4450
437	26.6	0.26	0.028	0.0015	0.0305	28.8	2.55	4460
438	34.3	0.78	0.037	0.0017	0.0367	37.8	2.45	4470
439	38.7	0.56	0.030	0.0012	0.0189	34.7	2.46	4480
440	31.1	0.32	0.024	0.0017	0.0248	37.7	2.74	4490
441	36.0	0.77	0.020	0.0016	0.0390	40.6	2.46	4500
442	35.0	0.62	0.027	0.0022	0.0275	32.6	2.55	4510
443	28.5	0.48	0.021	0.0026	0.0257	41.5	2.39	4520
444	34.2	1.06	0.025	0.0024	0.0211	31.0	2.62	4530
445	29.6	0.72	0.029	0.0025	0.0200	35.3	2.39	4540
446	38.8	0.51	0.030	0.0023	0.0371	36.7	2.28	4550
447	32.5	0.62	0.028	0.0022	0.0180	39.6	2.39	4560
448	39.3	0.56	0.033	0.0023	0.0242	33.9	2.18	4570
449	30.8	0.59	0.036	0.0016	0.0119	31.1	2.56	4580
450	35.1	0.67	0.011	0.0023	0.0322	41.2	2.26	4590
451	32.4	0.36	0.012	0.0013	0.0278	36.9	2.43	4600
452	24.4	0.31	0.018	0.0022	0.0304	27.0	2.51	4610
453	28.8	0.64	0.010	0.0015	0.0244	36.8	2.45	4620
454	35.3	1.06	0.021	0.0015	0.0149	28.1	2.44	4630
455	32.4	0.45	0.022	0.0017	0.0237	38.6	2.30	4640
456	28.2	0.24	0.026	0.0013	0.0087	41.1	2.39	4650
457	30.0	0.48	0.026	0.0019	0.0210	34.6	2.51	4660
458	33.6	0.40	0.019	0.0025	0.0522	31.3	2.31	4670
459	28.7	0.44	0.019	0.0018	0.0445	40.2	2.25	4680
460	36.9	0.68	0.029	0.0022	0.0350	33.1	2.32	4690
461	30.0	0.51	0.021	0.0020	0.0303	31.7	2.51	4700
462	39.9	0.36	0.015	0.0025	0.0345	30.0	2.36	4710
463	28.3	0.41	0.024	0.0018	0.0294	29.1	2.42	4720
464	33.4	0.17	0.025	0.0021	0.0358	36.5	2.18	4730
465	26.3	0.29	0.021	0.0032	0.0394	33.9	2.31	4740
466	29.7	0.15	0.028	0.0025	0.0121	38.5	2.32	4750
467	30.2	0.39	0.025	0.0015	0.0227	35.1	2.25	4760
468	34.3	0.22	0.022	0.0025	0.0244	34.4	2.55	4770
469	36.7	0.33	0.023	0.0015	0.0178	28.0	2.53	4780
470	33.7	0.45	0.027	0.0019	0.0122	32.0	2.21	4790
471	31.0	0.19	0.021	0.0021	0.0403	35.7	2.43	4800
472	36.0	0.53	0.017	0.0023	0.0329	33.5	2.29	4810
473	36.0	0.64	0.023	0.0017	0.0130	40.5	2.38	4820
474	33.1	0.25	0.025	0.0022	0.0116	27.3	2.40	4830
475	35.1	0.88	0.028	0.0028	0.0300	34.6	2.61	4840
476	34.4	0.08	0.024	0.0010	0.0160	35.8	2.44	4850
477	28.7	0.42	0.021	0.0014	0.0096	32.2	2.32	4860
478	35.8	0.12	0.028	0.0025	0.0222	35.8	2.50	4870

479	29.9	0.44	0.023	0.0018	0.0139	42.1	2.51	4880
480	30.1	0.16	0.030	0.0019	0.0347	30.7	2.41	4890
481	33.3	0.37	0.023	0.0024	0.0519	33.8	2.68	4900
482	31.2	0.33	0.024	0.0031	0.0041	29.3	2.38	4910
483	32.2	0.20	0.023	0.0013	0.0347	38.3	2.35	4920
484	35.1	0.05	0.018	0.0015	0.0299	30.2	2.46	4930
485	37.2	0.71	0.017	0.0019	0.0140	31.5	2.24	4940
486	31.8	1.09	0.017	0.0019	0.0361	41.2	2.35	4950
487	34.0	1.12	0.035	0.0020	0.0132	38.7	2.33	4960
488	31.6	0.39	0.022	0.0018	0.0011	32.1	2.57	4970
489	33.5	0.53	0.030	0.0025	0.0108	39.3	2.49	4980
490	34.5	0.40	0.026	0.0015	0.0319	32.5	2.47	4990
491	30.1	0.56	0.036	0.0020	0.0298	35.7	2.51	5000
492	33.6	0.27	0.030	0.0024	0.0364	42.6	2.51	5010
493	35.2	0.01	0.015	0.0021	0.0310	44.3	2.40	5020
494	32.9	0.53	0.022	0.0016	0.0403	33.4	2.23	5030
495	39.5	0.18	0.030	0.0020	0.0002	35.2	2.18	5040
496	30.1	0.01	0.026	0.0018	0.0215	39.5	2.40	5050
497	29.7	1.16	0.038	0.0016	0.0204	37.9	2.60	5060
498	25.4	0.48	0.023	0.0026	0.0240	34.3	2.50	5070
499	36.5	0.66	0.013	0.0018	0.0372	34.4	2.53	5080
500	36.3	0.89	0.027	0.0016	0.0161	31.9	2.62	5090
501	32.3	0.05	0.018	0.0016	0.0279	25.8	2.34	5100
502	36.5	0.66	0.024	0.0020	0.0008	34.7	2.32	5110
503	33.4	0.69	0.031	0.0012	0.0130	30.3	2.54	5120
504	33.7	0.56	0.026	0.0012	0.0359	34.3	2.32	5130
505	33.1	0.58	0.026	0.0020	0.0033	45.8	2.66	5140
506	34.5	0.38	0.022	0.0013	0.0419	35.3	2.51	5150
507	33.0	0.76	0.023	0.0017	0.0186	41.6	2.32	5160
508	42.8	0.30	0.023	0.0023	0.0312	30.5	2.36	5170
509	27.8	0.31	0.006	0.0024	0.0101	40.5	2.46	5180
510	25.0	0.76	0.027	0.0027	0.0340	28.3	2.49	5190
511	28.1	1.02	0.031	0.0014	0.0249	34.1	2.54	5200
512	28.3	0.42	0.015	0.0023	0.0401	36.6	2.44	5210
513	30.8	0.39	0.014	0.0021	0.0179	38.0	2.28	5220
514	32.0	0.66	0.028	0.0026	0.0152	34.8	2.41	5230
515	31.7	0.86	0.014	0.0020	0.0148	30.6	2.21	5240
516	34.9	0.83	0.013	0.0023	0.0491	30.2	2.47	5250
517	34.2	0.62	0.029	0.0025	0.0212	32.2	2.47	5260
518	35.8	0.35	0.019	0.0017	0.0048	30.8	2.41	5270
519	39.8	0.73	0.032	0.0017	0.0360	32.9	2.29	5280
520	37.9	0.52	0.015	0.0013	0.0252	31.0	2.56	5290
521	27.3	0.95	0.020	0.0019	0.0205	40.3	2.52	5300
522	22.8	0.15	0.026	0.0021	0.0312	36.5	2.32	5310
523	36.5	0.58	0.028	0.0016	0.0353	36.6	2.24	5320

524	25.2	0.92	0.027	0.0020	0.0165	31.6	2.52	5330
525	32.9	0.39	0.025	0.0017	0.0262	36.6	2.47	5340
526	32.7	0.36	0.022	0.0017	0.0215	36.8	2.40	5350
527	41.2	0.27	0.020	0.0023	0.0174	31.1	2.43	5360
528	32.3	0.46	0.027	0.0023	0.0307	30.3	2.48	5370
529	30.5	0.49	0.021	0.0025	0.0337	26.9	2.35	5380
530	33.5	0.57	0.027	0.0014	0.0075	38.9	2.59	5390
531	33.5	0.28	0.031	0.0018	0.0380	30.8	2.44	5400
532	32.9	0.56	0.008	0.0022	0.0266	35.3	2.31	5410
533	30.1	0.36	0.035	0.0013	0.0223	35.6	2.34	5420
534	27.5	0.43	0.019	0.0029	0.0052	35.6	2.59	5430
535	33.9	0.30	0.033	0.0020	0.0221	32.6	2.32	5440
536	27.1	0.46	0.034	0.0017	0.0239	34.3	2.27	5450
537	28.6	1.60	0.014	0.0024	0.0261	34.0	2.54	5460
538	38.2	1.39	0.025	0.0021	0.0192	40.9	2.43	5470
539	30.9	0.89	0.046	0.0020	0.0357	30.3	2.66	5480
540	32.1	0.78	0.022	0.0016	0.0432	34.4	2.37	5490
541	36.5	0.17	0.027	0.0011	0.0400	39.6	2.48	5500
542	31.3	0.37	0.026	0.0015	0.0223	37.2	2.39	5510
543	37.1	0.36	0.032	0.0016	0.0288	30.6	2.45	5520
544	31.1	0.70	0.031	0.0022	0.0297	38.6	2.21	5530
545	37.0	0.68	0.017	0.0022	0.0167	23.3	2.42	5540
546	35.3	0.57	0.021	0.0015	0.0247	33.2	2.49	5550
547	31.8	0.44	0.026	0.0023	0.0171	41.7	2.39	5560
548	29.2	0.27	0.023	0.0022	0.0256	37.5	2.36	5570
549	28.5	0.54	0.041	0.0018	0.0437	38.6	2.40	5580
550	31.5	0.88	0.027	0.0015	0.0228	35.0	2.14	5590
551	30.8	0.66	0.027	0.0024	0.0153	33.7	2.56	5600
552	30.9	0.59	0.018	0.0018	0.0414	38.2	2.44	5610
553	37.0	0.74	0.015	0.0014	0.0351	44.7	2.46	5620
554	31.3	0.72	0.029	0.0021	0.0181	34.2	2.48	5630
555	37.6	0.08	0.022	0.0022	0.0151	41.2	2.43	5640
556	30.4	0.55	0.028	0.0012	0.0417	33.0	2.58	5650
557	36.9	0.41	0.018	0.0029	0.0253	33.5	2.27	5660
558	30.4	0.04	0.030	0.0008	0.0271	38.1	2.39	5670
559	33.3	0.16	0.012	0.0012	0.0290	31.3	2.53	5680
560	36.9	0.45	0.034	0.0025	0.0167	39.1	2.39	5690
561	30.9	0.79	0.030	0.0021	0.0375	28.2	2.48	5700
562	30.7	0.48	0.025	0.0017	0.0537	25.3	2.20	5710
563	40.5	0.62	0.016	0.0019	0.0077	34.6	2.44	5720
564	36.8	0.28	0.021	0.0023	0.0272	36.8	2.53	5730
565	30.8	0.09	0.026	0.0015	0.0359	40.5	2.12	5740
566	35.4	0.57	0.032	0.0024	0.0143	35.8	2.37	5750
567	31.1	0.26	0.017	0.0023	0.0260	39.1	2.25	5760
568	35.6	0.89	0.032	0.0019	0.0269	36.3	2.28	5770

569	38.5	1.03	0.043	0.0020	0.0170	38.2	2.47	5780
570	26.0	0.43	0.020	0.0016	0.0334	31.0	2.54	5790
571	37.1	0.90	0.027	0.0015	0.0395	35.0	2.37	5800

BIBLIOGRAPHY

[1] *AASHTO, LRFD Bridge Design Specifications*, Seventh. Washington D.C.: American Association of State Highway and Transportation Officials, 2014.

[2] “Caltrans Seismic Design Criteria Version 2.0,” 2019. [Online]. Available: http://ascelibrary.org/doi/pdf/10.1061/9780784411179.ch02.

[3] K. Wardhana and F. C. Hadipriono, “Analysis of recent bridge failures in the United States,” *J. Perform. Constr. Facil.*, vol. 17, no. 3, pp. 144–150, 2003, doi: 10.1061/(ASCE)0887-3828(2003)17:3(144).

[4] W. Cook, P. J. Barr, and M. W. Halling, “Bridge failure rate,” *J. Perform. Constr. Facil.*, vol. 29, no. 3, pp. 1–8, 2015, doi: 10.1061/(ASCE)CF.1943-5509.0000571.

[5] M. B. Koçyiğit and H. Akay, “Verevli Akarsu Köprülerinde Taban Oyulmalarının İncelenmesi,” in *III. Uluslararası Mesleki ve Teknik Bilimler Kongresi*, 2018, no. October, pp. 1445–1452.

[6] M. Ghosn, F. Moses, and J. Wang, “NCHRP Report 489. Design of Highway Bridges for Extreme Events,” WASHINGTON, D.C., 2003.

[7] M. Yanmaz, “Yıkılan Akarsu Köprüleri Üzerine Görüşler,” *Türkiye Mühendislik Haberleri*, pp. 137–141, 2002.

[8] A. M. Shirole and R. C. Holt, “Planning for a comprehensive bridge safety assurance program,” *Transport Research Record*, vol. 1290. pp. 137–142, 1991.

[9] J. Briaud and B. E. Hunt, “Bridge Scour & the Structural Engineer,” *Struct. Mag.*, no. December, pp. 58–61, 2006.

[10] M. Yanmaz and A. Caner, “Çaycuma Köprüsünün Çökmesi Üzerine Görüşler,”

2012.

[11] O. Dündar, M. P. Alpan, and M. Tanış, "Ülkemiz Köprü Gözlem ve Yönetemi Üzerine Karşılaştırmalı Bir Değerlendirme," 2017, no. October.

[12] K. N. Ramanathan, "Next generation seismic fragility curves for california bridges incorporating the evolution in seismic design philosophy," Georgia Institute of Technology, 2012.

[13] Ö. Avşar, "Fragility Based Seismic Vulnerability Assessement of Ordinary Highway Bridges in Turkey," Middle East Technical University, 2009.

[14] N. Basöz and A. S. Kiremidjian, "Evaluation of Bridge Damage Data from the Loma Prieta and Northridge, California Earthquakes, Technical Report MCEER-98-0004," New York, 1998.

[15] M. Shinozuka, M. Q. Feng, H. Kim, T. Uzawa, and T. Ueda, "Statistical analysis of fragility curves,Technical Report MCEER-03-0002," 2003.

[16] H. Yamazaki, F., Hamada, T., Motoyama, H., Yamauchi, "Earthquake Damage Assessment of Expressway Bridges in Japan," in *Technical Council on Lifeline Earthquake Engineering Monograph,16*, 1999, pp. 361–370.

[17] K. R. Karim and F. Yamazaki, "Effect of earthquake ground motions on fragility curves of highway bridge piers based on numerical simulation," *Earthq. Eng. Struct. Dyn.*, vol. 30, no. 12, pp. 1839–1856, Dec. 2001, doi: 10.1002/eqe.97.

[18] E. Choi, R. DesRoches, and B. Nielson, "Seismic fragility of typical bridges in moderate seismic zones," *Eng. Struct.*, vol. 26, no. 2, pp. 187–199, 2004, doi: https://doi.org/10.1016/j.engstruct.2003.09.006.

[19] B. G. Nielson, "Analytical fragility curves for highway bridges in moderate

seismic zones," *Environ. Eng.*, no. December, p. 400, 2005, doi: 10.1016/j.engstruct.2017.03.041.

[20] B. G. Nielson and R. DesRoches, "Analytical Seismic Fragility Curves for Typical Bridges in the Central and Southeastern United States," *Earthq. Spectra*, vol. 23, no. 3, pp. 615–633, Aug. 2007, doi: 10.1193/1.2756815.

[21] J. E. Padgett and R. DesRoches, "Sensitivity of Seismic Response and Fragility to Parameter Uncertainty," *J. Struct. Eng. ASCE*, vol. 133, no. 4, pp. 484–494, 2007, doi: 10.1061/(ASCE)0733-9445(2007)133.

[22] J. Zhong, P. Gardoni, D. Rosowsky, and T. Haukaas, "Probabilistic Seismic Demand Models and Fragility Estimates for Reinforced Concrete Bridges with Two-Column Bents," *J. Eng. Mech.*, vol. 134, no. 6, pp. 495–504, Jun. 2008, doi: 10.1061/(ASCE)0733-9399(2008)134:6(495).

[23] M. N. Choine, A. O'Connor, and J. E. Padgett, "A Seismic Reliability Assessment of Reinforced Concrete Integral Bridges Subject to Corrosion," *Key Eng. Mater.*, vol. 569–570, pp. 366–373, 2013, doi: 10.4028/www.scientific.net/KEM.569-570.366.

[24] J. Ghosh and P. Sood, "Consideration of time-evolving capacity distributions and improved degradation models for seismic fragility assessment of aging highway bridges," *Reliab. Eng. Syst. Saf.*, vol. 154, pp. 197–218, 2016, doi: https://doi.org/10.1016/j.ress.2016.06.001.

[25] S. Banerjee and G. Ganesh Prasad, "Seismic risk assessment of reinforced concrete bridges in flood-prone regions," *Struct. Infrastruct. Eng.*, vol. 9, no. 9, pp. 952–968, 2013, doi: 10.1080/15732479.2011.649292.

[26] G. G. Prasad and S. Banerjee, "The impact of flood-induced scour on seismic

fragility characteristics of bridges," *J. Earthq. Eng.*, vol. 17, no. 6, pp. 803–828, 2013, doi: 10.1080/13632469.2013.771593.

[27] S. Kameshwar and J. E. Padgett, "Multi-hazard risk assessment of highway bridges subjected to earthquake and hurricane hazards," *Eng. Struct.*, vol. 78, pp. 154–166, 2014, doi: https://doi.org/10.1016/j.engstruct.2014.05.016.

[28] X. Guo, Y. Wu, and Y. Guo, "Time-dependent seismic fragility analysis of bridge systems under scour hazard and earthquake loads," *Eng. Struct.*, vol. 121, pp. 52–60, 2016, doi: 10.1016/j.engstruct.2016.04.038.

[29] T. Yilmaz, "Risk Assessment of Highway Bridges under Multi-Hazard Effect of Flood-Induced Scour and Earthquake," The Pennsylvania State University, 2015.

[30] T. Yilmaz, S. Banerjee, and P. A. Johnson, "Uncertainty in risk of highway bridges assessed for integrated seismic and flood hazards," *Struct. Infrastruct. Eng.*, vol. 14, no. 9, pp. 1182–1196, 2018, doi: 10.1080/15732479.2017.1402065.

[31] L. F. V. Yuan, S. A. Argyroudis, E. Tubaldi, M. Pregnolato, and S. A. Mitoulis, "Fragility of Bridges Exposed to Multiple Hazards and Impact on Transport Network Resilience," in *Earthquake Risk and Engineering towards a Resilient World*, 2019, no. September, pp. 1–10.

[32] R. Pant, S. Thacker, J. W. Hall, D. Alderson, and S. Barr, "Critical infrastructure impact assessment due to flood exposure," *J. Flood Risk Manag.*, vol. 11, no. 1, pp. 22–33, 2018, doi: 10.1111/jfr3.12288.

[33] J. Lee, Y. J. Lee, H. Kim, S. H. Sim, and J. M. Kim, "A new methodology development for flood fragility curve derivation considering structural deterioration for bridges," *Smart Struct. Syst.*, vol. 17, no. 1, pp. 149–165, 2016, doi: 10.12989/sss.2016.17.1.149.

[34] H. Kim, S. H. Sim, J. Lee, Y. J. Lee, and J. M. Kim, “Flood fragility analysis for bridges with multiple failure modes,” *Adv. Mech. Eng.*, vol. 9, no. 3, pp. 1–11, 2017, doi: 10.1177/1687814017696415.

[35] D. Turner, “Fragility Assessment of Bridge Superstructures Under Hydrodynamic Forces,” Colorado State University, 2015.

[36] F. Kalendher, “Synthetic Damage Curves for Concrete Girder Bridge Decks Under Flood Hazard,” RMIT University, 2017.

[37] I. M. I. Qeshta, “Fragility and Resilience of Bridges Subjected to Extreme Wave-Induced Forces by,” Rmit University, 2019.

[38] K. R. MacKie and B. G. Nielson, “Uncertainty quantification in analytical bridge fragility curves,” *TCLEE 2009 Lifeline Earthq. Eng. a Multihazard Environ.*, vol. 357, p. 9, 2009, doi: 10.1061/41050(357)9.

[39] Y. K. Wen, B. R. Ellingwood, D. Veneziano, and J. Bracci, “Uncertainty modeling in earthquake engineering,” *MAE Cent. Proj.*, pp. 1–113, 2003, [Online]. Available: http://mae.cee.illinois.edu/research/research_briefs/Whitepaper.pdf.

[40] H. Bin Ma *et al.*, “Probabilistic seismic response and uncertainty analysis of continuous bridges under near-fault ground motions,” *Front. Struct. Civ. Eng.*, vol. 13, no. 6, pp. 1510–1519, 2019, doi: 10.1007/s11709-019-0577-8.

[41] A. Aviram, K. Mackie, and B. Stojadinovic, “Epistemic Uncertainty of Seismic Response Estimates for Reinforced concrete Bridges,” *Proc. 14th World Conf. Earthq. Eng.*, 2008.

[42] S. Banerjee and G. G. Prasad, “Analysis of Bridge Performance under the Combined Effect of Earthquake and Flood-Induced Scour,” in *ICVRAM and*

ISUMA 2011, 2011, no. Did, pp. 360–367.

[43] A. Alipour, B. Shafei, and M. Shinozuka, “Reliability-based calibration of load and resistance factors for design of rc bridges under multiple extreme events: Scour and earthquake,” *J. Bridg. Eng.*, vol. 18, no. 5, pp. 362–371, 2013, doi: 10.1061/(ASCE)BE.1943-5592.0000369.

[44] Z. Wang, J. E. Padgett, and L. Dueñas-Osorio, “Risk-consistent calibration of load factors for the design of reinforced concrete bridges under the combined effects of earthquake and scour hazards,” *Eng. Struct.*, vol. 79, pp. 86–95, 2014, doi: 10.1016/j.engstruct.2014.07.005.

[45] M. Ghosn and P. D. Johnson, “Reliability Analysis of Bridges under The Combined Effect of Scour and Earthquakes,” in *8th ASCE Specialty Conference on Probabilistic Mechanics and Structural Reliability*, 2000, pp. 1–6.

[46] P. A. Johnson and D. A. Dock, “Probabilistic Bridge Scour Estimates,” vol. 124, no. 1992, pp. 750–754, 1998.

[47] P. A. Johnson, “Comparison of pier-scour equations using field data,” *J. Hydraul. Eng.*, vol. 121, no. 8, pp. 626–629, 1995, doi: 10.1061/(ASCE)0733-9429(1995)121:8(626).

[48] P. A. Johnson, “Reliability-based pier scour engineering,” vol. 118, no. 10, pp. 1344–1358, 1993.

[49] A. Pizarro and E. Tubaldi, “Quantification of modelling uncertainties in bridge scour risk assessment under multiple flood events,” *Geosci.*, vol. 9, no. 10, 2019, doi: 10.3390/geosciences9100445.

[50] Y. M. Chiew, “Local Scour at Bridge Piers,” Auckland University, 1984.

[51] H. L. Lee and L. W. Mays, “Hydraulic uncertainties in flood levee capacity,” *J. Hydraul. Eng.*, vol. 112, no. 10, pp. 928–934, 1986, doi: 10.1061/(ASCE)0733-9429(1986)112:10(928).

[52] B. Y. Tung, “Mellin Transform Applied to Uncertainty Analysis in Hydrology/Hydraulics,” *J. Hydraul. Eng.*, vol. 116, no. 5, pp. 659–674, 1990.

[53] P. A. Johnson, “Uncertainty of hydraulic parameters,” *J. Hydraul. Eng.*, vol. 122, no. 2, pp. 112–114, 1996, doi: 10.1061/(ASCE)0733-9429(1996)122:2(112).

[54] P. A. Johnson, P. E. Clopper, L. W. Zevenbergen, and P. F. Lagasse, “Quantifying uncertainty and reliability in bridge scour estimations,” *J. Hydraul. Eng.*, vol. 141, no. 7, pp. 1–9, 2015, doi: 10.1061/(ASCE)HY.1943-7900.0001017.

[55] A. M. Yanmaz, “Uncertainty of local scouring parameters around bridge piers,” *Turkish J. Eng. Environ. Sci.*, vol. 25, no. 2, pp. 127–137, 2001.

[56] L. A. Arneson, L. W. Zevenbergen, P. F. Lagasse, and P. E. Clopper, “Evaluating Scour at Bridges Fifth Edition,” *Hydraul. Eng. Circ.*, no. 18, p. 340, 2012.

[57] R. K. W. Chee, “Live-bed scour at bridge piers,” Auckland, 1982.

[58] P. A. Johnson and B. M. Ayyub, “Assessing time-variant bridge reliability due to pier scour,” *J. Hydraul. Eng.*, vol. 119, no. 7, p. 874, 1993, doi: 10.1061/(ASCE)0733-9429(1993)119:7(874).

[59] B. Melville, D. M. Sheppard, and H. Demir, *Scour at Wide Piers and Long Skewed Piers, NCHRP Report 682*. Washington, D.C.: National Academies Press, 2011.

[60] P. A. Johnson, “Fault Tree Analysis of Bridge Failure Due to Scour and Channel

Instability,” vol. 5, no. March, pp. 35–41, 1999.

[61] A. M. Yanmaz and I. Üstün, “Generalized reliability model for local scour around bridge piers of various shapes,” *Turkish J. Eng. Environ. Sci.*, vol. 25, no. 6, pp. 687–698, 2001.

[62] A. M. Yanmaz and M. Çalamak, “Akarsu Köprü Temellerindeki Oyulma Riskinin Değerlendirilmesi,” *Tek. Dergi/Technical J. Turkish Chamb. Civ. Eng.*, vol. 27, no. 3, pp. 7533–7549, 2016.

[63] A. M. Yanmaz and O. Cicekdag, “Composite reliability model for local scour around cylindrical bridge piers,” *Can. J. Civ. Eng.*, vol. 28, no. 3, pp. 520–535, 2001, doi: 10.1139/cjce-28-3-520.

[64] Ö. Köse and A. M. Yanmaz, “Köprü kenar ayaklanndaki oyulma güvenilirliği,” *Tek. Dergi/Technical J. Turkish Chamb. Civ. Eng.*, vol. 21, no. 1, pp. 4919–4934, 2010.

[65] M. Muzzammil, N. A. Siddiqui, and A. F. Siddiqui, “Reliability considerations in bridge pier scouring,” *Struct. Eng. Mech.*, vol. 28, no. 1, pp. 1–18, 2008.

[66] M. Khalid, M. Muzzammil, and J. Alam, “A reliability-based assessment of live bed scour at bridge piers,” *ISH J. Hydraul. Eng.*, vol. 00, no. 00, pp. 1–8, 2019, doi: 10.1080/09715010.2019.1584543.

[67] R. Hosseini and A. Amini, “Scour depth estimation methods around pile groups,” *KSCE J. Civ. Eng.*, vol. 19, no. 7, pp. 2144–2156, 2015, doi: 10.1007/s12205-015-0594-7.

[68] E. M. Laursen and A. Toch, “Scour around bridge piers and abutments,” *Iowa Hwy. Res. Board*, 1956.

[69] C. R. Neill, “River bed scour, a review for bridge engineers,” 1964.

[70] H. W. Shen, “Scour near piers,” *River Mech.*, vol. II, no. 23, 1971.

[71] H. N. C. Breusers, G. Nicollet, and H. W. Shen, “Local scour around cylindrical piers,” *J. Hydr. Res.*, vol. 15, no. 3, pp. 211–252, 1977.

[72] S. C. Jain and E. E. Fischer, “Scour around circular bridge piers at high Froude numbers,” Washington D.C., 1979.

[73] S. Hancu, “Sur Ie calcul des affouillements locaux dams la zone des piles de ponts,” in *Proc., 14th IAHR Congr.*, 1971, pp. 299–313.

[74] D. C. Froehlich, “Analysis of onsite measurements of scour at piers,” in *ASCE Nat. Hydr. Engrg. Conf.*, 1988.

[75] B. W. Melville and A. J. Sutherland, “Design method for local scour at bridge piers,” *J. Hydr. Engrg.*, vol. 114, no. 10, pp. 1210–1226, 1988.

[76] J. S. Jones, “Comparison of Prediction Equations for Bridge Pier and Abutment Scour.,” *Transp. Res. Rec.*, vol. 2, pp. 202–209, 1984.

[77] M. N. Landers and D. S. Mueller, “Evaluation of Selected Pier-Scour Equations Using Field Data,” *Transp. Res. Rec.*, vol. 1523, no. 1, pp. 186–195, Jan. 1996, doi: 10.1177/0361198196152300123.

[78] “AASHTO LRFD Bridge Design Specifications,” Washington ,DC, 2012.

[79] “Korean Highway Bridge Design Specification (KHBDS),” Seoul, 2010.

[80] F. Kalendher, S. Setunage, D. Robert, and H. Mohaseni, “Fragility Curves for concrete girder bridges under flood hazard,” in *Proceedings of the Ninth International Conference on Bridge Maintenance, Safety, Risk, Management (IABMAS 2018)*, 2018, p. 2945.

[81] *Bridge Design-Design Loads, AS 5100.2-2004*. Australia, 2004.

[82] W. Lokuge, C. Fraser, and W. Karunasena, “Proceedings of the 25th Australasian Conference on Mechanics of Structures and Materials,” in *Proceedings of the 25th Australasian Conference on Mechanics of Structures and Materials (ACMSM25)*, 2020, vol. 37, pp. 407–418, doi: 10.1007/978-981-13-7603-0.

[83] *Cement and Concrete Association of Australia Guide to Concrete Construction*. Australia, 2002.

[84] B. Jordan, “Analysis of bridges subjected to flood loadings based on different design standards,” University of Southern Queensland, 2015.

[85] *THE DESIGN OF HIGHWAY BRIDGES FOR HYDRAULIC ACTION, BA 59/94*, vol. 1, no. section 3. European, 1994.

[86] Indian Road Congress, *Standard Specifications and Code of Practice for Road Bridges*. India, 2014.

[87] J. B. Bradley, D. L. Richards, and C. D. Bahner, “Debris Control Structures: Evaluation and Countermeasures,” Washington, D.C., 2005. [Online]. Available: www.fhwa.dot.gov/engineering/hydraulics/pubs/04016/hec09.pdf.

[88] C. Paralo, C. J. Apelt, and M. A. Jempson, “Debris Force on Highway Bridges, NCHRP Report 445.” National Academy Press, Washington D.C., p. 90, 2000.

[89] A. Caner, *Türkiye Köprü Tasarım Klavuzu*. Turkey, 2019.

[90] A. S. Nowak, “Calibration of LRFD Bridge Design Code, NCHRP Report 368,” Washington D.C., 1999.

[91] Y. Zhang, “Probabilistic Structural Seismic Performance Assessment Methodology and Application to an Actual Bridge-Foundation-Ground System,”

University of California, San Diego, 2006.

[92] E. Choi, “Seismic analysis and retrofit of mid-America bridges,” 2002.

[93] J. Ghosh, “Parameterized Seismic Reliability Assessment and Life-Cycle Analysis of Aging Highway Bridges,” Rice University, 2013.

[94] B. Ellingwood and H. Hwang, “Probabilistic Descriptions of Resistance of Safety-Related Structures in Nuclear Plants,” *Nucl. Eng. Des.*, 1985.

[95] K.-C. Yeh and Y.-K. Tung, “Uncertainty and Sensitivity Analyses of Pit-Migration Model,” *Jounrnal Hydraul. Eng.*, vol. 119, no. 2, pp. 262–283, 1993.

[96] W. L. Mays and Y. K. Tung, *Hydro Systems Engineering and Management*. New York: McGraw-Hill, 1992.

[97] M. A. Cesare, “FIRST-ORDER ANALYSIS OF OPEN CHANNEL FLOW,” *J. Hydraul. Eng.*, vol. 117, no. 2, pp. 242–247, 1991.

[98] L. De Doncker, P. Troch, R. Verhoeven, K. Bal, P. Meire, and J. Quintelier, “Determination of the Manning roughness coefficient influenced by vegetation in the river Aa and Biebrza river,” *Environ. Fluid Mech.*, vol. 9, no. 5, pp. 549–567, 2009, doi: 10.1007/s10652-009-9149-0.

[99] “Hydraulic Engineering Center(1986) : Accuracy of Computed Water Surface Profiles,” Davis, CA, 1986.

[100] Z. Wang, “Risk Based Design and Associated Transportation Networks Under Natural Hazards,” Rice University, 2014.

[101] M. N. Sheikh, H. H. Tsang, T. J. McCarthy, and N. T. K. Lam, “Yield curvature for seismic design of circular reinforced concrete columns,” *Mag. Concr. Res.*, vol. 62, no. 10, pp. 741–748, 2010, doi: 10.1680/macr.2010.62.10.741.

[102] M. D. McKay, “Latin hypercube sampling as a tool in uncertainty analysis of computer models,” *Proc. - Winter Simul. Conf.*, pp. 557–564, 1992, doi: 10.1145/167293.167637.

[103] F. Akgul, “Bridge management in Turkey: a BMS design with customised functionalities,” *Struct. Infrastruct. Eng.*, vol. 12, no. 5, pp. 647–666, 2016, doi: 10.1080/15732479.2015.1035284.

[104] “Caltrans 2006, Seismic Design Criteria Version 1.4,” Sacramento, CA., 2006.

[105] “ATC, 1996, ATC-32 ,Improved Seismic Design Criteria for California Bridges: Provisional Recommendations,” Redwood City, California, 1996.

[106] N. M. J. Priestly, G. M. Calvi, and F. Seible, *Seismic Design and Retrofit of Bridges*. Joh Wiley & Sons, Inc, 1996.

[107] T. Yilmaz and S. Banerjee, “Impact spectrum of flood hazard on seismic vulnerability of bridges,” *Struct. Eng. Mech.*, vol. 66, no. 4, pp. 515–529, 2018, doi: 10.12989/sem.2018.66.4.515.

[108] Caltrans, “Seismic Design Criteria Version 1.7,” *Calif. Dep. Transp. Sacramento, CA, U.S.*, no. April, 2013.

[109] F. McKenna, “OpenSees: A Framework for Earthquake Engineering Simulation,” *Comput. Sci. Eng.*, vol. 13, no. 4, pp. 58–66, 2011, doi: 10.1109/MCSE.2011.66.

[110] J. B. Mander, M. J. N. Priestley, and R. Park, “Theoretical Stress-Strain Model for Confined Concrete,” *J. Struct. Eng.*, vol. 114, no. 8, pp. 1804–1826, 1989.

[111] F. Zwerneman and K. A. Digre, “SS: New API Codes: Updates, New Suite of Standards: API RP 2A-WSD, the 23rd Edition,” in *Offshore Technology Conference*, Apr. 2010, p. 9, doi: 10.4043/20837-MS.

[112] A. M. Yanmaz, *Köprü Hidroliği*. ODTÜ Geliştirme Vakfı Yayıncılık, 2002.

[113] F. Liang, C. R. Bennett, R. L. Parsons, J. Han, and C. Lin, “A literature review on behavior of scoured piles under bridges,” *Geotech. Spec. Publ.*, vol. 41022, no. 186, pp. 482–489, 2009, doi: 10.1061/41022(336)62.

[114] A. Mondoro and D. M. Frangopol, “Risk-based cost-benefit analysis for the retrofit of bridges exposed to extreme hydrologic events considering multiple failure modes,” *Eng. Struct.*, vol. 159, no. April 2017, pp. 310–319, 2018, doi: 10.1016/j.engstruct.2017.12.029.

[115] C. Lin, J. Han, C. Bennett, and R. L. Parsons, “Case history analysis of bridge failures due to scour,” *Clim. Eff. Pavement Geotech. Infrastruct. - Proc. Int. Symp. Clim. Eff. Pavement Geotech. Infrastruct. 2013*, pp. 204–216, 2014, doi: 10.1061/9780784413326.021.

[116] M. L. Yurtseven, “Köprü Ayakları Arkasında Oluşan Oyulmaların İncelenmesi,” İstanbul Teknik Üniversitesi, 2005.

[117] Z. Wang, L. Dueñas-Osorio, and J. E. Padgett, “Influence of scour effects on the seismic response of reinforced concrete bridges,” *Eng. Struct.*, vol. 76, pp. 202–214, 2014, doi: 10.1016/j.engstruct.2014.06.026.

[118] B. Melville and S. Coleman, *Bridge Scour*. Water Resources Publications,LLC, 2000.

[119] P. F. Lagasse, P. E. Clopper, L. W. Zevenbergen, W. J. Spitz, and L. G. Girard, “NCHRP REPORT 653, Effects of Debris on Bridge Pier Scour,” 2010.

[120] L. A. A. P.F. Lagasse, L.W. Zevenbergen, W.J. Spitz, “Stream Stability at Highway Structures, Fourth Edition,” 2012.

[121] J. He and Z.-F. Fu, “1 - Overview of modal analysis,” J. He and Z.-F. B. T.-M. A. Fu, Eds. Oxford: Butterworth-Heinemann, 2001, pp. 1–11.

[122] Y. Y. Ko, J. S. Chiou, Y. C. Tsai, C. H. Chen, H. Wang, and C. Y. Wang, “Evaluation of flood-resistant capacity of scoured bridges,” *J. Perform. Constr. Facil.*, vol. 28, no. 1, pp. 61–75, 2014, doi: 10.1061/(ASCE)CF.1943-5509.0000381.

[123] A. Amini, B. W. Melville, T. M. Ali, and A. H. Ghazali, “Clear-water local scour around pile groups in shallow-water flow,” *J. Hydraul. Eng.*, vol. 138, no. 2, pp. 177–185, 2012, doi: 10.1061/(ASCE)HY.1943-7900.0000488.

[124] S. Masanobu, F. M. Q., L. Jongheon, and N. Toshihiko, “Statistical Analysis of Fragility Curves,” *J. Eng. Mech.*, vol. 126, no. 12, pp. 1224–1231, Dec. 2000, doi: 10.1061/(ASCE)0733-9399(2000)126:12(1224).

[125] C. A. Cornell, F. Jalayer, R. O. Hamburger, and D. A. Foutch, “Probabilistic Basis for 2000 SAC Federal Emergency Management Agency Steel Moment Frame Guidelines,” *J. Struct. Eng.*, vol. 128, no. April 2002, pp. 526–533, 2002, doi: 10.1061/(ASCE)0733-9445(2002)128:4(526).

[126] O. C. Celik and B. R. Ellingwood, “Seismic fragilities for non-ductile reinforced concrete frames - Role of aleatoric and epistemic uncertainties,” *Struct. Saf.*, vol. 32, no. 1, pp. 1–12, 2010, doi: 10.1016/j.strusafe.2009.04.003.

[127] B. S. Kevin Mackie, “Seismic Demands for Performance-Based Design of Bridges,” 2003. doi: 10.1061/(ASCE)BE.1943-5592.0000827.

[128] M. J. Moyer and M. J. Kowalsky, “Influence of tension strain on buckling of reinforcement in concrete columns,” *ACI Struct. J.*, vol. 100, no. 1, pp. 75–85, 2003, doi: 10.14359/12441.

VITA

Personal Information

Surname, Name: Kanpara Cıvaş, Züleyha

Place and date of birth: Turkey/Kocaeli/İzmit – 05.10.1993

Phone: +90 544 635 1523

e-mail: zuleyhakanpara@gmail.com

Education

Özyeğin University (Istanbul/Turkey) M.Sc. Civil Engineering Department	**09.2018-09.2020**
Izmir Institute of Technology (Izmir/ Turkey) B.Sc. Civil Engineering Department (the first degree of class)	**09.2012-06.2017**

Scientific Participations

1. Structural Dynamics Workshop, Izmir Institute of Technology. 9-19 September 2019, Izmir/Turkey
2. 2nd ICOCEE Cappadocia (2017), International Conference on Civil and Environmental Engineering. 8- 10 May 2017, Nevsehir/Turkey

Journal Articles

1. Erdem T. K., Bilgiç E., Kanpara Cıvaş Z. "A New Method to Quantify the Robustness of Self-Consolidating Grouts." Construction and Building Materials, vol. 229, 2019, p. 116849., doi:10.1016/j.conbuildmat.2019.116849.

Conference Papers

1. Kanpara Cıvaş Z., Aygın O. C., Yılmaz T., "A Sensitivity Study for Seismic Response Assessment of Highway Bridges with Uncertain Modeling, Scour, and Deterioration Parameters", "9th Turkish Conference on Earthquake Engineering (9TCEE)", İstanbul, Turkey, 2-4 June 2021.

2. Erdem T.K., Bilgiç E., Kanpara Z., "An Investigation on the Factors Affecting the Range of Superplasticizers for Workable Self-Consolidating Grouts", 2nd International Conference on Civil and Environmental Engineering (Cappadocia-2017), Nevşehir, Turkey, 8 – 10 May 2017, 1667-1675.